(14) AFIT/GAE/AA/79D-9

(10) Roy Edward La Froth

(6) THRUST VECTORING TO ELIMINATE THE VERTICAL STABILIZER.

(9) Masters THESIS

AFIT/GAE/AA/79D-9 Roy E. La Froth
Capt USAF

(11) Dec 79

(12) 134

Approved for public release; distribution unlimited

AFIT/GAE/AA/79D-9

THRUST VECTORING TO ELIMINATE THE VERTICAL STABILIZER

THESIS

Presented to the Faculty of the School of Engineering

of the Air Force Institute of Technology

Air Training Command

in Partial Fulfillment of the

Requirements for the Degree of

Master of Science

by

Roy E. La Froth, B.S.A.E.

Capt USAF

Graduate Aeronautical Engineering

December 1979

Preface

This study represents my effort to determine what is needed in an active thrust vector controller to provide the directional stability and control given by the vertical stabilizer and rudder on an F-111.

I would like to thank my advisor, Captain James T. Silverthorn of Aeronautics and Astronautics of the Air Force Institute of Technology faculty, for his excellent guidance.

I would also like to thank my sponsor, Lieutenant Robert (Rob) Crombe of the Air Force Flight Dynamic Laboratory for his support and assistance in obtaining an understanding of the flying qualities requirements.

I wish especially to thank my wife, Brigitte, for typing this thesis. Her patience and perseverance during the entire project was an encouragement.

Contents

List of Figures

List of Tables

List of Symbols

a_y	lateral acceleration (ft/sec)
b	wing span (ft)
C_D	drag coefficient
$C_{\ell_\beta} = \frac{\partial C_\ell}{\partial \beta}$	variation of rolling moment coefficient with sideslip angle (1/deg)
$C_{n_\beta} = \frac{\partial C_n}{\partial \beta}$	variation of yawing moment coefficient with sideslip angle (1/deg)
$C_{y_\beta} = \frac{\partial C_y}{\partial \beta}$	variation of side force coefficient with sideslip angle (1/deg)
$C_{\ell_p} = \frac{\partial C_\ell}{\partial p}$	variation of rolling moment coefficient with roll rate (1/rad)
$C_{n_p} = \frac{\partial C_n}{\partial p}$	variation of yawing moment coefficient with roll rate (1/rad)
$C_{y_p} = \frac{\partial C_y}{\partial p}$	variation of side force coefficient with roll rate (1/rad)
$C_{\ell_r} = \frac{\partial C_\ell}{\partial r}$	variation of rolling moment coefficient with yaw rate (1/rad)
$C_{n_r} = \frac{\partial C_n}{\partial r}$	variation of yawing moment coefficient with yaw rate (1/rad)
$C_{y_r} = \frac{\partial C_y}{\partial r}$	variation of side force coefficient with yaw rate (1/rad)
$C_{\ell_\delta} = \frac{\partial C_\ell}{\partial \delta}$	variation of rolling moment coefficient with control angle
$C_{n_\delta} = \frac{\partial C_n}{\partial \delta}$	variation of yawing moment coefficient with control angle (1/deg)
$C_{y_\delta} = \frac{\partial C_y}{\partial \delta}$	variation of side force coefficient with control angle (1/deg)
g	acceleration due to gravity (ft/sec^2)
Ixx	moment of inertia about the X axis ($slug\text{-}ft^2$)
Ixz	product of inertia ($slug\text{-}ft^2$)

I_{zz}	moment of inertia about the z axis (slug-ft^2)
K_β	β feedback gain
K_r	r feedback gain
l_t	distance from the aircraft center of gravity to engine nozzle (ft)
$L_{\dot{\beta}}$	dimensional variation of rolling moment with rate of change of sideslip angle (1/sec)
L_β	dimensional variation of rolling moment with sideslip angle (1/sec^2)
L_p	dimensional variation of rolling moment with roll rate (1/sec)
L_r	dimensional variation of rolling moment with yaw rate (1 /sec)
L_δ	dimensional variation of rolling moment with control deflection (1/sec^2)
MAC	mean aerodynamic center
$N_{\dot{\beta}}$	dimensional variation of yawing moment with rate of change of sideslip angle (1/sec)
N_β	dimensional variation of yawing moment with sideslip angle (1/sec^2)
N_p	dimensional variation of yawing moment with roll rate (1/sec)
N_r	dimensional variation of yawing moment with yaw rate (1/sec)
N_δ	dimensional variation of yawing moment with control deflection (1/sec^2)
p	perturbed roll rate (rad/sec)
q	dynamic pressure $\frac{1}{2} \rho V_t^2$ (lb/ft^2)
r	perturbed yaw rate (rad/sec)
S	wing area (ft^2)
s	Laplace variable
u_o	longitudinal equilibrium velocity along the body X axis
V_t	steady state forward velocity (ft/sec)

v	perturbed side velocity (ft/sec)
v_g	side velocity due to a gust (ft/sec)
W	weight (lb)
w_o	aircraft steady state downward velocity (ft/sec)
$Y_{\dot{\beta}}$	dimensional variation of lateral force with rate of change of sideslip angle (ft/sec)
Y_β	dimensional variation of lateral force with sideslip angle (ft/sec^2)
Y_p	dimensional variation of lateral force with roll rate (ft/sec)
Y_r	dimensional variation of lateral force with yaw rate (ft/sec)
Y_δ	dimensional variation of lateral force with cnntrol deflection (ft/sec^2)

Greek Symbols

β	sideslip angle (rad)
β_g	sideslip angle due to a side gust (rad)
ϕ	perturbed bank angle (rad)
α	angle of attack (deg)
γ	flight path angle (deg)
θ_o	steady state pitch attitude from the horizon (deg)
ω	frequency (rad/sec)
ω_n	dutch roll frequency (rad/sec)
δ_a	aileron surface deflection (rad,deg)
δ_r	rudder surface deflection (rad,deg)
δ_v	thrust vector deflection (rad,deg)
ζ	dutch roll damping ratio
ρ	air density (slug/ft^3)
Φ	power spectral density

Abstract

Root locus analysis techniques are used to design an active thrust vector control system to provide the directional stability for an F-111 without the vertical stabilizer. A linear analysis of the lateral-directional modes is performed for the aircraft both with and without the vertical stabilizer. The aircraft with the vertical stabilizer is used as a baseline. Computer time histories for discrete atmospheric turbulence and a covariance analysis for random turbulence are used for the evaluation. It is found that the thrust vector control produces a response as good as or better than the baseline aircraft.

Requirements for the thrust vector deflection and rate of deflection are generated. The lowest possible rate of deflection for acceptable flying qualities is shown to be 1 rad/sec.

THRUST VECTORING TO ELIMINATE THE VERTICAL STABILIZER

I. Introduction

There is increasing concern over the vulnerability of modern jet fighter aircraft to detection by radar and optical means. In looking at ways to reduce detection there has been much work on electronically masking an aircraft to radar, although these techniques do little to reduce the optical profile. When one views a jet fighter from a top view (or bottom view), the wings constitute the largest part of the aircraft's cross section. Since they have been designed specifically to give the aircraft its required lift and flight characteristics, there is no apparent potential for improvement of the cross section. From a side view of the aircraft it is seen that, besides the fuselage, the cockpit and the vertical stabilizer are areas in which to improve the cross section. Reduction of the height of the cockpit will not help very much and would reduce the pilot's visibility. Reduction of the size or elimination of the vertical stabilizer and rudder would greatly improve the radar cross section and optical profile. The problem is that the vertical stabilizer provides the aircraft's directional stability and therefore its reduction or elimination could cause the aircraft to be directionally unstable. Therefore, a means to provide the directional stabilility and yaw characteristics that the vertical stabilizer and rudder provide is needed. Thrust vectoring of the jet engine nozzle using an active control system could be the means.

Another problem with the vertical stabilizer is that at the high angles of attack modern jet fighter aircraft are capable of, the stabilizer may be blanked to the free stream by the wing-body combination. An aircraft with an active thrust vector control (TVC) would not be as susceptible to reduced lateral-directional stability at high angles of attack.

Furthermore, if the vertical stabilizer could be reduced or eliminated, both a reduction in drag and weight would be realized. Of course, these benefits must be compared with the increased complexity and weight and the reduction in longitudinal thrust associated with thrust vectoring.

Purpose

The purpose of this thesis is to determine the static and dynamic requirements of lateral-directional thrust vectoring (magnitude and rate) adequate to replace the vertical stabilizer on a specific aircraft. In other words, this thesis will determine what is needed in an active TVC to provide the same directional stability and control now given by the vertical stabilizer and rudder. Also, the stability and control advantages of such a concept are to be indicated.

Aircraft

The aircraft utilized in this study is the F-111 Transonic Aircraft Technology (TACT) program aircraft. The F-111 is a supersonic, variable wing sweep, twin engine fighter aircraft. A physical description of the F-111 TACT aircraft is in Appendix 1. The TACT program (Ref 1:1) was a supercritical airfoil research program to

demonstrate the performance advantages of a supercritical wing. Since wind tunnel data for this aircraft in both a tail-on* and tail-off configuration was available (from the Flying Qualities Group of the Air Force Flight Dynamic Laboratory), it was a convenient choice for this present study.

Scope

Linear analysis and design methods were used to approach the problem. Since it was initially assumed that the longitudinal perturbations would be small, only the lateral-directional aircraft modes were examined. The limitation of this assumption is discussed in Chapters IV and V. A full design study of the aircraft covering its complete flight envelope was not practical for this thesis. Instead the study was restricted to two-steady level cruise conditions.

The analyses and design were performed at cruise conditions of Mach 0.8 at 40000 ft. altitude and at Mach 2.0 at 30000 ft. Since the first is a low thrust, low dynamic pressure condition, it is believed to be the a worst case cruise condition with respect to damping of the dutch roll mode with the TVC. On the other hand, the second flight condition is a high thrust, high dynamic pressure condition and therefore represents an easier design case. Table 1 summarizes these two flight conditions. The stability derivatives for the two flight cases in the tail-on and tail-off configurations are shown in Appendix 2.

The system was evaluated using both discrete and random atmospheric turbulence simulation. The tail-on aircraft, including its

*Tail-on refers to the aircraft with the vertical stabilizer and tail-off refers to the TVC aircraft without the vertical stabilizer.

Table 1

Flight Conditions

	Flt. Cond. 1	Flt. Cond. 2
Mach No.	0.8	2.0
Altitude (ft)	40000	30000
Airspeed (ft/sec)	774	1990
Dynamic Pressure (lb/ft^2)	176	1764
Density ($slugs/ft^3$)	5.873×10^{-4}	8.907×10^{-4}
Flight Path angle (deg)	0	0
Angle at attack (deg)	9	2
Weight (lb)	68000	68000
Wing Sweep (deg)	26	58
Center of Gravity (% MAC)	32.5	32.5
Required Thrust (lb)	6350	44980
Ixx ($slug-ft^2$)	89500	59000
Ixz ($slug-ft^2$)	3500	4720
Izz ($slug-ft^2$)	456000	442000

yaw stability augmentation system (SAS), was used as a basis for comparison. A sensitivity study was performed to determine the effects of thrust variation, feedback gain and TVC actuator time constant variation. The TVC actuator requirements to provide acceptable flying qualities were specified. No attempt was made to model any specific two-dimensional TVC nozzle. Only the deflection of the thrust vector is specified. In its undeflected position the thrust vector is assumed to be along the aircraft body roll axis.

Organization

The second chapter of this thesis presents the lateral-directional small perturbation equations of motion utilized in this study.

Chapter III describes the design of the thrust vector controller. Listed first are the flying qualities requirements which the design is to meet. The block diagram of the yaw control system is shown and then the root locus analysis of the controller is presented. The feedback gain selections are provided along with the transfer functions of the closed loop system with the yaw SAS. Then a comparison is made with the tail-on yaw SAS and verification that the flying qualities requirements are satisfied from the eigenvalues of the characteristic equation.

The results of the evaluation of the yaw SAS to three types of input are presented in Chapter IV. A computer program was developed to integrate the aircraft equations of motion to provide time histories for a pulse rudder pedal input. A comparison is made with the tail-on aircraft. Next, the response to discrete atmospheric turbulence is shown. The model for the turbulence is a 1-COS discrete side gust.

The aircraft response to this gust is found using the same integration program as before. Again, a comparison with the tail-on configuration is made. The effect of random atmospheric turbulence is next examined using the Dryden form of the power spectral density and a computer program which does a covariance analysis. Results of a study of the effects of the variation of thrust, gains, and actuator time constant (each independently) on the response to atmospheric turbulence are presented.

Chapter V then discusses the effects on the dutch roll mode of applying limits to the thrust vector excursion and slew rate using the discrete atmospheric turbulence input. The results show the minimum thrust vector excursion and rate requirements for the discrete gust environment to satisfy the dutch roll requirements.

Conclusions and recommendations are presented in the final chapter of this thesis.

II. Aircraft Equations of Motion

This chapter presents the lateral-directional small perturbation equations of motion (Ref 2:6.47) written in the body axis system. These equations were used in the design of the thrust vector control law (Chapter III) and the evaluation of the controller (Chapters IV and V). The equations are.

Lateral Acceleration

$$\dot{v} - w_o\, p + u_o\, r = Y_{\dot{\beta}}\dot{\beta} + Y_\beta \beta + Y_p p + Y_r r + g \cos\theta_o\, \phi + Y_{\delta_a}\, \delta_a + Y_{\delta_v}\, \delta_v \qquad (1)$$

Roll Acceleration

$$\dot{p} - \frac{Ixz}{Ixx}\, \dot{r} = L_{\dot{\beta}}\dot{\beta} + L_\beta \beta + L_p p + L_r r + L_{\delta_a}\, \delta_a + L_{\delta_v}\, \delta_v \qquad (2)$$

Yaw Acceleration

$$\dot{r} - \frac{Ixz}{Izz}\, \dot{p} = N_{\dot{\beta}}\dot{\beta} + N_\beta \beta + N_p p + N_r r + N_{\delta_a}\, \delta_a + N_{\delta_v}\, \delta_v \qquad (3)$$

Kinematic

$$\dot{\phi} = p + r \tan\theta_o \qquad (4)$$

The quantities v, p, r, ϕ and β represent the aircraft's perturbation side velocity, roll rate, yaw rate, bank angle and sideslip angle respectively. The subscript "$_o$" represents equilibrium values and the quantities Y_β, Y_p, L_p, etc. are the dimensional stability and control derivatives (Ref 2:6.46). The term δ_a is the aircraft perturbation aileron deflection while δ_v represents thrust

vector deflection. The δ_v terms are replaced with δ_r (rudder deflection) in the tail-on cases. Appendix 3 gives the sign convention for δ_v and derives the TVC dimensional derivatives.

It is generally assumed that the $\dot{\beta}$ derivatives are negligible (Ref 2:4.82). Then, noting that:

$$v = V_t \beta$$

and:

$$\dot{v} = V_t \dot{\beta}$$

where V_t is the aircrafts total velocity.

Equation 1 can be rewritten as:

$$\dot{\beta} = \frac{Y_\beta}{V_t}\beta + \frac{(w_o + Y_p)}{V_t} p + \frac{(Y_r - u_o)}{V_t} r + \frac{g \cos \theta_o}{V_t} \phi + \frac{Y_{\beta_a}}{V_t} \beta_a \quad \frac{Y_{\beta_v}}{V_t} \beta_v \tag{5}$$

Simultaneous solution of Equations (2) and (3) for $\dot{p}$ and $\dot{r}$ and introduction of primed dimensional derivatives into these equations, gives:

$$\dot{p} = L'_\beta \beta + L'_p p + L'_r r + L'_{\delta a} \delta_a + L'_{\delta_v} \delta_v \tag{6}$$

$$\dot{r} = N'_\beta \beta + N'_p p + N'_r r + N'_\delta \delta_a + N'_{\delta_v} \delta_v \tag{7}$$

The primed derivatives are defined as:

$$L'_i = \frac{L_i + \frac{Ixz}{Izz} N_i}{1 - \frac{Ixz^2}{Ixx\ Izz}}$$

$$N_i' = \frac{N_i + \frac{Ixz}{Izz} L_i}{1 - \frac{Ixz^2}{Ixx\ Izz}}$$

where the subscript, "i", represents β, p, r, δ_a, δ_v.

Finally, the lateral acceleration can be expressed as:

$$a_y = Y_\beta \beta + Y_p p + Y_{\delta_a} \delta_a + Y_{\delta_v} \delta_v \qquad (8)$$

III. Thrust Vector Control Law Development

This chapter presents the control laws as developed for the TVC yaw stability augmentation system (SAS). The requirements for the aircraft dutch roll mode, roll mode and spiral mode are presented. The block diagram of the TVC yaw SAS is shown and compared with the tail-on yaw SAS. The root locus plots for the tail-off aircraft and yaw SAS are shown and then the lateral modes for the closed loop system are compared with the requirements and the tail-on aircraft modes.

Computer Programs

Existing computer programs and library subprograms available through the Aeronautical System Division's (ASD) computer system were utilized in the TVC control law development. In order to use the root locus analysis method, the aircraft lateral-directional transfer functions needed to be obtained. A program written by J. M. Griffin (Ref 3) accepts the lateral non-dimensional stability derivatives as input and computes the lateral-directional transfer functions in both polynomial form and factored form. The transfer functions of the variables, β, p, r and a_y with aileron and rudder (or thrust vector) input are provided as output. It also provides the dutch roll frequency and damping ratio, roll time constant and spiral time constant.

Another very useful computer program, Total, (Ref 4) in the AFIT library of the ASD computer system was used for the root locus analysis. The program was accessed interactively. Transfer functions were

provided as input to obtain the root locus digital printout and plots used for analysis and design.

Requirements

The lateral-directional flying qualities requirements for the dutch roll mode, roll mode and spiral stability were taken from the Air Force Flight Dynamics Laboratory (AFFDL) flying qualities specification (Ref 5:182,206,220). The requirements are specified for a class IV (highly maneuverable) aircraft, category A (flight phase that requires rapid maneuvering or precise flight control), level 1 (flying qualities clearly adequate for mission accomplishment) flying qualities.

The three lateral-directional modes (Ref 2:6.53) can be obtained from the roots of the characteristic equation for the aircraft. The dutch roll mode is represented by a complex pair of roots in the s-plane so the flying qualities requirements are specified in terms of frequency and damping ratio. The roll mode normally appears in the characteristic equation as a root on the s-plane real axis. Its requirement is specified in terms of the roll mode time constant which implies a response requirement to a step (aileron) input. The spiral mode is often divergent so the requirement is specified as a time to double amplitude. The requirements for these three modes are as follows:

Dutch Roll Mode - $\omega_n \geq 1$ rad/sec

$$\zeta \geq 0.19$$

$$\zeta\omega_n \geq 0.35 \text{ rad/sec}$$

Roll Mode - $1/\tau_r \geq$ 1 per sec

Spiral Stability-Minimum time to double amplitude = 12 sec

or $1/\tau_s \geq -0.057$ per sec

Coupled Roll/Spiral is unacceptable.

System Analysis

By looking at the non-dimensional stability derivatives (Appendix 2) it can be seen that for each flight condition the stability derivatives are different for the tail-on and tail-off configurations. The stability derivative of particular interest here is C_{n_β} since this derivative must be positive for directional stability (Ref 6:112-113). Therefore, it can be seen directly from Appendix 2 that removal of the vertical stabilizer causes the aircraft to be directionally unstable (C_{n_β} is negative). The effect of the removal of the vertical stabilizer can be seen from the large changes in C_{y_β}, C_{y_p}, C_{n_p} and C_{n_r}. In order to restore this lost directional stability a feedback control system to a thrust vectoring device is to be used. Figure 1 is a block diagram of the control system proposed to correct this lack of directional stability. Sideslip (β) feedback is used in the inner loop with yaw rate (r) feedback in the outer loop. The β feedback basically increases the dutch roll frequency and the r feedback provides the dutch roll damping.

The thrust vector actuator was selected with a 0.1 second time constant. This was believed to be representative of an actuator for this type of application. The washout circuit time constant was

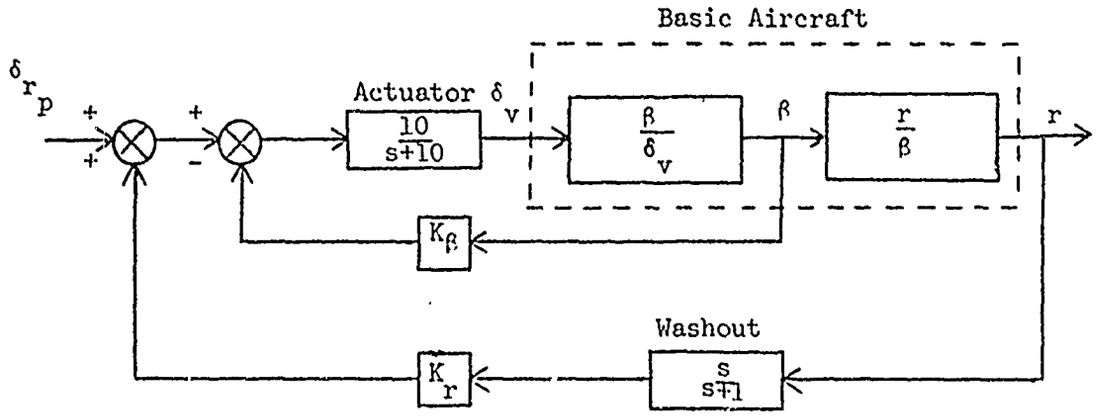

Figure 1 Tail-off Yaw SAS

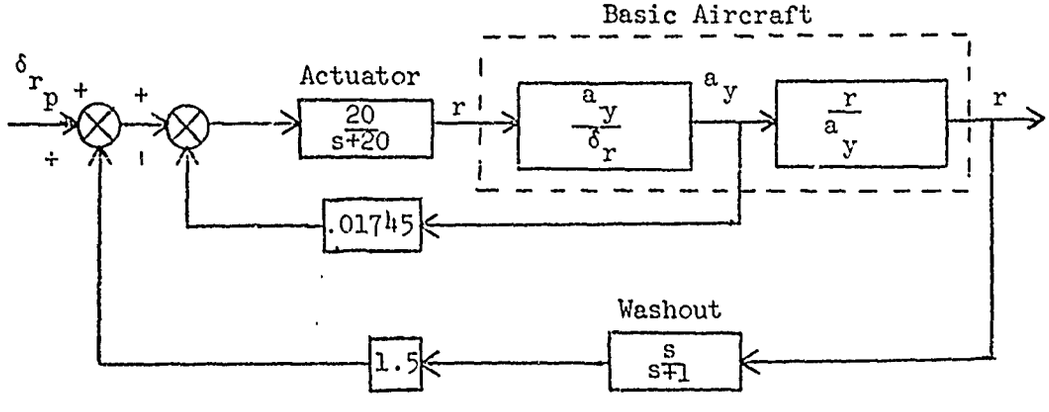

Figure 2 Tail-on Yaw SAS

selected to be consistant with the tail-on washout time constant of .1 second. The effect of washout time constant will be discussed later in this chapter. A simplified block diagram of the tail-on yaw SAS is shown in figure 2. The configuration of this yaw SAS is basically the same as the tail-off yaw SAS except that the lateral acceleration (a_y) feedback was used in the inner loop. The rudder actuator is modelled with a 0.05 second time constant so it is a faster actuator than the one selected for the TVC configuration.

A root locus of the inner loop (β feedback) of the tail-off yaw SAS at Mach 0.8 is shown in figure 3. Of particular interest here is the coupled roll-spiral mode in the right-half s-plane. This condition is unacceptable from the flying qualities requirements standpoint. The dutch roll poles are located at $-0.60 \pm 0.45j$. By increasing the feedback gain the roll-spiral roots can be moved back to the real axis. As this is done the dutch roll mode goes unstable but the frequency is increased above the minimum requirement of 1 rad/sec. Closure of the yaw SAS outer loop stabilizes the dutch roll as shown in figure 4. The outer loop gain is selected to maximize the product of the dutch roll frequency and damping ratio ($\zeta\omega_n$). This will minimize the time to damp the transient response. As seen in figure 4 the roll and spiral modes are now uncoupled (as they should). The gains selected were:

Inner Loop $K_\beta = 16.22$

Outer Loop $K_r = 6.35$

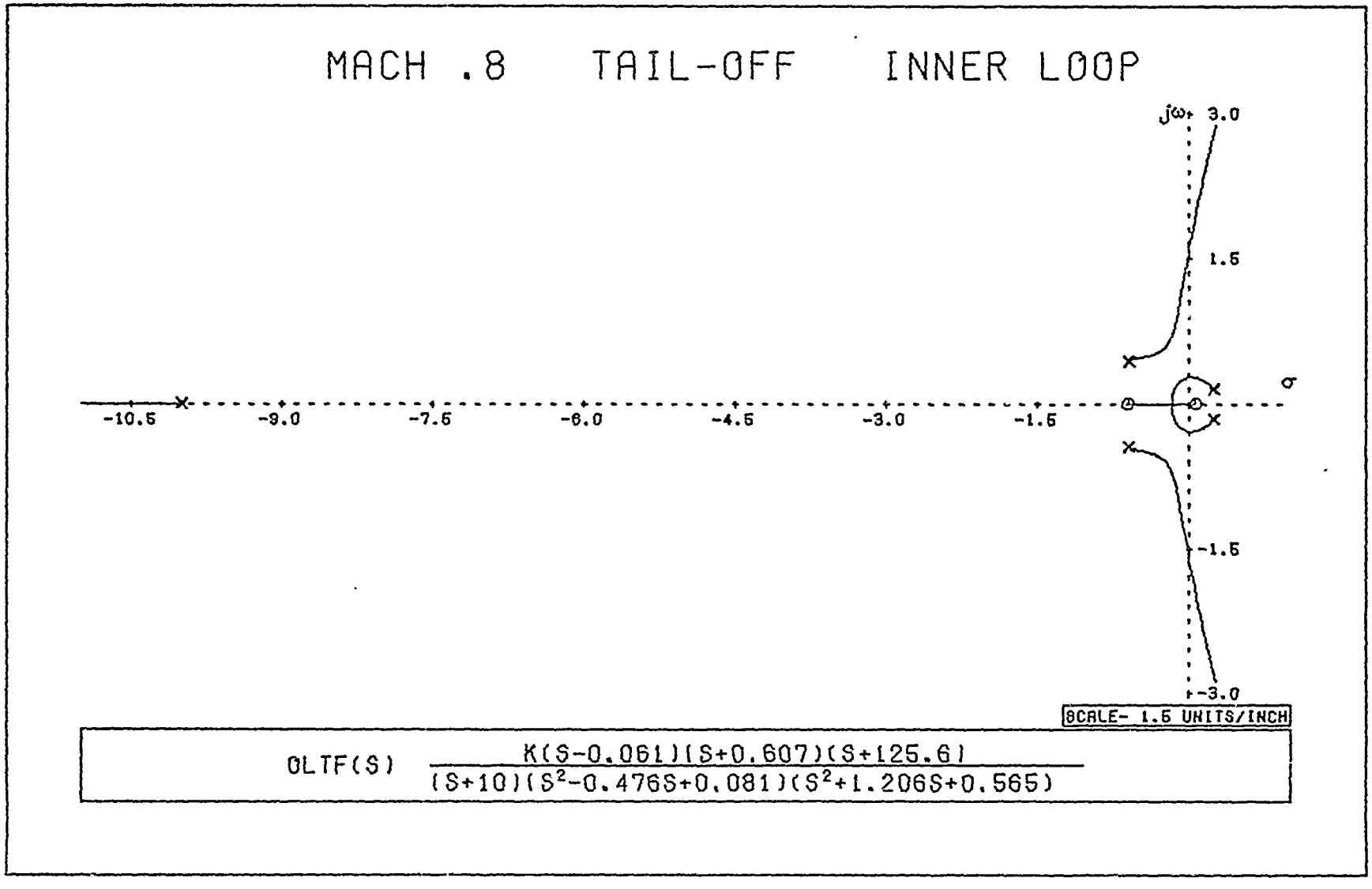

Figure 3.Yaw SAS · Inner Loop Root Locus Flt. Cond. 1

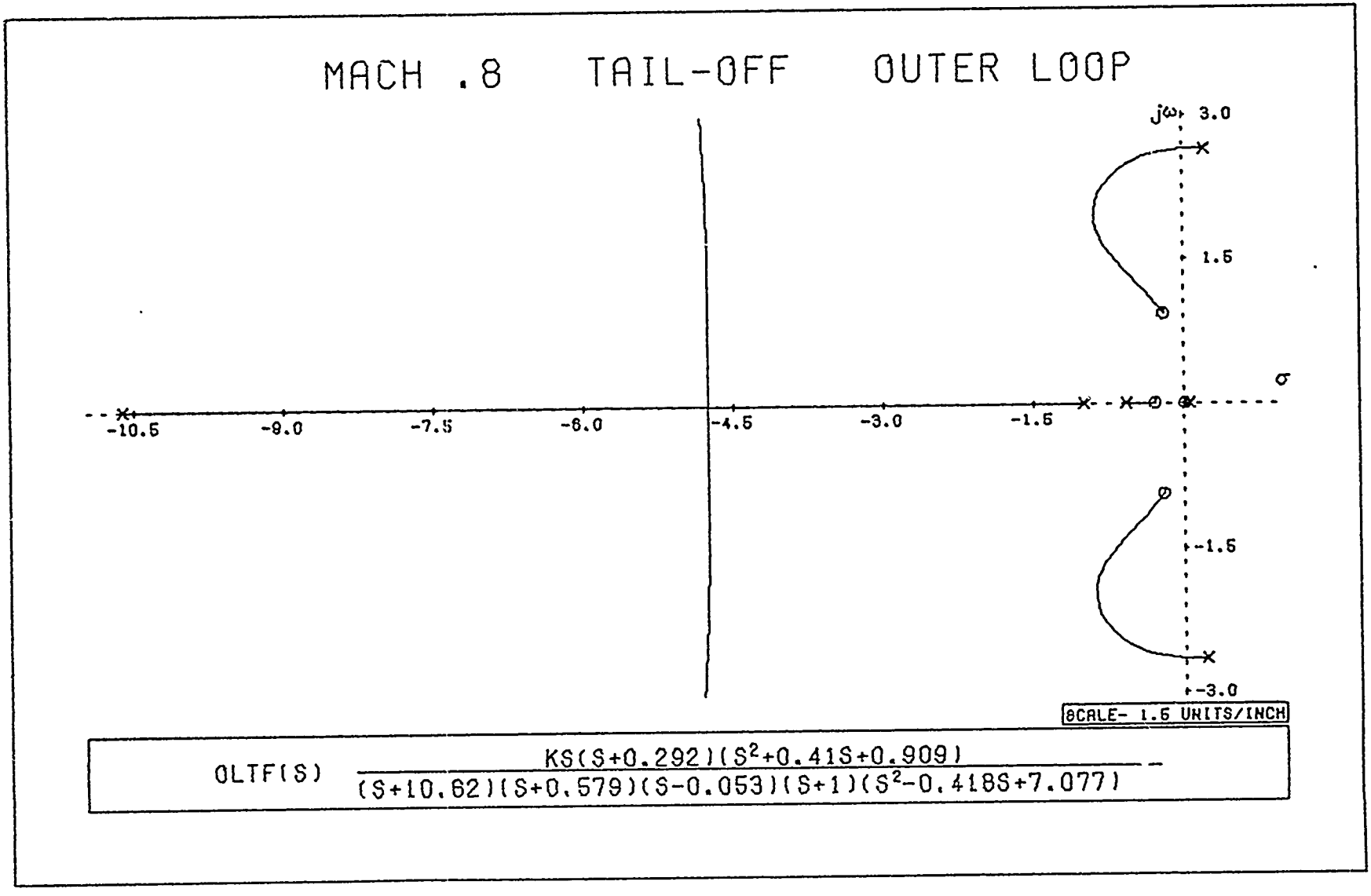

Figure 4. Yaw SAS Outer Loop Root Locus Flt.Cond. 1

The closed loop transfer function is:

$$\frac{r}{\delta_{r_p}} = \frac{-4.76\,(s + .292)(s + .205 \pm .931j)(s + 1)}{(s + .469)(s - .045)(s + .893 \pm 2.06j)(s + 4.01)(s + 5.5)}$$

This can be compared with the closed loop transfer function for the Mach 0.8 tail-on aircraft (and yaw SAS):

$$\frac{r}{\delta_{r_p}} = \frac{-20.44\,(s + .268 \pm .7j)(s + .334)(s + 1)}{(s - .016)(s + .446 \pm 1.2j)(s + .517)(s + 2.83)(s + 14.3)}$$

Table 2 shows the dutch roll frequency and damping, roll time constant and the spiral time constant for the Mach 0.8 tail-off case as compared with the flying qualities specification requirements and with the tail-on case. This table indicates that the tail-off aircraft exceeds the dutch roll specification requirement. The tail-off configuration has a higher frequency and damping than the tail-on configuration which suggests a better transient response than the tail on. The spiral divergence criteria is met for the tail-off aircraft but the roll time constant is too high. No attempt will be made here to correct this problem but only to suggest that roll augmentation would correct the problem. Another way to correct the problem would be to increase the washout time constant sufficiently but this will be discussed later in this chapter.

Table 2

Mach 0.8 Lateral Flying Qualities of Interest

	Dutch Roll			Roll	Spiral
	ω_n	ζ	$\zeta\omega_n$	$1/\tau_r$	$1/\tau_s$
	(rad/sec)		(rad/sec)	(1/sec)	(1/sec)
Requirement	1 (min)	0.19 (min)	0.35 (min)	1 (min)	-0.057 (min)
Tail-off	2.24	0.4	0.89	0.47	-0.045
Tail-on	1.28	0.35	0.45	2.86	-0.016

The Mach 2 case was handled in much the same way as the Mach 0.8 case but new feedback gains had to be selected. The root locus of the inner loop of the yaw SAS is shown in figure 5. This time the tail-off aircraft does not have a coupled roll-spiral or a dutch roll mode but the roots are all on the real axis. By increasing the feedback gain the poles at 2.9 and 0.022 form the dutch roll mode. The pole at -3.15 couples for a small range of gain with the pole at -1.43 but then they return to the real axis to form a roll mode and spiral mode. The dutch roll is unstable for all values of gain but the yaw rate feedback will stabilize this mode. An inner loop gain was selected which produced a good dutch roll root locus (figure 6). The gains selected were:

$K_\beta = 6.43$

$K_r = 1.34$

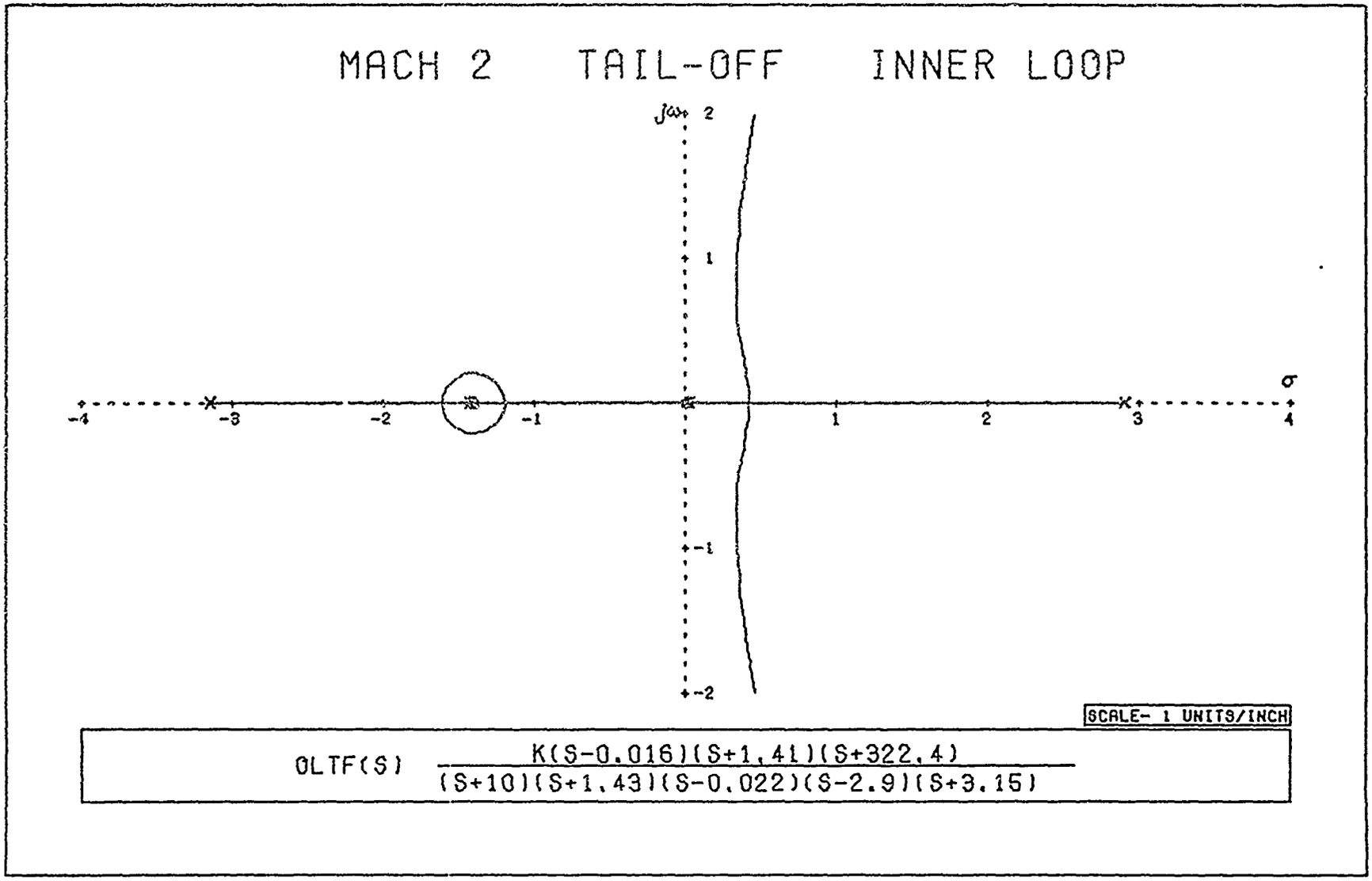

Figure 5. Yaw SAS Inner Loop Root Locus Flt. Cond. 2

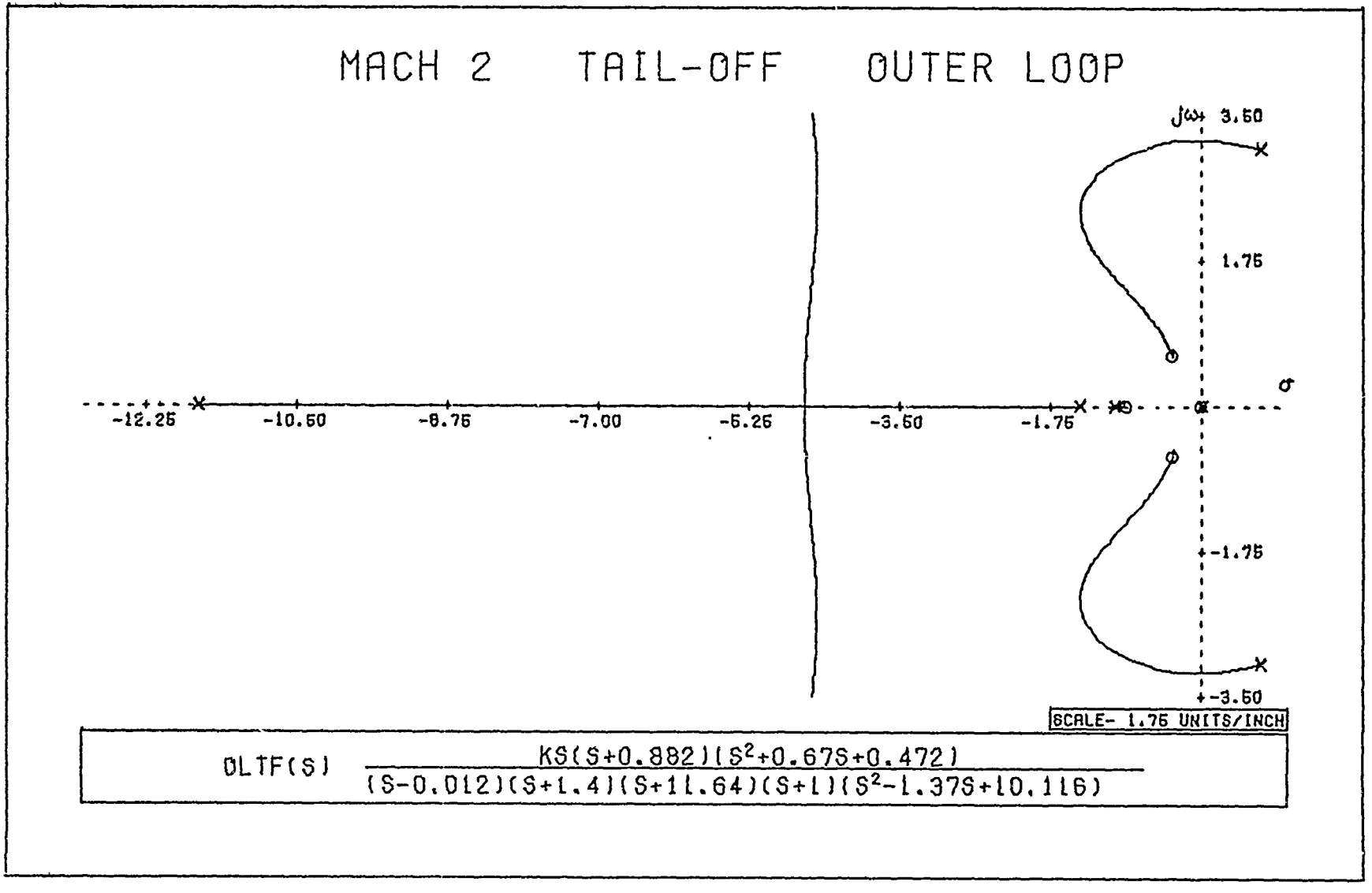

Figure 6. Yaw SAS Outer Loop Root Locus Flt. Cond. 2

The transfer function for the closed loop system (figure 1) is:

$$\frac{r}{\delta_{r_p}} = \frac{-32.8\,(s + .882)(s + .335 \pm .6j)(s + 1)}{(s + .96)(s - .0108)(s + 1.24 \pm 2.76j)(s + 4.03)(s + 5.2)}$$

For comparison the transfer function for the tail-on aircraft with its yaw SAS (figure 2) is:

$$\frac{r}{\delta_{r_p}} = \frac{-42\,(s + .65 \pm 1.05j)(s + .65)(s + 1)}{(s + .009)(s + 2.12 \pm 6.17j)(s + .94)(s + 2.77)(s + 7.37)}$$

Table 3 shows the dutch roll frequency and damping, roll time constant and the spiral time constant for the Mach 2 tail-off case as compared with the flying qualities specification requirements and the Mach 2 tail-on case. While the tail-off aircraft exceeds the specification requirement, the tail-on aircraft has a much higher frequency and $\zeta\omega_n$ parameter which indicates that it will have a shorter transient response than the tail-off aircraft. The roll and spiral time constants satisfy the specification requirements.

Table 3

Mach 2 Lateral Flying Qualities of Interest

	Dutch Roll			Roll	Spiral
	ω_n	ζ	$\zeta\omega_n$	$1/t_r$	$1/t_r$
	(rad/sec)		(rad/sec)	(1/sec)	(1/sec)
Requirement	1 (min)	0.19 (min)	0.35 (min)	1 (min)	-0.057 (min)
Tail-off	3.0	0.41	1.24	4.0	-0.0108
Tail-on	6.5	0.32	2.12	2.78	0.009

Effects of Washout Time Constant

As indicated previously the washout circuit for the tail-off design was selected to be consistent with that in the tail-on yaw SAS. The effect on the dutch roll of changing from the 1 second time constant was examined for flight condition 1. The result is that as the time constant is decreased the root locus of the dutch roll collapses toward the imaginary axis. Figure 7 shows the effect of 0.83 second washout time constant. If the washout time constant is increased the result is that the dutch roll root locus expands away from the imaginary axis producing much better dutch roll characteristics. Figures 8 and 9 show the effect of a 1.25 second and a 2 second time constant respectively.

If a washout time constant on the order of 2 seconds could be tolerated, the washout pole would be to the right of the roll pole (figure 9) and the branch associated with the roll mode would move to the left. There would then be no problem in satisfying the flying qualities roll time constant requirement.

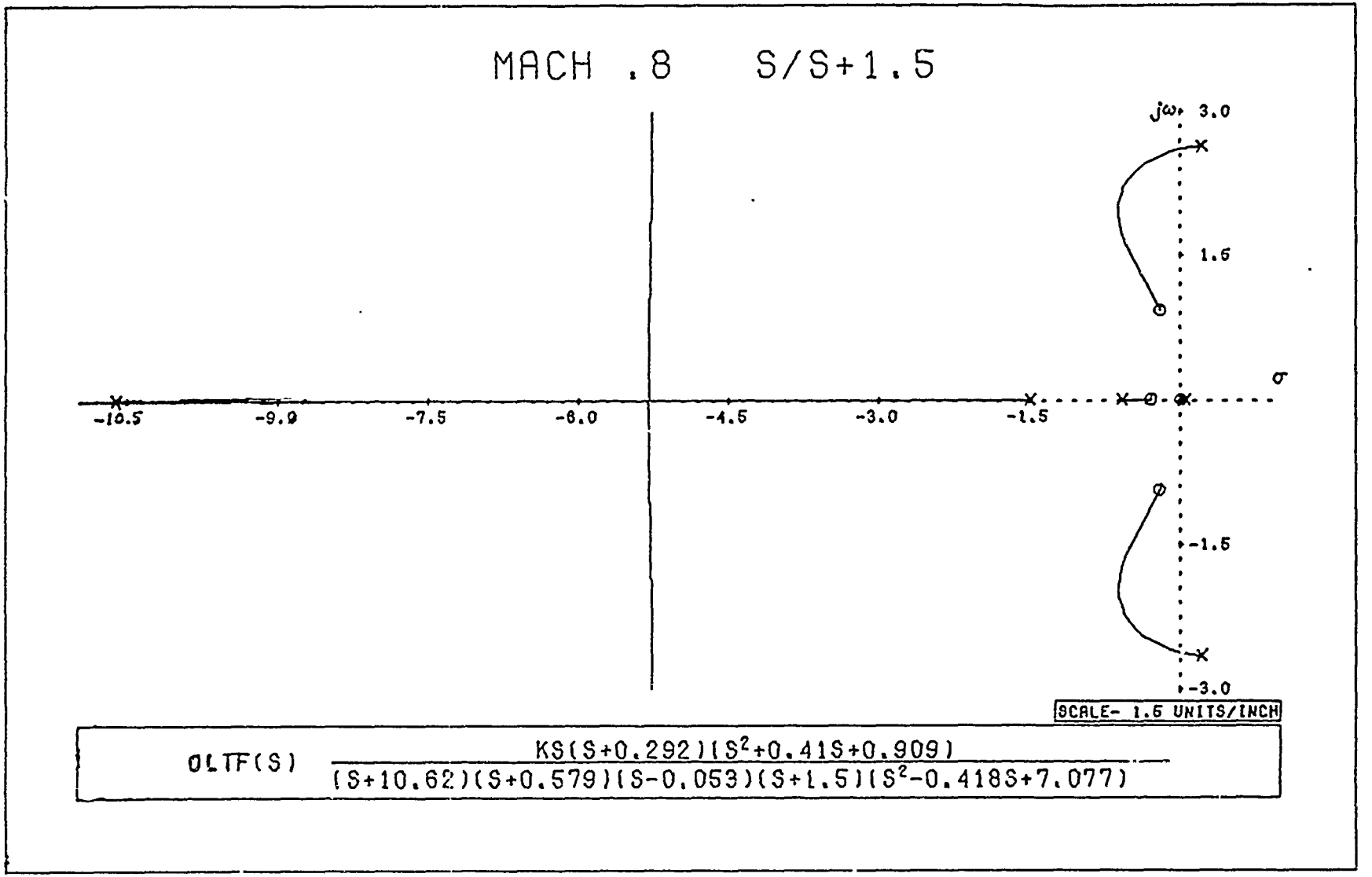

Figure 7. Effect of a .83 sec Washout Time Constant Flt. Cond. 1

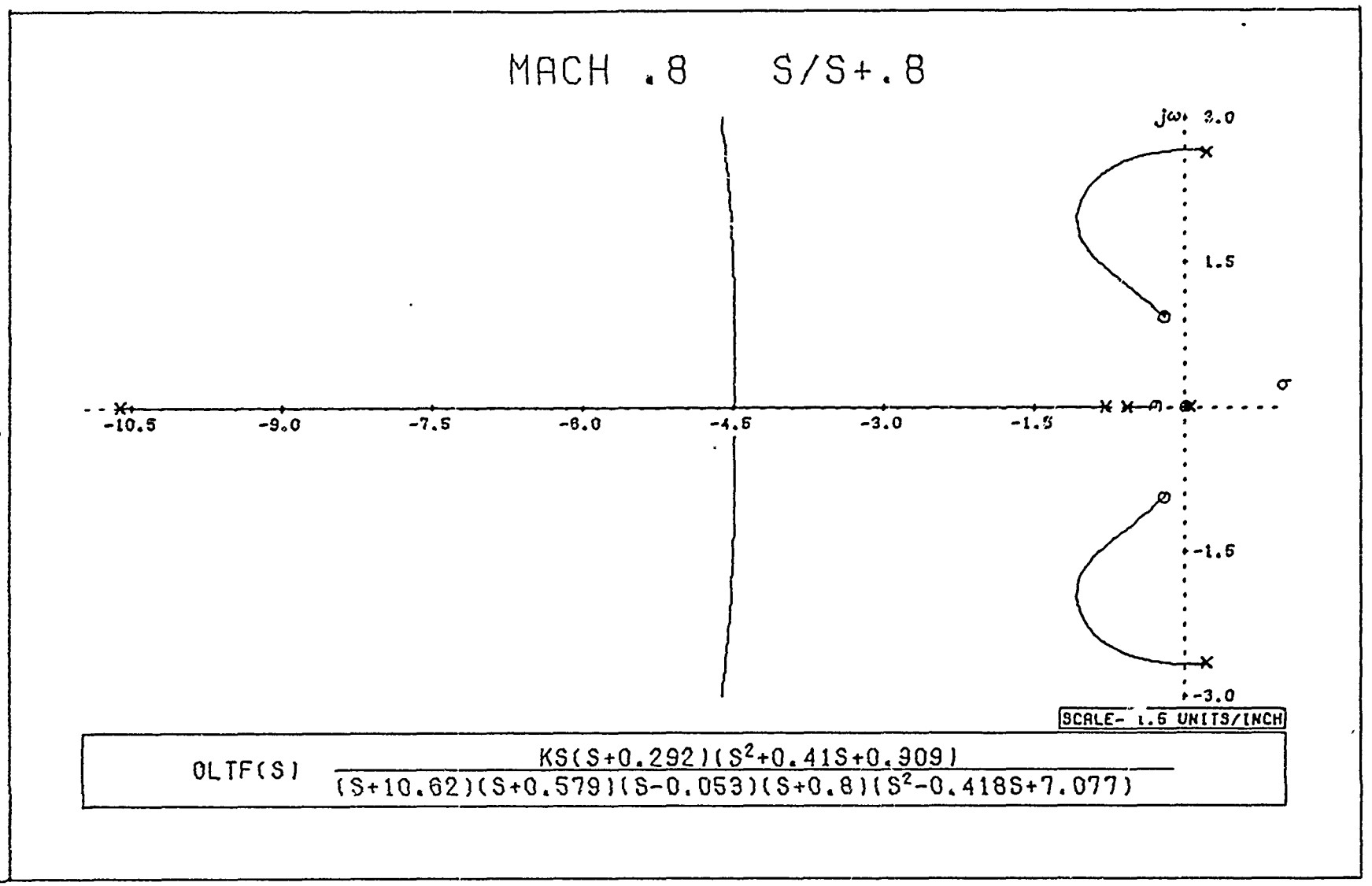

Figure 8. Effect of a 1.25 sec Washout Time Constant Flt. Cond. 1

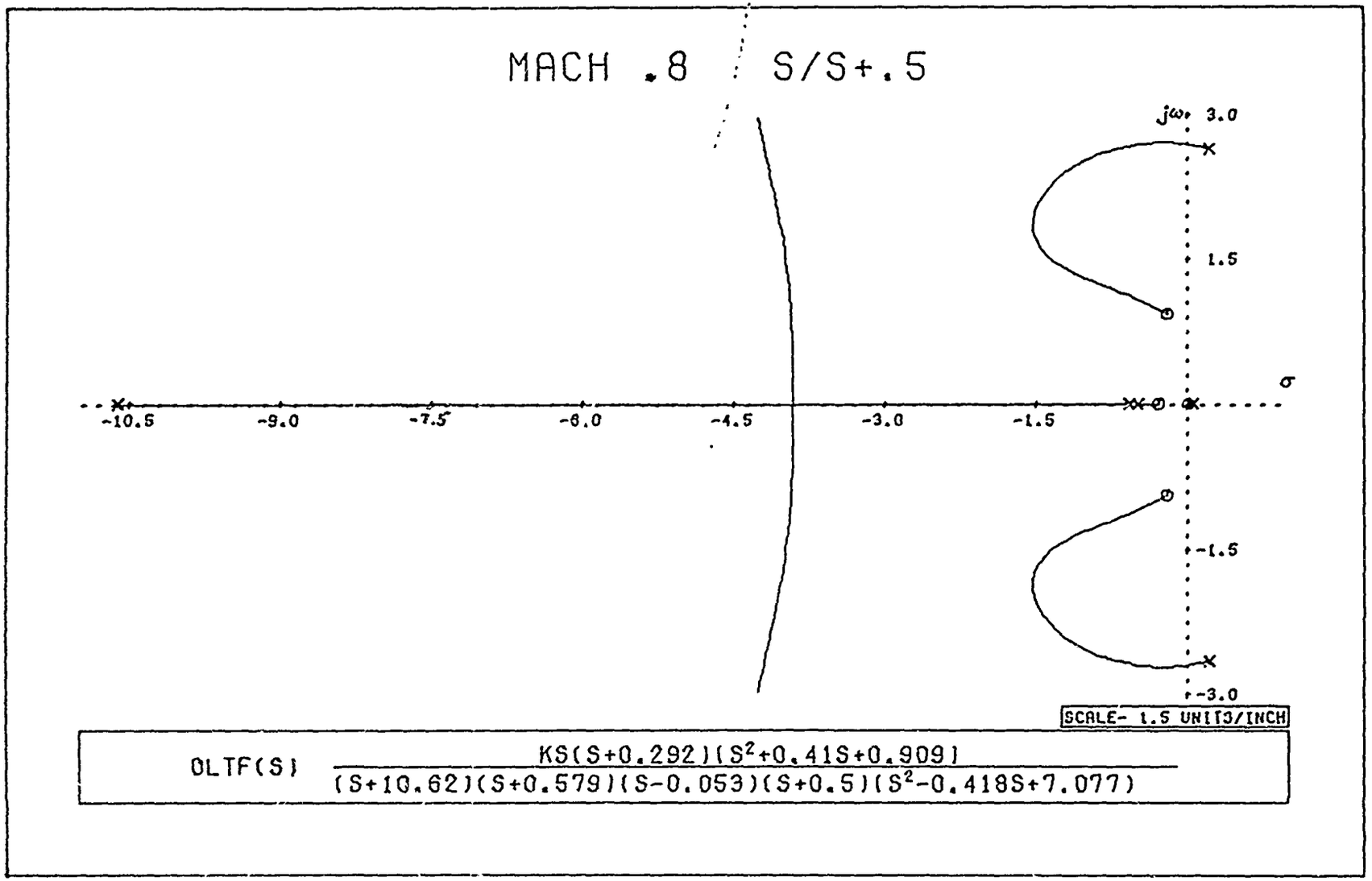

Figure 9. Effect at a 2 sec. Washout Time Constant Flt. Cond. 1

at a subsonic cruise condition. However, it takes the tail-on aircraft longer to damp the disturbance. This would be expected as the dutch roll frequency and damping are less than that of the tail-off aircraft at this flight condition. Figure 19 shows plots of p and ϕ for the tail-on aircraft. The bank angle seeks a steady state value of about 9 degrees whereas the tail-off aircraft continued to roll, but, at a slow rate. After 10 seconds the tail-off aircraft only rolled 3 3 degrees. This reflects the long roll mode time constant.

The Mach 2 tail-off rudder pulse responses are shown in figures 20-25. Figure 20 shows the pulse rudder input, δ_v, and $\dot{\delta}_v$ plots. The variables a_y, β and r plots are shown in figure 21. Again, the yaw SAS is functioning properly although this time the magnitude of a_y, β and r are larger since the thrust is larger than the Mach 0.8 case. The response damps out quickly (less than 4 sec.) which would be expected from the high dutch roll frequency and damping ratio. The plots of p and ϕ are shown in figure 22. In this case the bank angle reached a steady value.

Figure 23 shows the Mach 2 tail-on a_y, β and r pulse rudder plots. The magnitudes of these variables are not as high as in the tail-off case and the system damps out faster (3 sec.). This would be expected as the product of the dutch roll frequency and damping ratio is higher. The rudder position and rate plots are shown on figure 24 and reflect the high dutch roll frequency. The higher a_y in the tail-off case reflects the high thrust at this flight condition. The plots of ϕ and p are shown in figure 25. For this flight case the bank angle reached a lower steady state value than the tail-off

(Ref 5:448) were used to calculate the appropriate value for v_y. In order to get a β gust term (β_g) the following relation is used:

$$\beta_g = - \frac{v_g}{V_t}$$

The discrete β_g is then input through the β term in the equations of motion.

Random Turbulence

To complement the evaluation of the aircraft and control system to atmospheric turbulence, the effect of continuous random turbulence needs to be considered. The reason is that if a measure of the velocity of gusts on a given flight path were made, the magnitude of the gusts would be of a random nature. Therefore, continuous random turbulence is described statistically. Again only side gusts will be considered since the study is limited to the lateral-directional modes.

In straight, steady level flight through a turbulent atmosphere it is important to minimize the unwanted motion (error) caused by the turbulence. In order to statistically measure how well the SAS is performing, mean square error is utilized since the average value of the gusts is assumed to be zero. The power spectral density, Φ, is utilized to obtain the mean square error for an aircraft and control system. The random turbulence model is represented in figure 10. The input used to evaluate the performance of the system is white noise which has a constant power spectral density (= 1). There are several textbooks which give a treatise on random atmospheric turbulence. Blakelock is one (Ref 6: Chapter 9).

The Dryden form of the power spectral density for the side gust is utilized and is defined as:

$$\Phi_{v_g}(\omega) = \sigma_v \frac{Lv}{V_t} \frac{1 + 3\left(\frac{Lv}{V_t}\omega\right)^2}{1 + \left[\left(\frac{Lv}{V_t}\omega\right)^2\right]^2}$$

where Lv and σ_v are parameters specified in reference 5 (p 447-448). The transfer functions for the shaping filter ($T_{v_g}(j\omega)$) can be obtained by performing spectral factorization of $\Phi_{v_g}(\omega)$. That is:

$$\Phi_{v_g}(\omega) = T_{v_g}(j\omega)\, T_{v_g}(-j\omega)$$

Then:

$$T_{v_g}(j\omega) = \sigma_v \sqrt{\frac{Lv}{V_t}} \frac{1 + \sqrt{3}\ \frac{Lv}{V_t}\ j\omega}{(1 + \frac{Lv}{V_t}\ j\omega)^2}$$

Then by replacing $j\omega$ with s and dividing by V_t yields.

$$T_{\beta_g}(s) = \sigma_v \sqrt{\frac{Lv}{V_t}} \frac{1 + \sqrt{3}\ \frac{Lv}{V_t}\ s}{(1 + \frac{Lv}{V_t}\ s)^2}$$

which is utilized in the continuous random turbulence model. The values (thunderstorm levels) for Lv and σ_v used are:

Lv = 1750 ft.

σ_v = 21 ft/sec

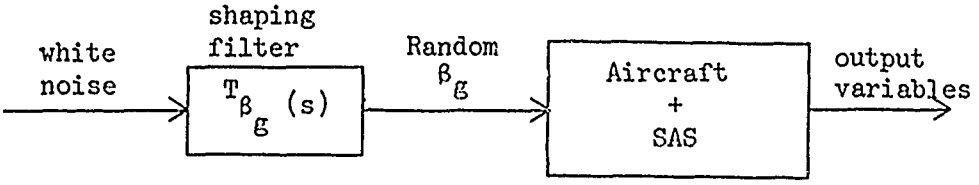

Figure 10 - Continuous Random Model Block Diagram

Computer Models/Programs

In order to obtain time response plots for the pulse rudder pedal input and the discrete atmospheric turbulence input, an integration and plot computer program was created. The integration was done using a library Runge-Kutta integration subroutine (ODE) on the CC6600 library of the ASD computer system. The aircraft and control system modeled in state variable form were provided as input to this program. The form of the program input is:

$$\dot{\overline{X}} = A\,\overline{X} + G\,\beta_g + B\,\delta_{r_p}$$

where $\overline{X}$ is the aircraft state vector, δ_{r_p} is pilot rudder pedal inputs, and β_g is gust inputs.

Figure 11 shows the block diagram of the state space model used for the tail-off configurations. The only differences in the model for the tail-on aircraft are the a_y feedback and the different actuator dynamics. The state equations in matrix form are shown in figure 12. The gust term (β_g) enters each of the state equations through the β term. For the pilots rudder pedal input the G matrix is a null matrix. For the discrete gust input the B matrix is a null

matrix. The output of the computer program is time response plots (0-10 second) for β + β_g, p, r, ϕ, δ_v, $\dot{\delta}_v$, a_y, and β_g (or δ_{r_p}) and a listing at 0.05 second increments for these variables.

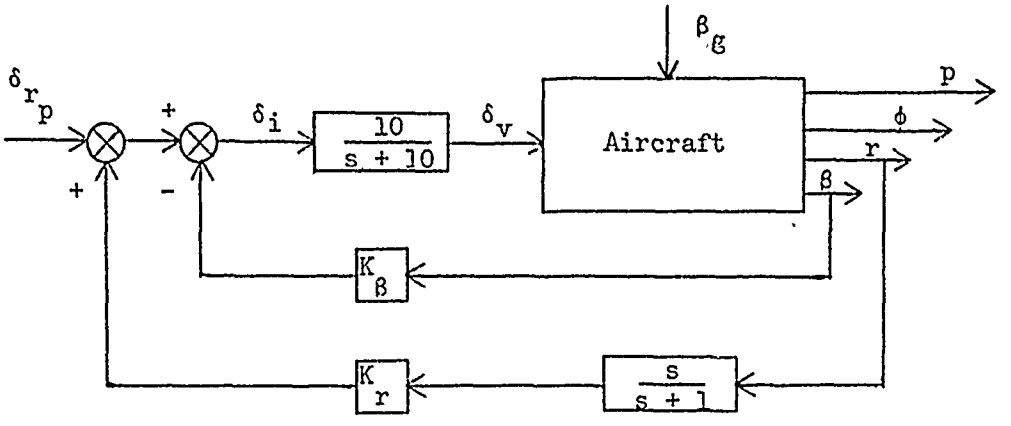

Figure 11 Tail-off State Space Model

An existing computer program developed by Capt J. T. Silverthorn (AFIT Department of Aeronautics and Astronautics), which performs a covariance analysis (Ref 7:89) was utilized to evaluate the response of the aircraft to random atmospheric turbulence. The inputs to the program are the aircraft and control system state equations augmented with the state equations for the shaping filter to model the atmospheric power spectral density function. The power spectral density function adds two states to the basic aircraft and control system A matrix (figure 12). A listing of this program is shown in Appendix 5.

Response To A Rudder Pedal Input

In order to determine the effectiveness of thrust vectoring to generate a yawing moment, a comparison with the tail-on rudder

$$\begin{bmatrix} \dot{\beta} \\ \dot{p} \\ \dot{r} \\ \dot{\phi} \\ \dot{\delta}_v \\ \dot{r}_f \end{bmatrix} = \begin{bmatrix} \frac{Y_\beta}{V_t} & \frac{w_o + Y_p}{V_t} & \frac{u_o - Y_r}{V_t} & \frac{g \cos \Theta_o}{V_t} & \frac{Y_{\delta v}}{V_t} & 0 \\ L'_\beta & L'_p & L'_r & 0 & L'_{\delta v} & 0 \\ N'_\beta & N'_p & N'_r & 0 & N'_{\delta v} & 0 \\ 0 & 1 & \tan \Theta_o & 0 & 0 & 0 \\ 10\ K_\beta & 0 & 0 & 0 & -10 & 10 \\ K_r N'_\beta & K_r N'_p & K_r N'_r & 0 & K_r N'_{\delta v} & -1 \end{bmatrix} \begin{bmatrix} \beta \\ p \\ r \\ \phi \\ \delta_v \\ r_f \end{bmatrix} + \begin{bmatrix} \frac{Y_\beta}{V_t} \\ L'_\beta \\ N'_\beta \\ 0 \\ 10\ K_\beta \\ K_r N'_\beta \end{bmatrix} \beta_g + \begin{bmatrix} 0 \\ 0 \\ 0 \\ 0 \\ 1 \\ 0 \end{bmatrix} \delta_{r_p} .$$

Figure 12. Integration Program Input Matrix

effectiveness was made. This was expressed in terms of yawing moment/degree of thrust vector deflection ($Izz\ N_{\delta_v}$) compared with the yawing moment/degree of rudder deflection ($Izz\ N_{\delta_r}$). This is plotted in figure 13 for different Mach numbers at 30000 ft. altitude. What is indicated is that for the subsonic Mach numbers the rudder generates a higher control yawing moment than does thrust vectoring. Note the low thrust condition at Mach 0.8. But when the thrust is increased sufficiently in the supersonic regime, the thrust vector generates a higher control yawing moment.

A command rudder (δ_{r_p}) pulse of 3 degrees for 1 second duration was applied to the system to observe the response. In figure 14 is a 0-10 sec. plot of the input and plots of the position of the thrust vector (δ_v) and rate which the thrust vector is moving ($\dot{\delta}_v$) for the Mach 0.8 tail-off case. It can be seen from the δ_v plot that the yaw SAS is resisting the input as it should do initially. Figure 15 shows plots of a_y, β and r where the dutch roll mode can be seen. Notice that a_y has the same shape as δ_v which indicates that the lateral acceleration is primarily the result of thrust vectoring. The amplitudes of a_y and β are small and the time to damp out is less than 5 seconds. Figure 16 shows plots of p and ϕ.

The same rudder pulse was applied to the tail-on aircraft to compare its response to that of the tail-off aircraft. Figure 17 shows plots of the rudder position and rate. Figure 18 shows plots of a_y, β and r which indicate larger amplitudes than for the tail-off. This reflects what was shown in figure 13 that the rudder control effectiveness is greater than the thrust vector control effectiveness

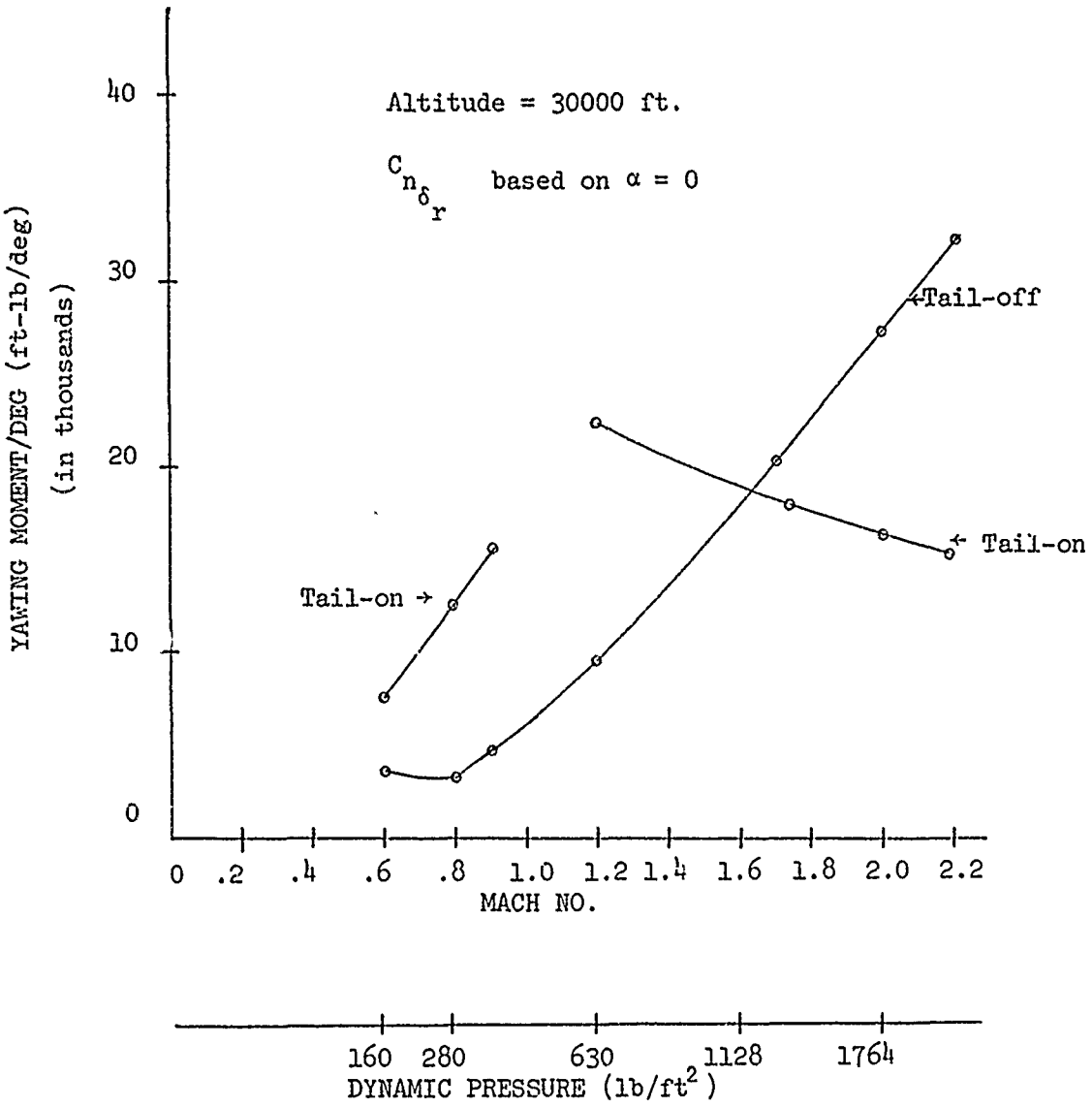

Figure 13. Yawing Moment/Degree of Thrust Vector (tail-off) or Rudder (Tail-on) Deflection

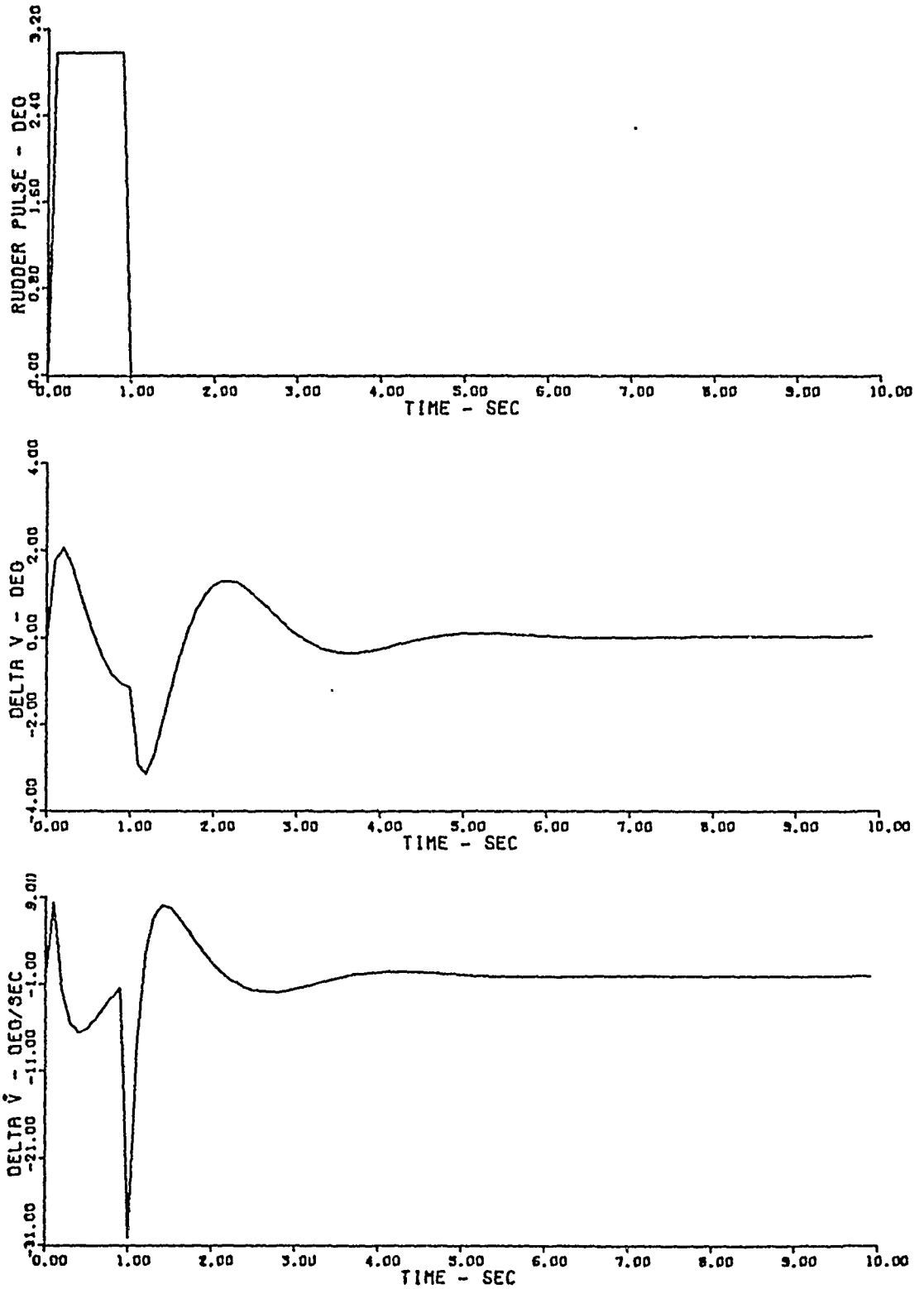

Figure 14. Flt. Cond. 1, Tail-off, Rudder Pedal Input

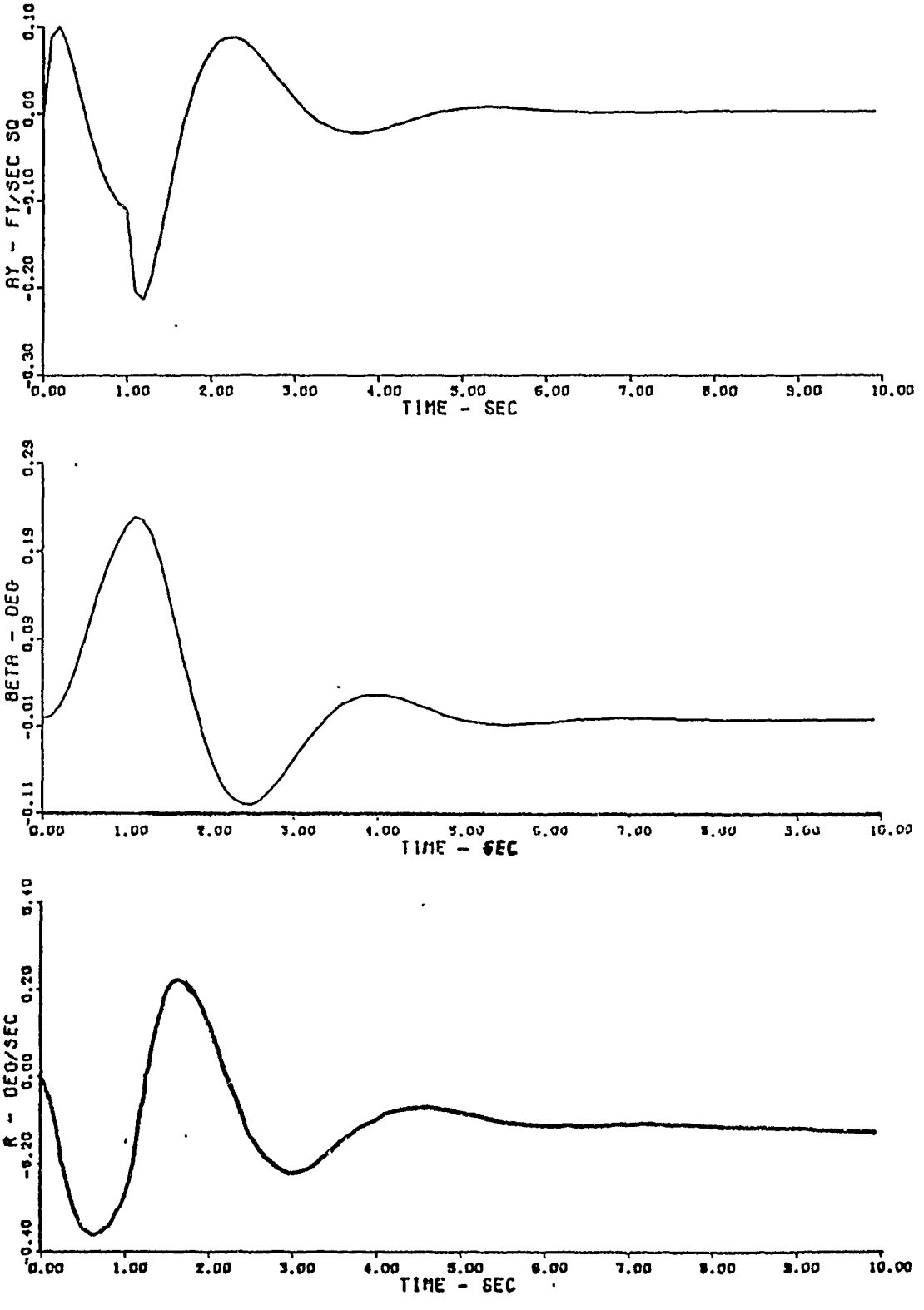

Figure 15. Flt. Cond. 1, Tail-off, Rudder Pedal Input

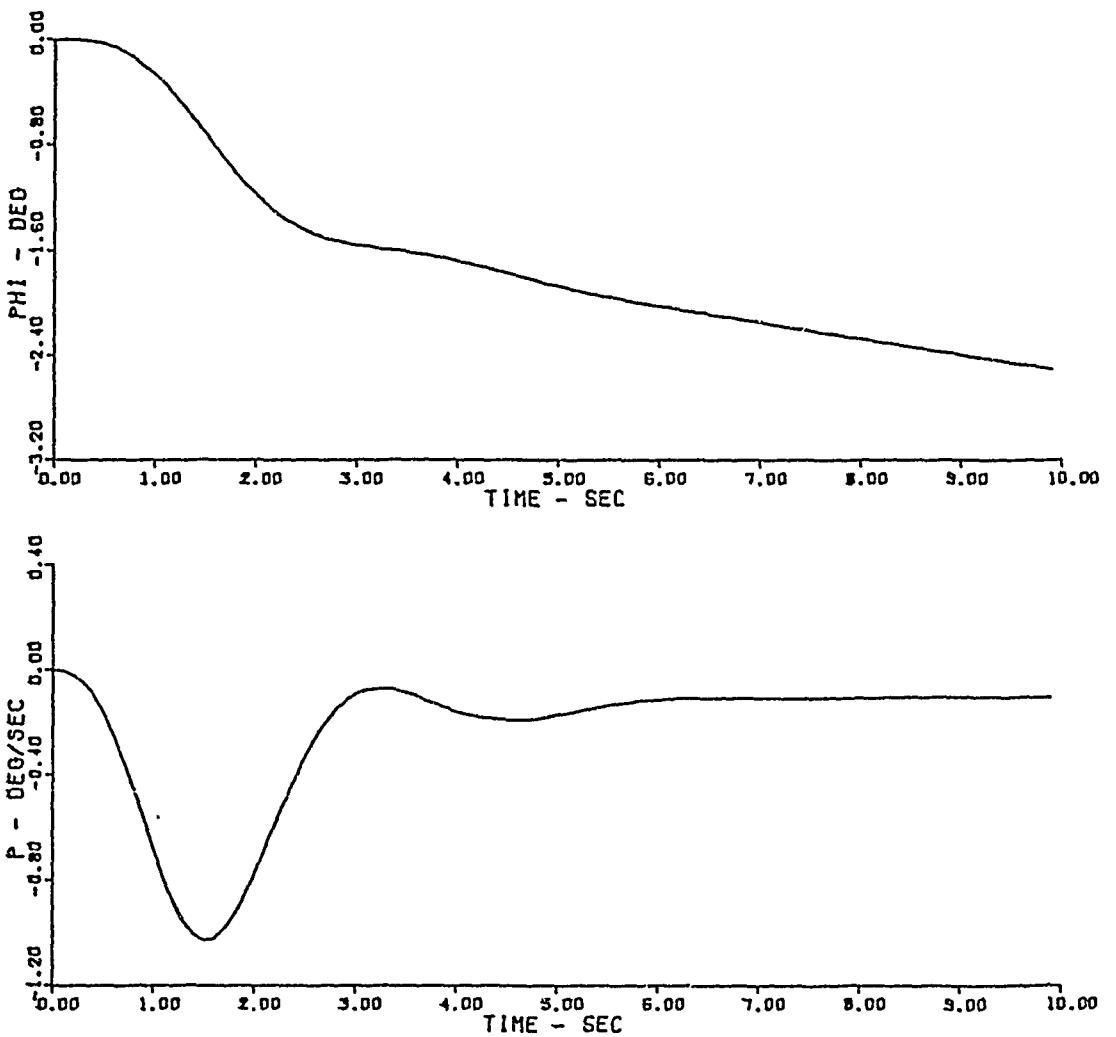

Figure 16. Flt. Cond. 1, Tail-off, Rudder Pedal Input

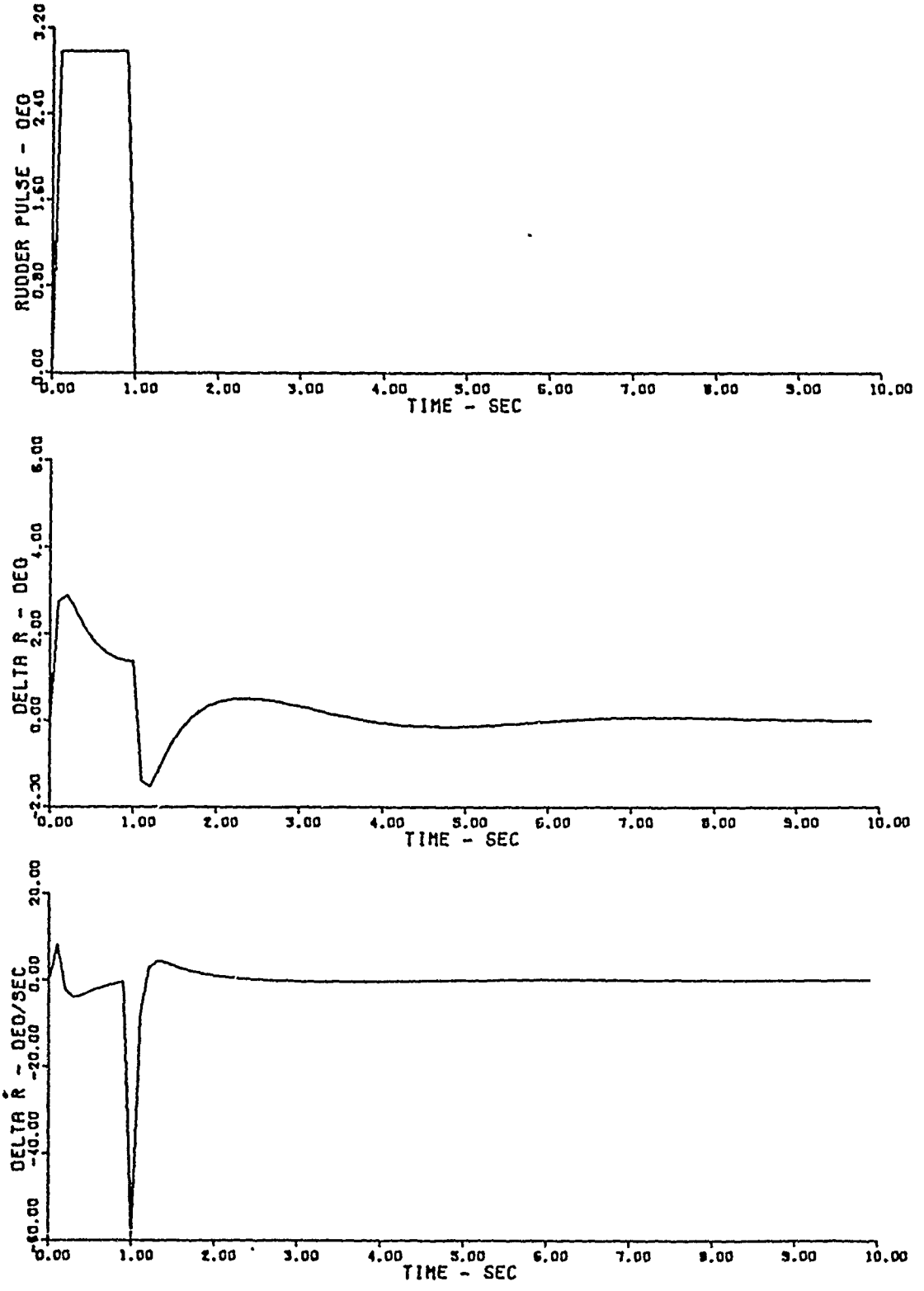

Figure 17. Flt. Cond. 1, Tail-on, Rudder Pedal Input

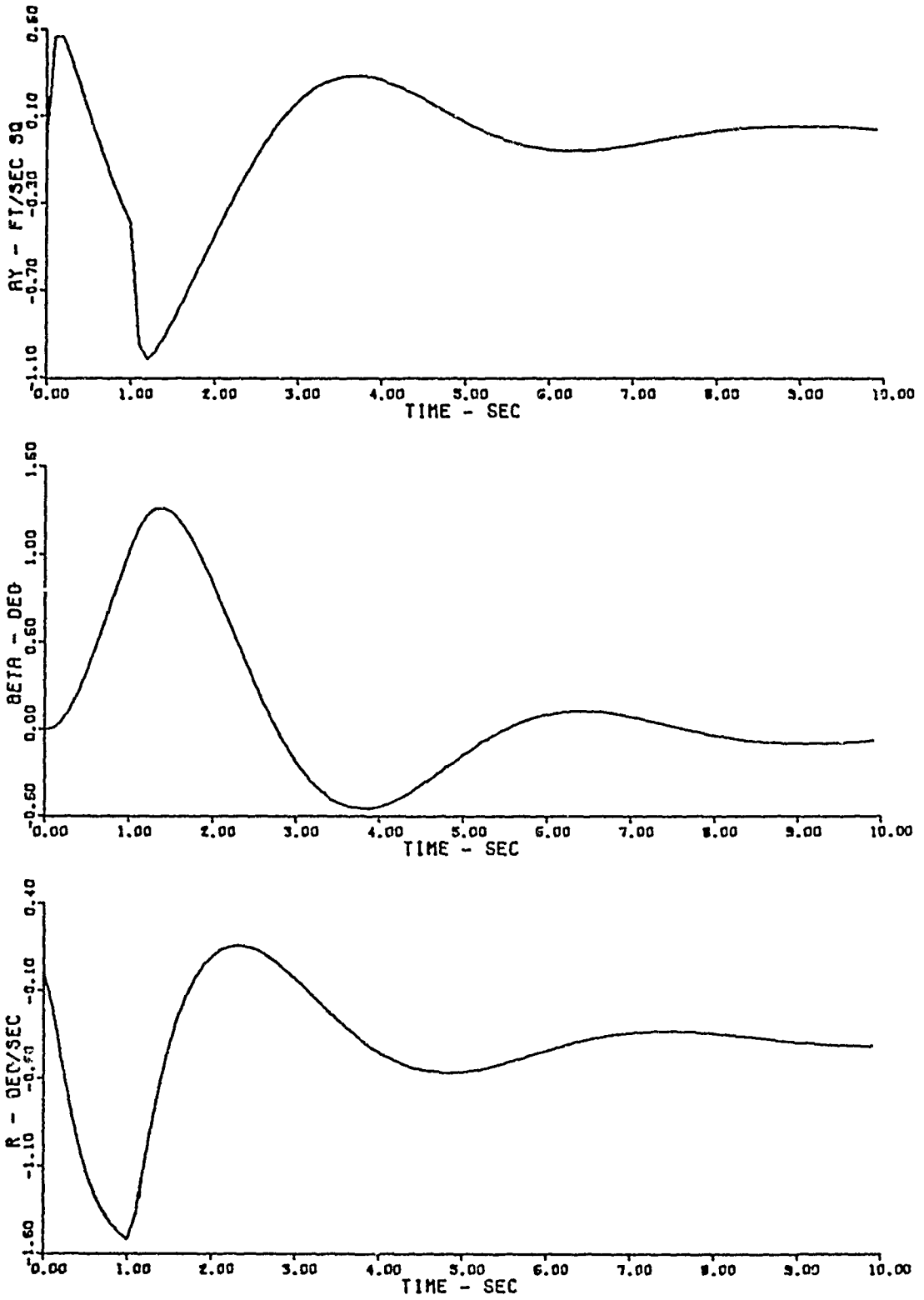

Figure 18. Flt. Cond. 1, Tail-on Rudder Pedal Input

at a subsonic cruise condition. However, it takes the tail-on aircraft longer to damp the disturbance. This would be expected as the dutch roll frequency and damping are less than that of the tail-off aircraft at this flight condition. Figure 19 shows plots of p and ϕ for the tail-on aircraft. The bank angle seeks a steady state value of about 9 degrees whereas the tail-off aircraft continued to roll, but, at a slow rate. After 10 seconds the tail-off aircraft only rolled 3 3 degrees. This reflects the long roll mode time constant.

The Mach 2 tail-off rudder pulse responses are shown in figures 20-25. Figure 20 shows the pulse rudder input, δ_v, and $\dot{\delta}_v$ plots. The variables a_y, β and r plots are shown in figure 21. Again, the yaw SAS is functioning properly although this time the magnitude of a_y, β and r are larger since the thrust is larger than the Mach 0.8 case. The response damps out quickly (less than 4 sec.) which would be expected from the high dutch roll frequency and damping ratio. The plots of p and ϕ are shown in figure 22. In this case the bank angle reached a steady value.

Figure 23 shows the Mach 2 tail-on a_y, β and r pulse rudder plots. The magnitudes of these variables are not as high as in the tail-off case and the system damps out faster (3 sec.). This would be expected as the product of the dutch roll frequency and damping ratio is higher. The rudder position and rate plots are shown on figure 24 and reflect the high dutch roll frequency. The higher a_y in the tail-off case reflects the high thrust at this flight condition. The plots of ϕ and p are shown in figure 25. For this flight case the bank angle reached a lower steady state value than the tail-off

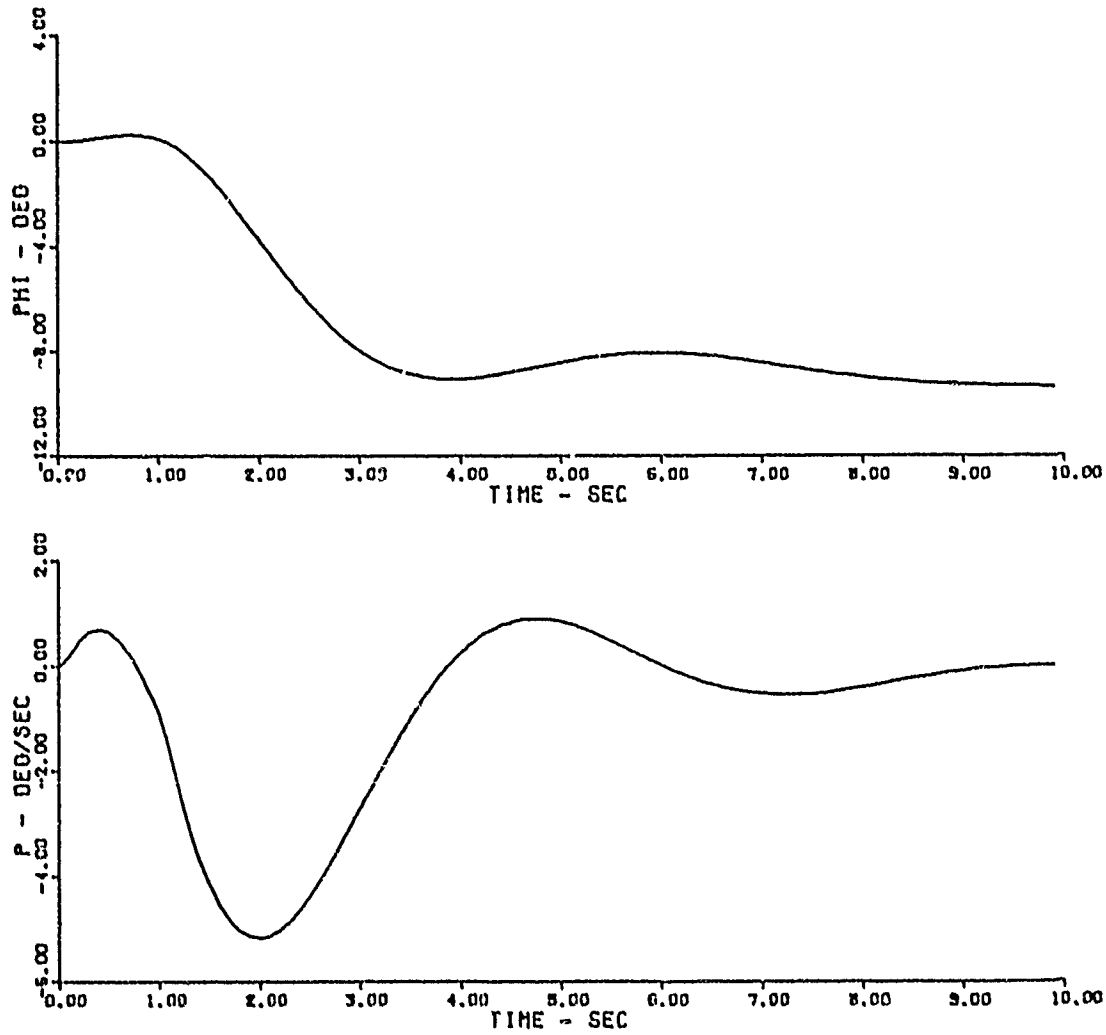

Figure 19. Flt. Cond. 1, Tail-on Rudder Pedal Input

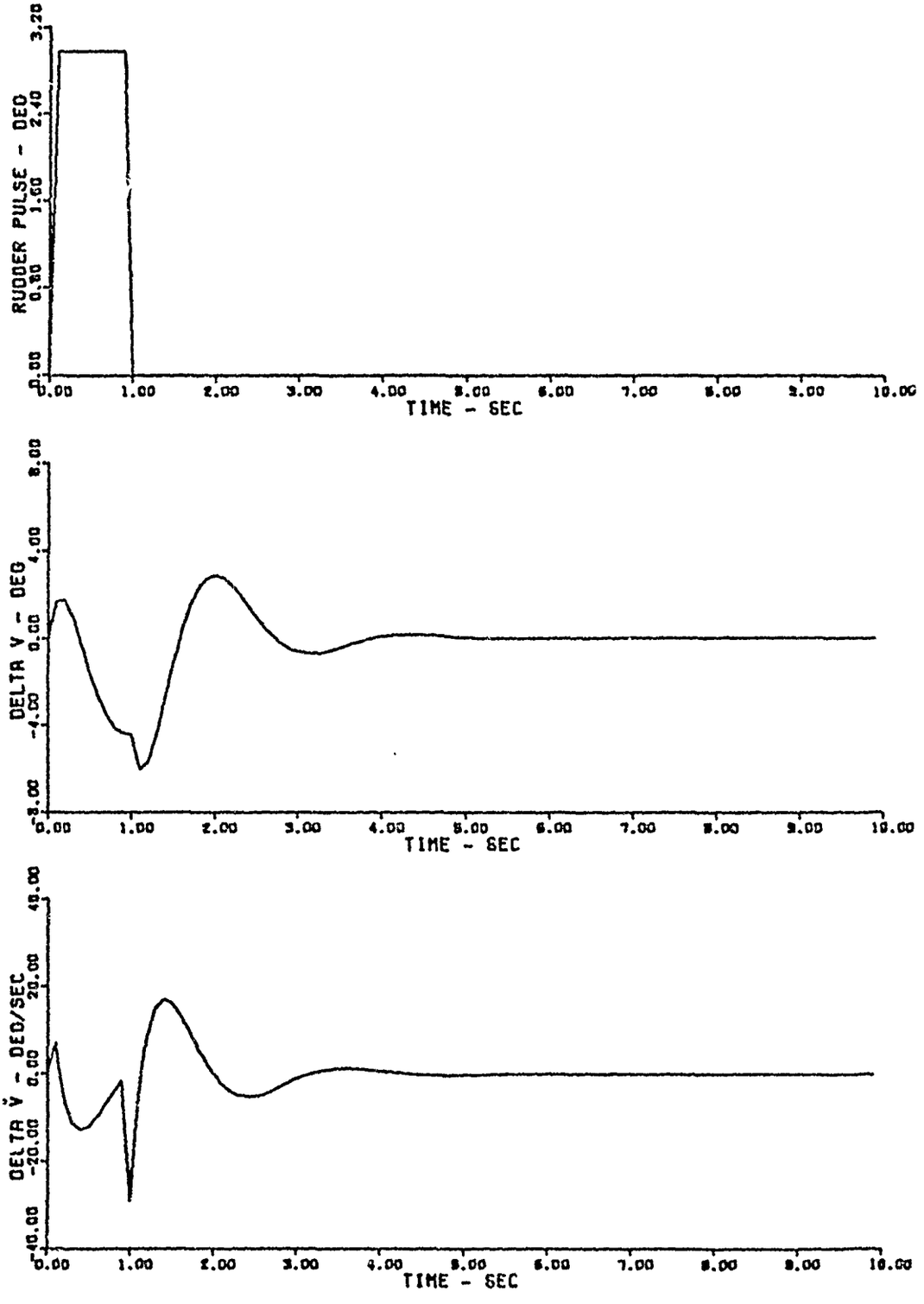

Figure 20. Flt. Cond. 2, Tail-off, Rudder Pedal Input

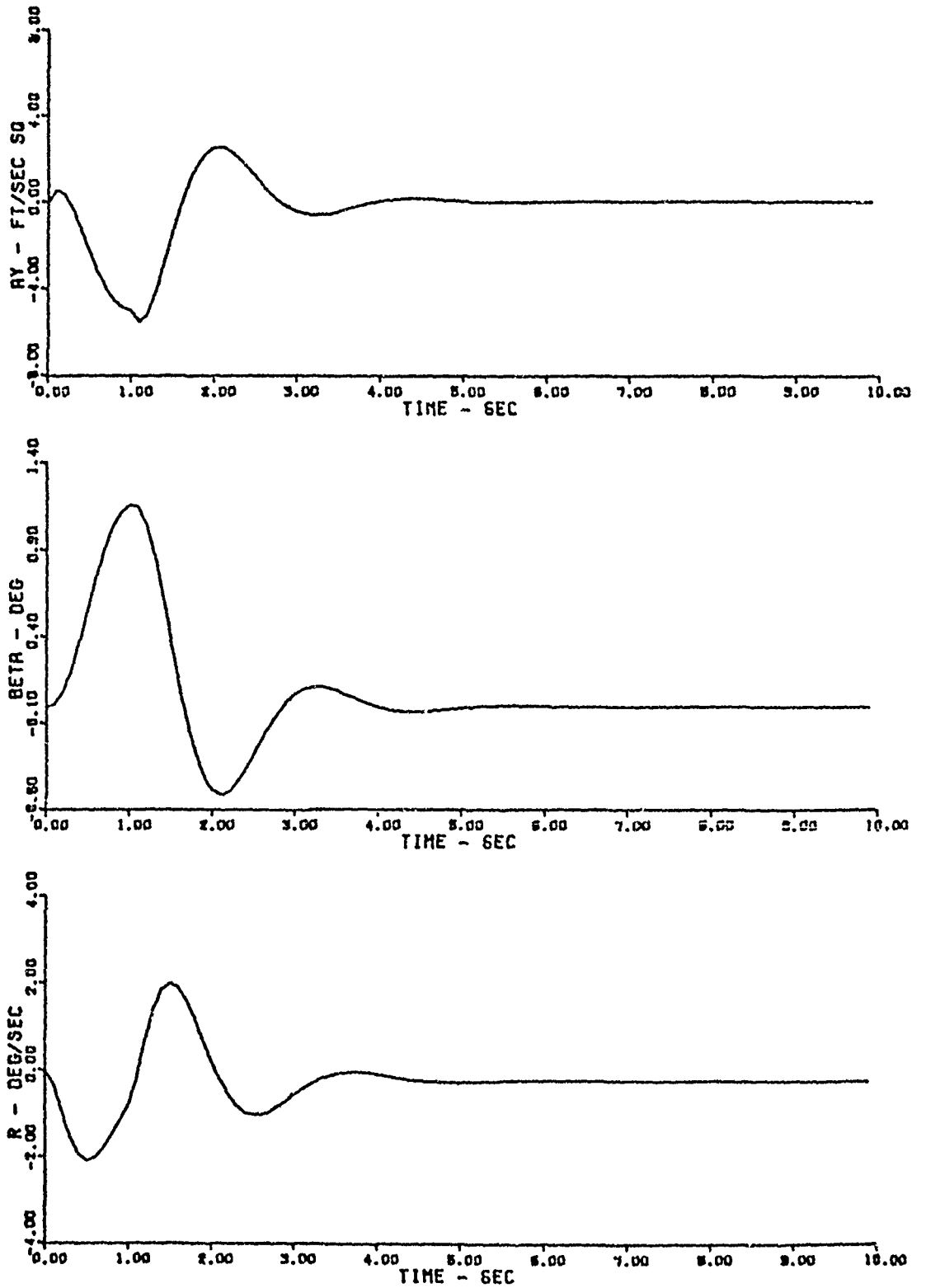

Figure 21. Flt. Cond. 2, Tail-off Rudder Pedal Input

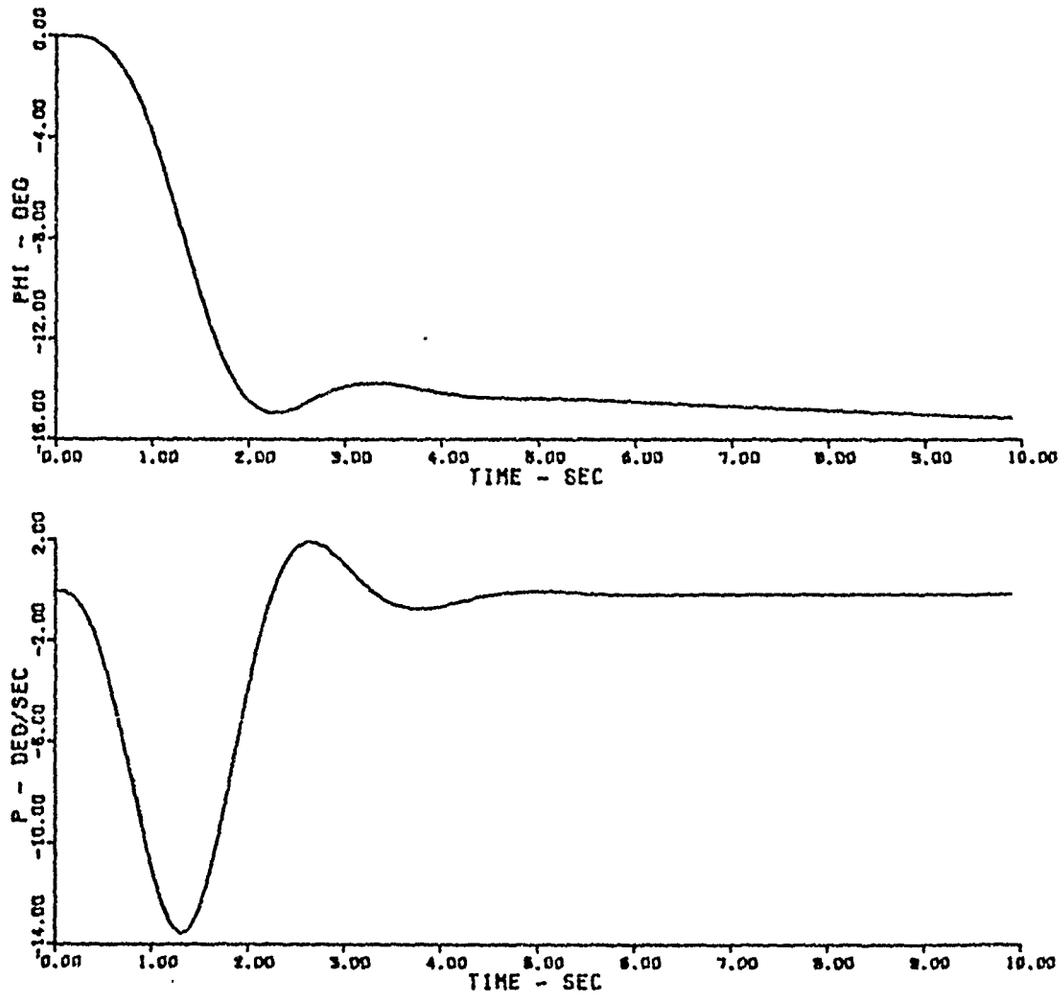

Figure 22. Flt. Cond. 2, Tail-off, Rudder Pedal Input

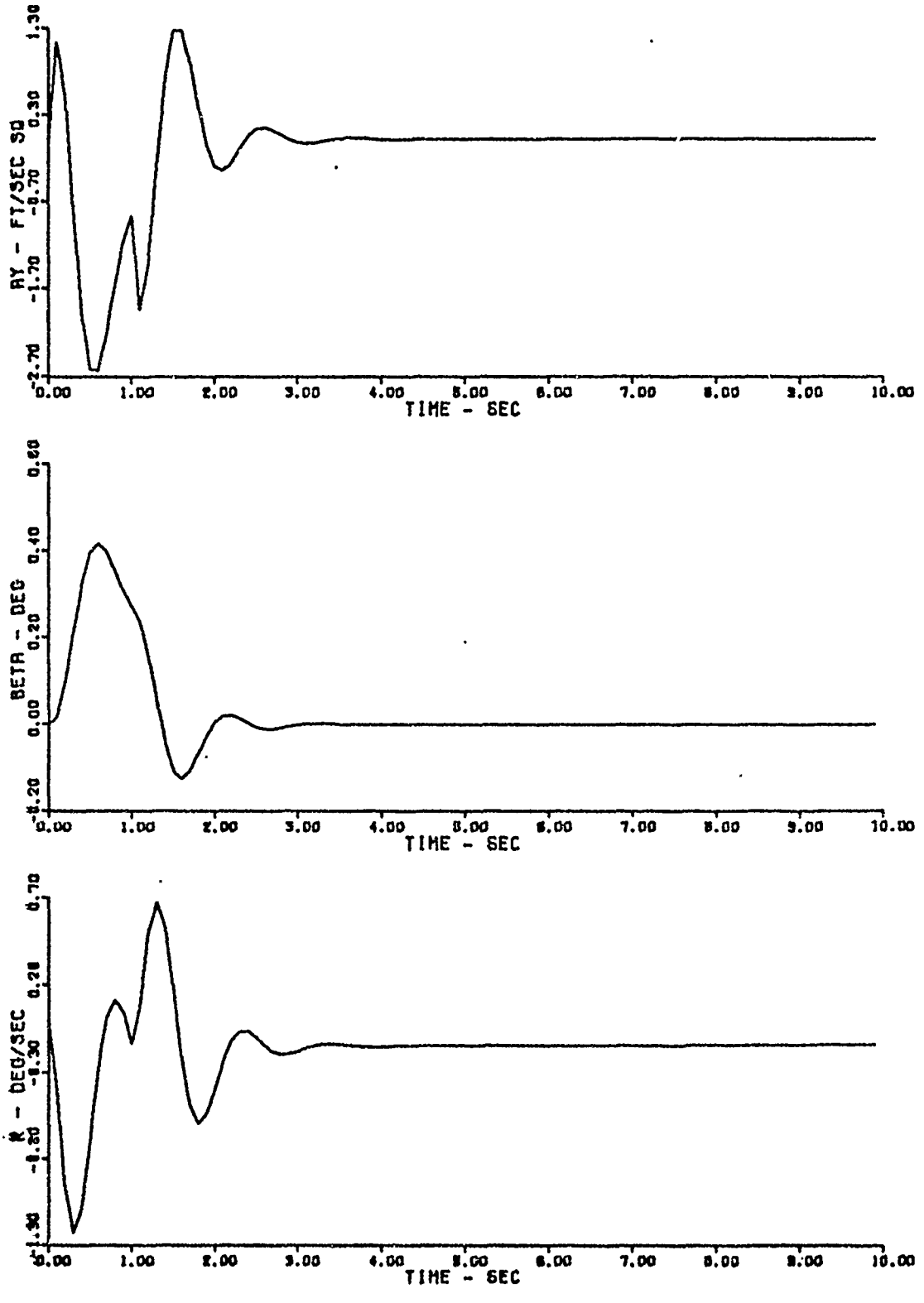

Figure 23. Flt. Cond. 2, Tail-on, Rudder Pedal Input

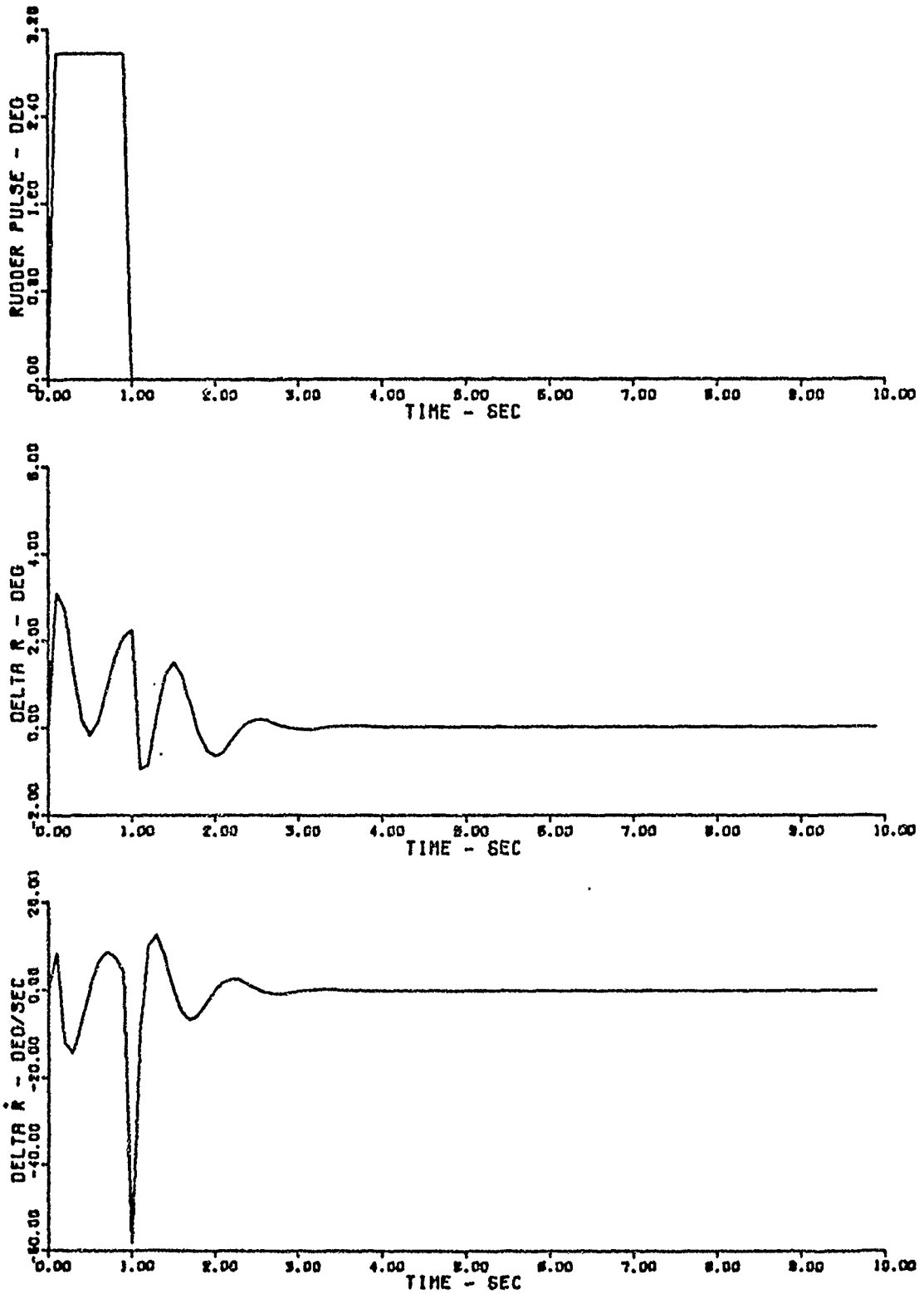

Figure 24. Flt. Cond. 2, Tail-on, Rudder Pedal Input

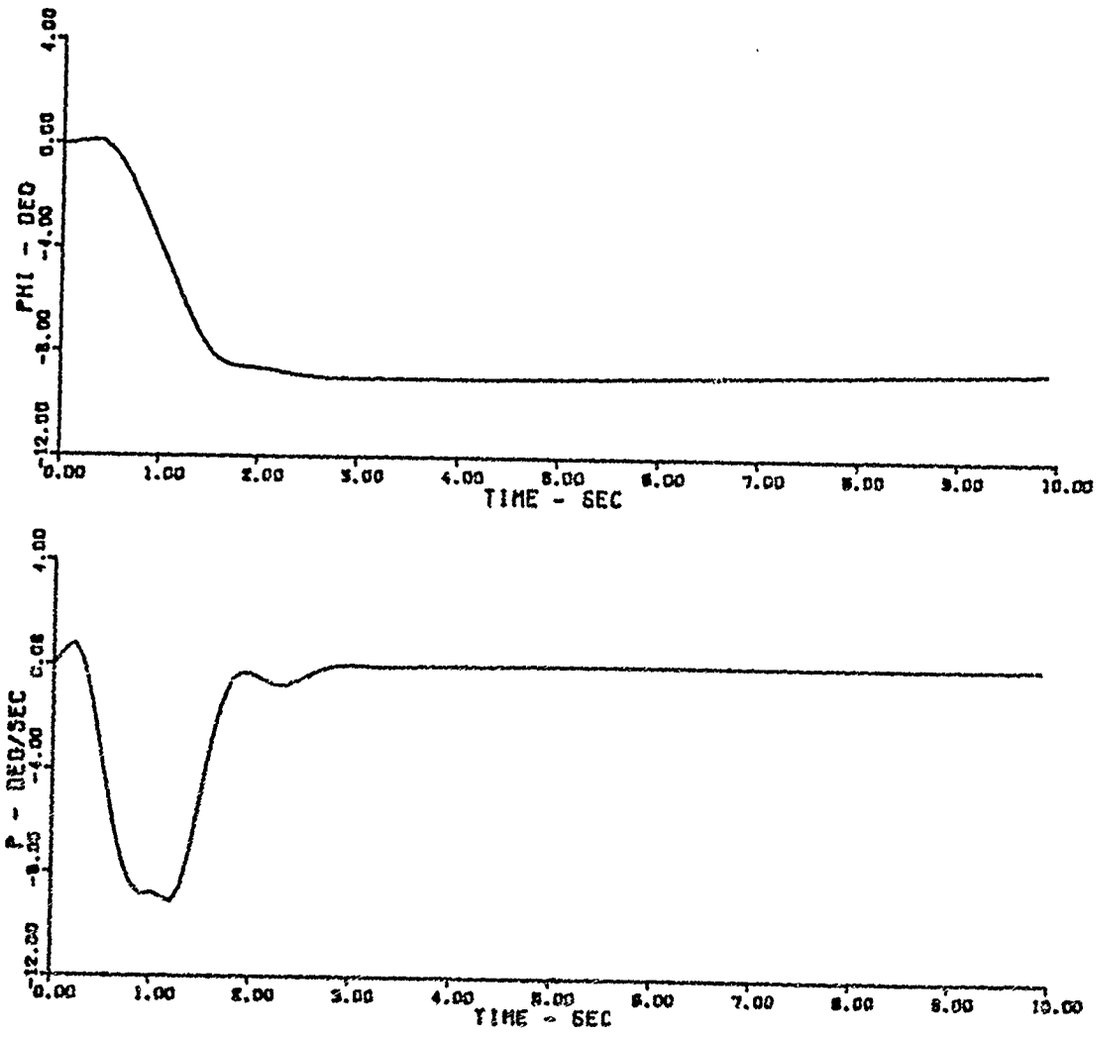

Figure 25. Flt. Cond. 2, Tail-on, Rudder Pedal Input

aircraft due to the shorter time to damp the dutch roll mode.

Response To Discrete Atmospheric Turbulence

In order to properly evaluate the response of the aircraft and SAS to discrete (1 - COS) atmospheric turbulence, the gust frequency which excites the aircraft the most (resonance) must be found. A log magnitude frequency response (Bode plot) of the system to a sinusoidal input could be useful in finding the resonant frequency. Noting the half angle formula:

$$\sin\left[\frac{\omega}{2}\right] = \pm \left[\frac{1 - \cos \omega}{2}\right]^{1/2}$$

Where: ω = frequency

a relationship of a sinusoidal input to a 1 - COS input can be seen. Basically, th resonant frequency of a sinusoidal input is $\frac{1}{2}$ that of the 1 - COS input. Frequency response plots of β/β_g and a_y/β_g are shown in figures 26 and 27 for the Mach 0.8 tail-off [illegible]t case. The resonant frequency is shown to be about 2 rad/sec. It might be expected that the resonant frequency for a 1 - COS discrete input would be about 4 rad/sec.

A frequency sensitivity study was done using the integration program described earlier in this chapter. The results indicated that a gust frequency of 3 rad/sec produced the largest values of β and a_y (Table 4). A gust frequency of 4 rad/sec excited the TVC, with the highest δ_v excursion. For the tail-on aircraft a gust frequency of 2 rad/sec produced the largest values of β and a_y. From Table 4 it is seen that as the gust frequency increases the peak thrust vector excursion increases until a 4 rad/sec gust is

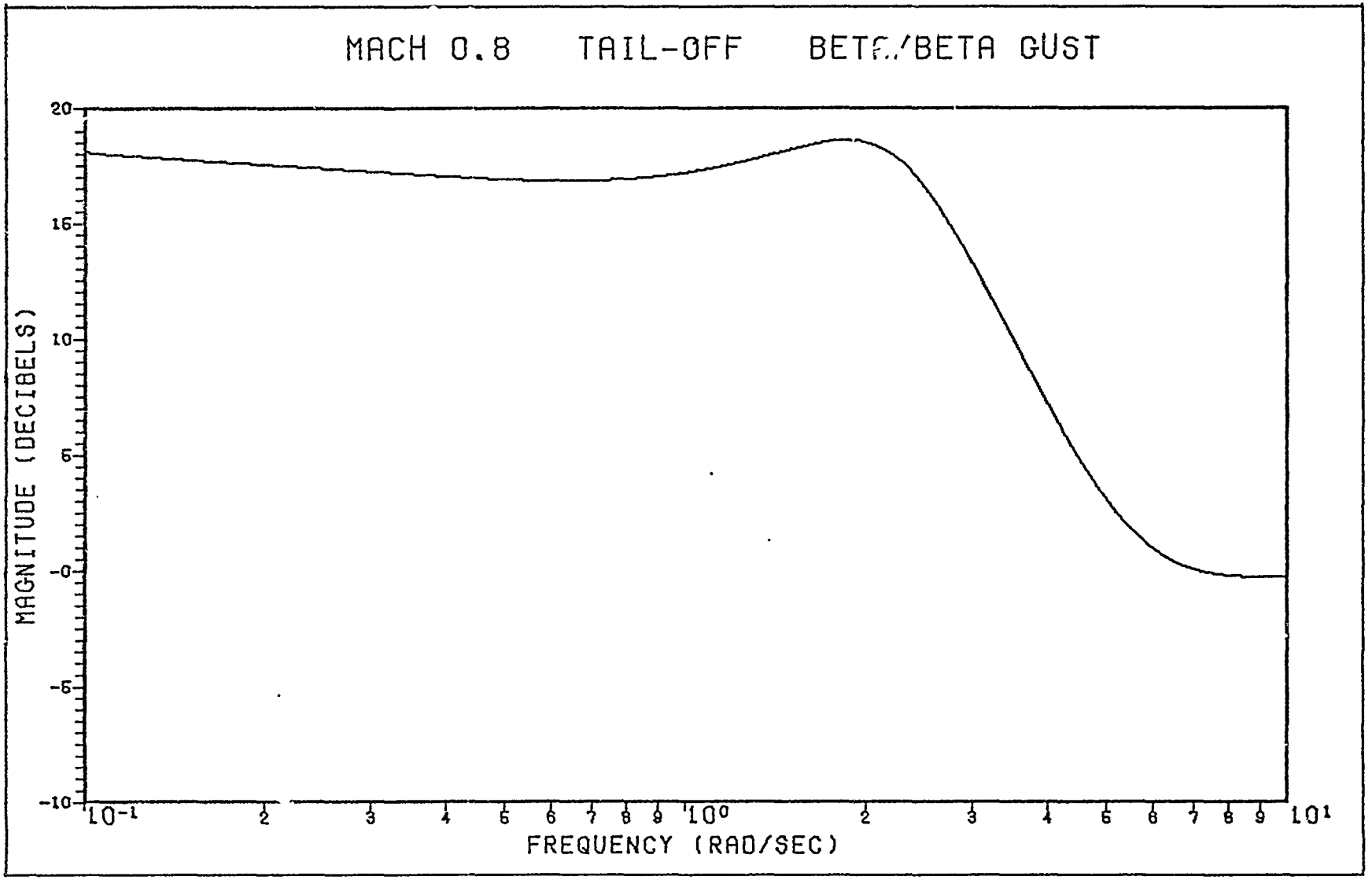

Figure 26. Flt. Cond. 1. Tail-off, Frequency Response

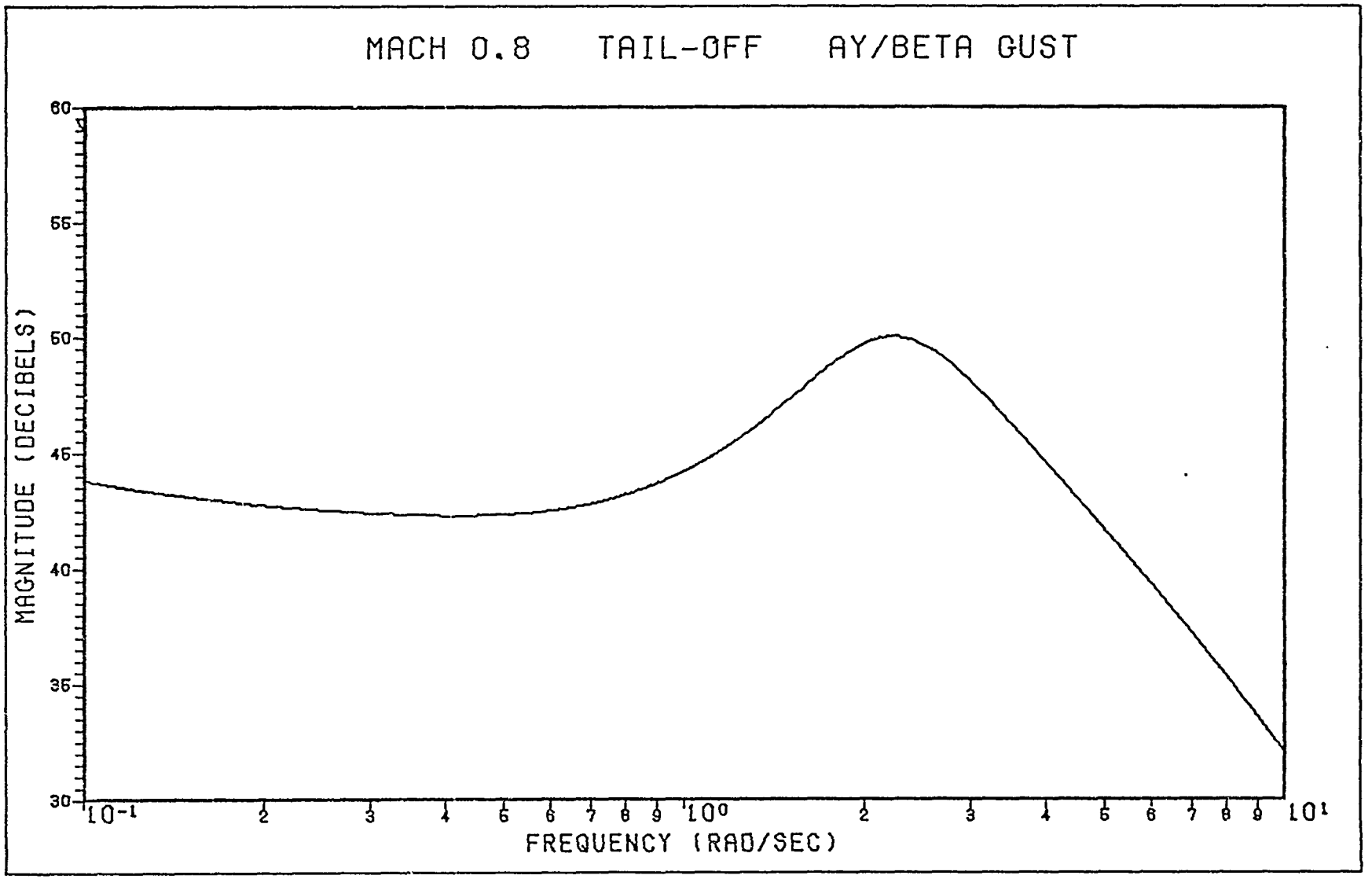

Figure 27. Flt. Cond. 1, Tail-off, Frequency Response

Table 4

Mach 0.8 Discrete Gust Frequency Sensitivity Study

Peak Magnitudes								
	Tail-off				Tail-on			
Discrete β_g Frequency (rad/sec)	β (deg)	a_y (ft/sec^2)	δ_v (deg)	$\dot{\delta}_v$ (deg/sec)	β (deg)	a_y (ft/sec^2)	δ_r (deg)	$\dot{\delta}_r$ (deg/sec)
1.6	2.17	2.16	18.0	29.0	3.48	3.00	0.97	2.60
2.0	2.88	2.52	25.8	46.6	3.66	2.75	1.22	3.41
2.24	3.05	2.57	28.4	55	3.43	2.48	1.35	3.55
2.56	3.29	2.71	32.3	68.2	3.25	2.26	1.39	4.00
3.0	3.46	2.83	36.1	86.5	2.93	2.00	1.50	4.23
4.0	3.17	2.73	37.9	119	2.12	1.48	1.54	4.56
4.5	2.93	2.62	37.3	129	1.85	1.30	1.52	5.04
5.0	2.66	2.45	35.8	139	1.61	1.14	1.48	5.47

reached but the rate continues to climb with gust frequency. The same is true for the tail-on rudder excursion and rate but the magnitudes are much smaller.

The frequency response plots for the Mach 2 case are shown in Figures 28 and 29. The resonant frequency to a sinusoidal input is 2.5 rad/sec. A frequency sensitivity study using the discrete gust input was also done for the Mach 2 flight condition. Table 5 shows the results. For this case higher frequencies excited the system since the dutch roll frequencies for both tail-on and tail-off were higher than in the Mach 0.8 case. For the Mach 2 tail-off case a gust frequency of 5 rad/sec produced the largest values of β and a_y. The largest value for δ_v was also produced at this frequency but $\dot{\delta}_v$ increased with the gust frequency. The tail-on aircraft has a higher dutch roll frequency (6.53 rad/sec) than the tail-off aircraft so the largest values of β and a_y occurred at a higher gust frequency of 6 rad/sec. For this flight case the values for the rudder excursion and rates were comparable to the thrust vector excursion and rates. This would be expected as the yawing moment due to thrust vectoring (figure 13) is much higher at the Mach 2 flight condition.

Time response plots were run for the Mach 0.8 flight condition at a gust frequency of 4 rad/sec. This frequency was chosen as it most excited the TVC. Time response plots for the tail-off aircraft are shown in figure 30-32 and the tail-on plots are shown in figures 33-35. From figure 30 the β_g input can be seen and also the δ_v and $\dot{\delta}_v$ time responses. Figure 31 shows the a_y, β and r time responses.

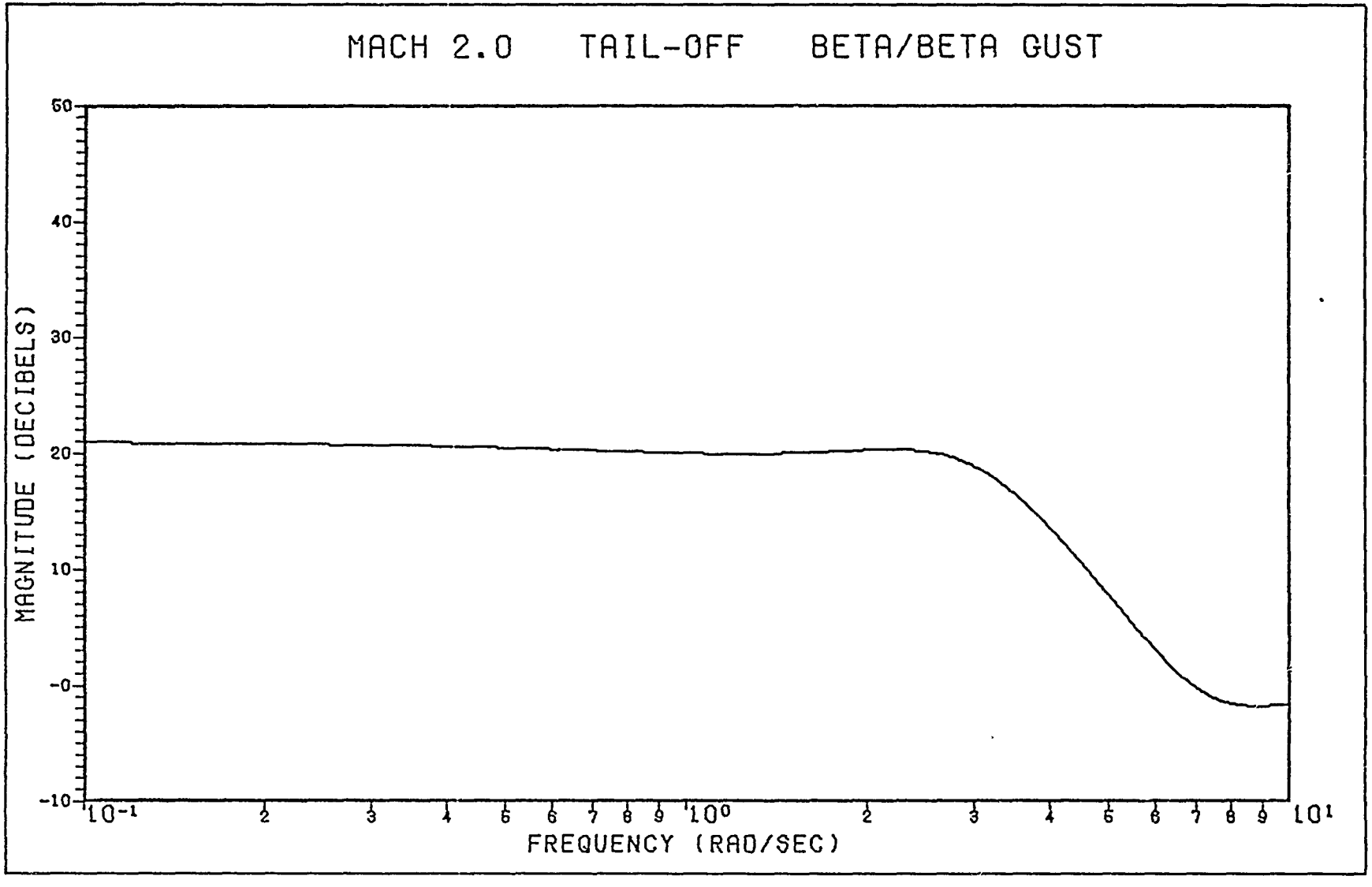

Figure 28. Flt. Cond. 2, Tail-off, Frequency Response

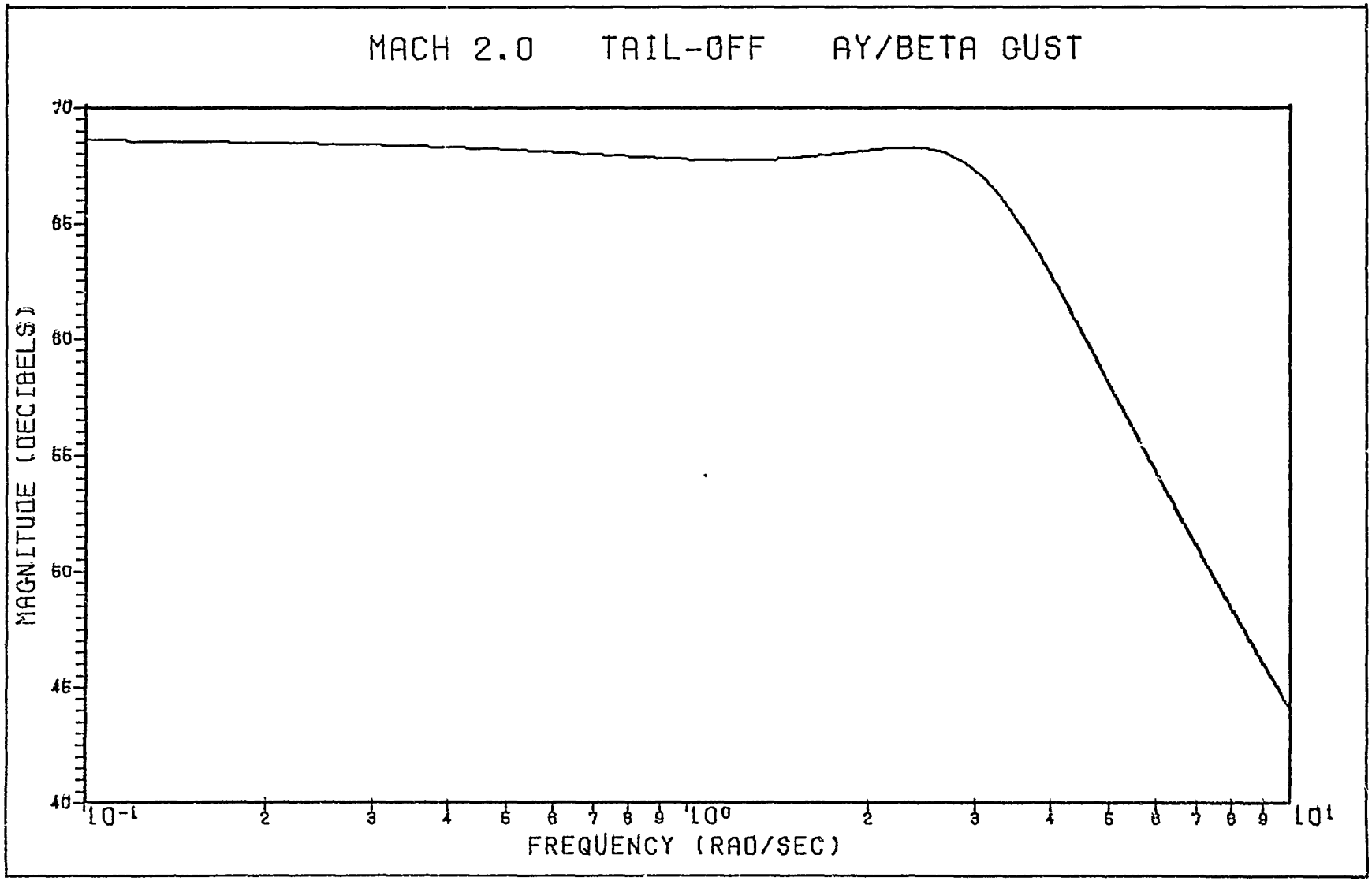

Figure 29. Flt. Cond. 2, Tail-off, Frequency Response

Table 5

Mach 2 Discrete Gust Frequency Sensitivity Study

Peak Magnitudes

Discrete β_g Frequency (rad/sec)	Tail-off				Tail-on			
	β (deg)	a_y (ft/sec^2)	δ_v (deg)	$\dot{\delta}_v$ (deg/sec)	β (deg)	a_y (ft/sec^2)	δ_r (deg)	$\dot{\delta}_r$ (deg/sec)
1.5	0.62	6.63	2.53	4.21	0.17	9.54	0.44	2.15
3	1.64	8.96	7.75	22.2	0.57	11.7	2.82	12.2
5	1.80	9.00	9.86	38.2	1.17	14.9	7.73	45.5
6	1.66	8.43	9.72	45.0	1.28	14.4	8.42	58.4
7	1.50	7.72	9.08	49.3	1.28	13.3	9.09	69.1
8	1.45	6.88	8.34	50.9	1.20	12.0	9.14	67.0

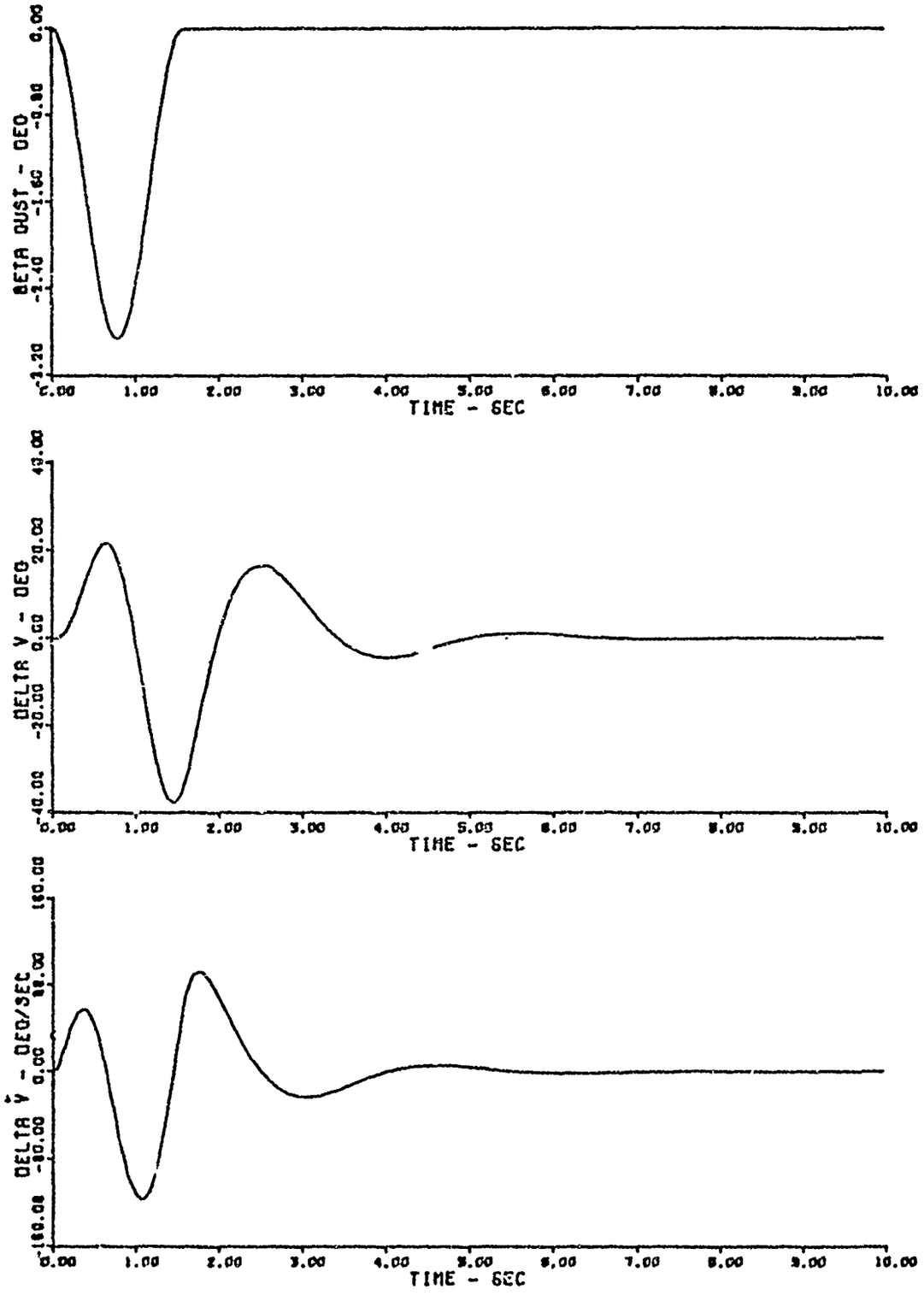

Figure 30. Flt. Cond. 1, Tail-off, Discrete Atmospheric Turbulence

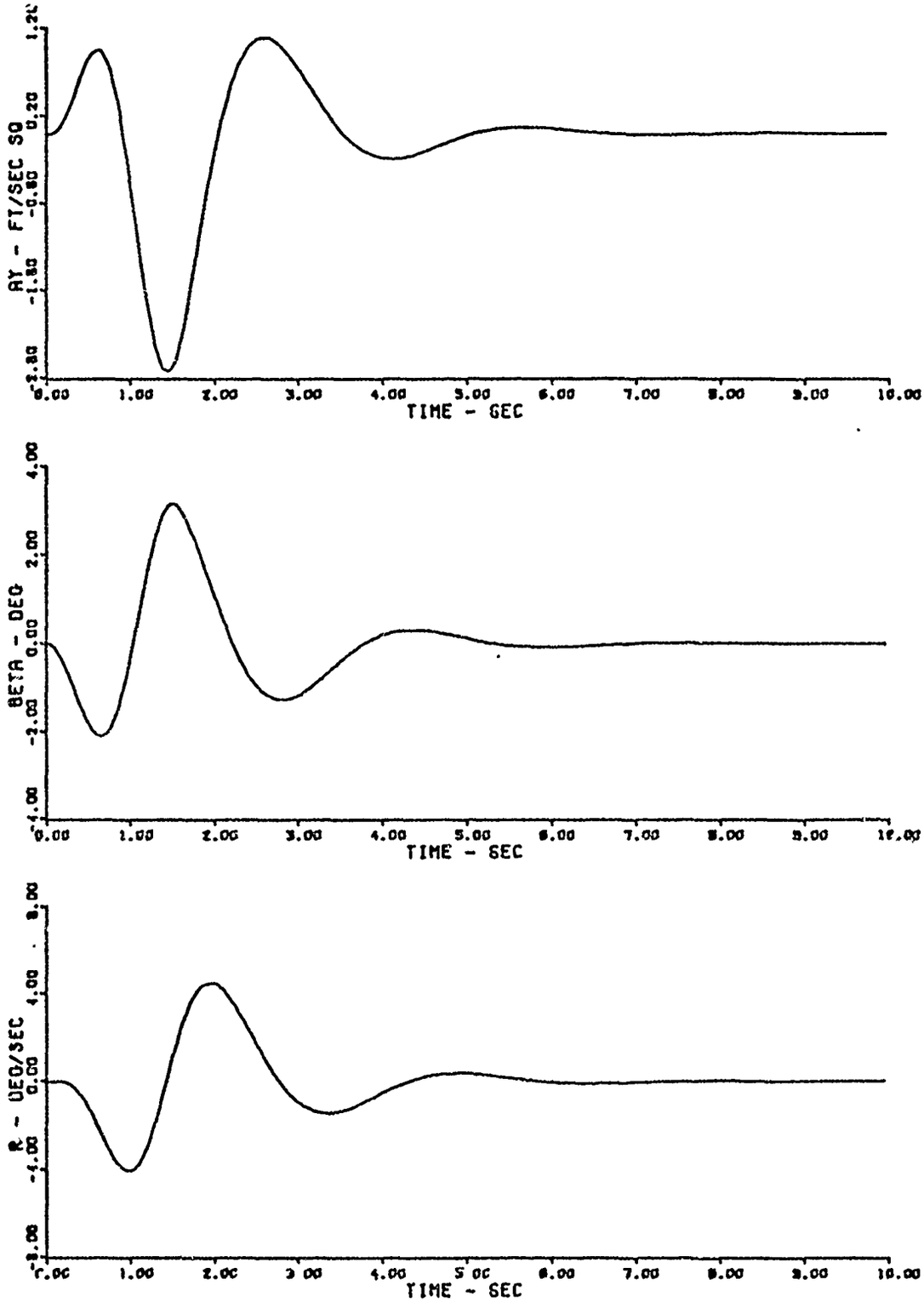

Figure 31. Flt. Cond. 1, Tail-off, Discrete Atmospheric Turbulence

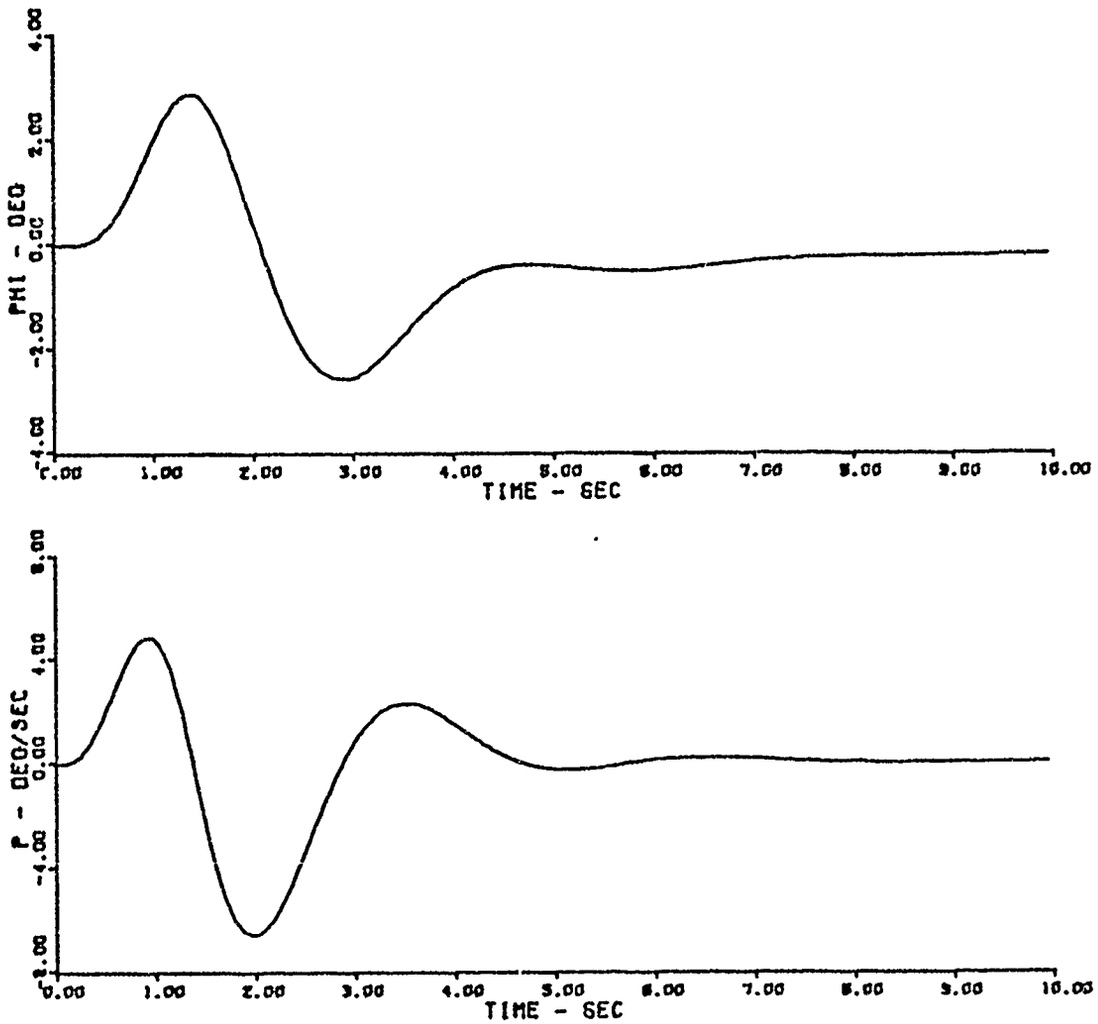

Figure 32. Flt. Cond. 1, Tail-off, Discrete Atmospheric Turbulence

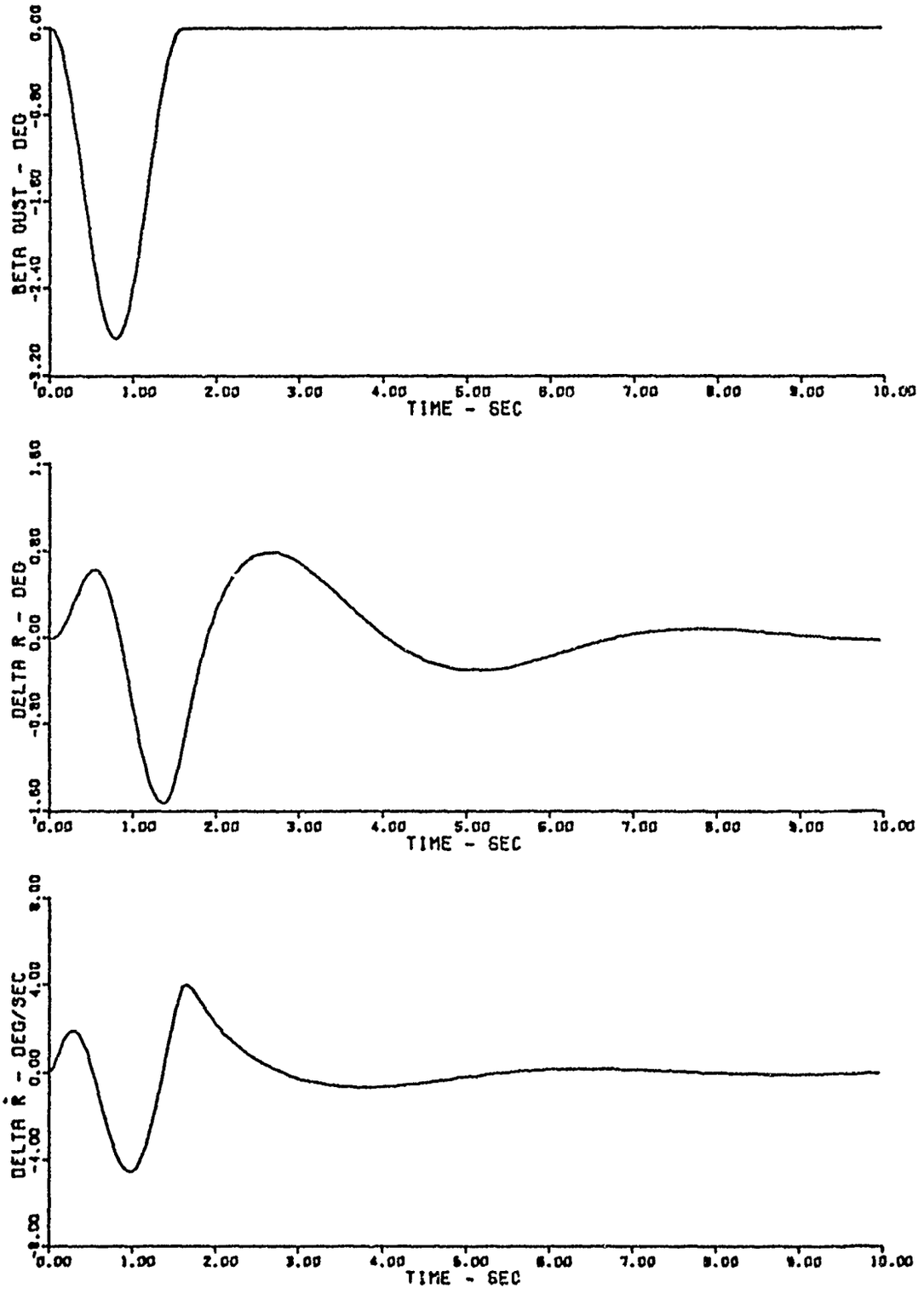

Figure 33. Flt. Cond. 1, Tail-on, Discrete Atmospheric Turbulence

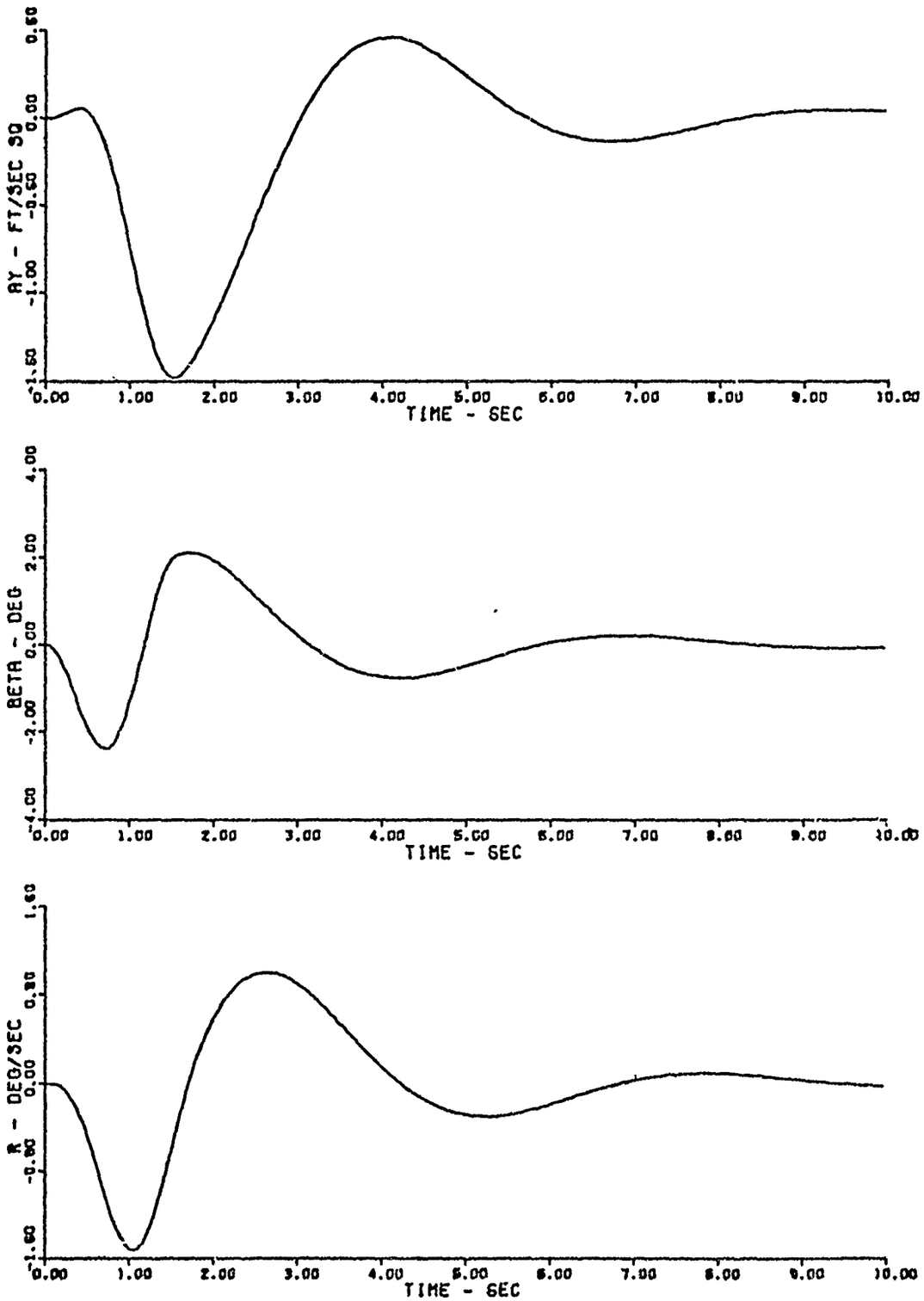

Figure 34. Flt. Cond. 1, Tail-on, Discrete Atmospheric Turbulence

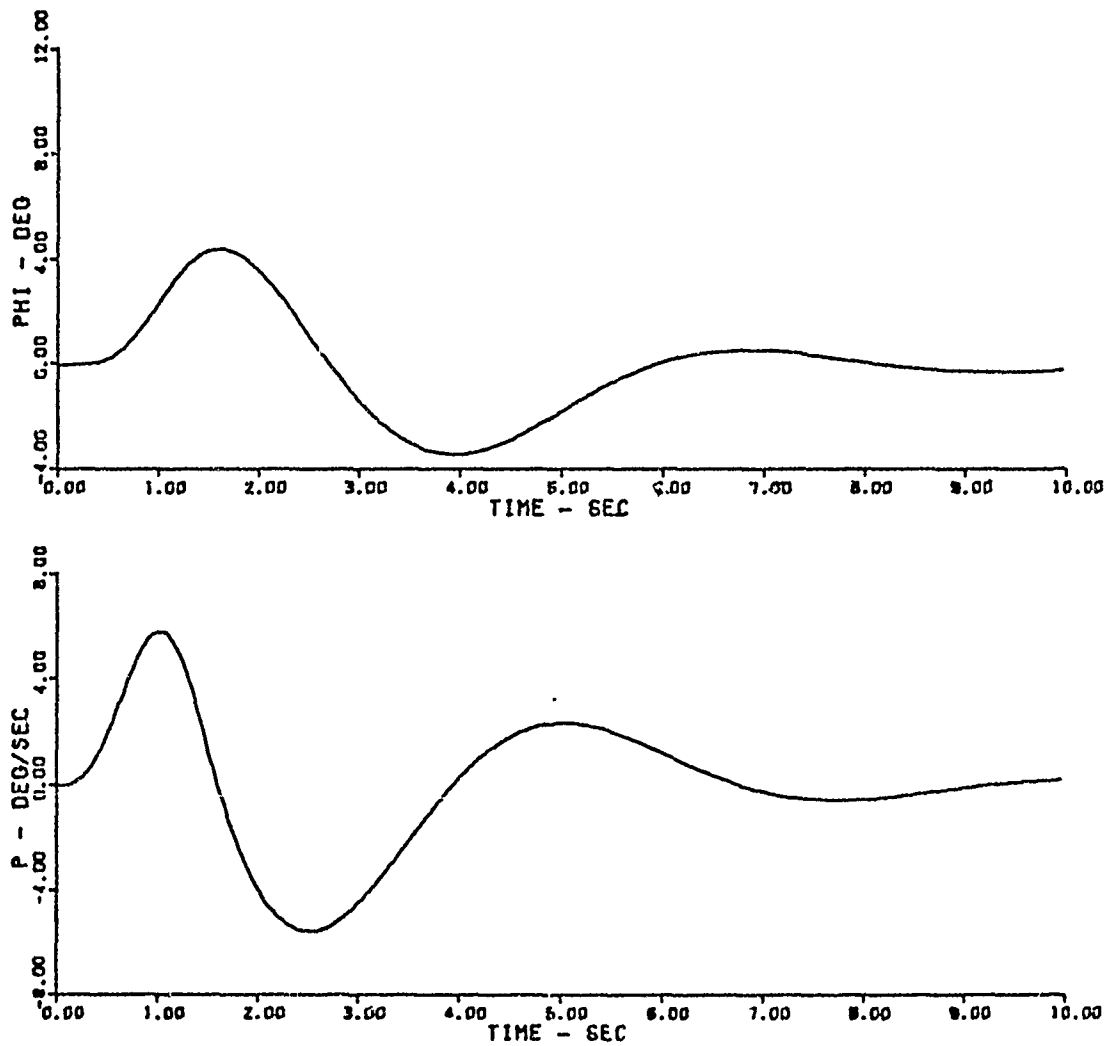

Figure 35. Flt. Cond. 1, Tail-on, Discrete Atmospheric Turbulence

In comparing a_y and β parameters to those of the tail-on aircraft responses in figure 34 it is seen that the tail-off case produces larger values of β and a_y but damps out faster. Since the tail-off aircraft has a larger dutch roll frequency and damping than the tail-on aircraft the faster damping would be expected. Looking at the δ_v and $\dot{\delta}_v$ time responses one realizes the price which must be paid for this stability. δ_v peaks at 38 degrees and $\dot{\delta}_v$ peaks at 119 deg/sec (as indicated in table 4). In comparing the ϕ and p parameters in figures 32 (tail-off) and 35 (tail-on) the same type of transient behavior is displayed as the other aerodynamic parameters except for a slightly larger bank angle in the tail-on case than in the tail off case.

For the Mach 2 flight condition a discrete gust frequency of 5 rad/sec was used since this excited the tail-off aircraft the most. This was also anticipated from the frequency response study. Time response plots for the tail-off aircraft are shown in figures 36-38. The input β_g can be seen in figure 36 along with δ_v and $\dot{\delta}_v$ and it is immediately noticed that the magnitudes of δ_v and $\dot{\delta}_v$ are much lower and more reasonable than the Mach 0.8 flight condition. From figure 37 the transient response is seen to damp much faster than in the Mach 0.8 case due to the higher dutch roll frequency and damping. The high dutch roll frequency (6.5 rad/sec) of the tail-on aircraft can be seen in figures 39 and 40 as the transient response is of high frequency and damps out quicker than the tail-off aircraft. The tail-off aircraft provides a softer response than the tail-on aircraft as the lateral acceleration is lower although β is slightly larger. Figure 41 shows the time responses of ϕ and p.

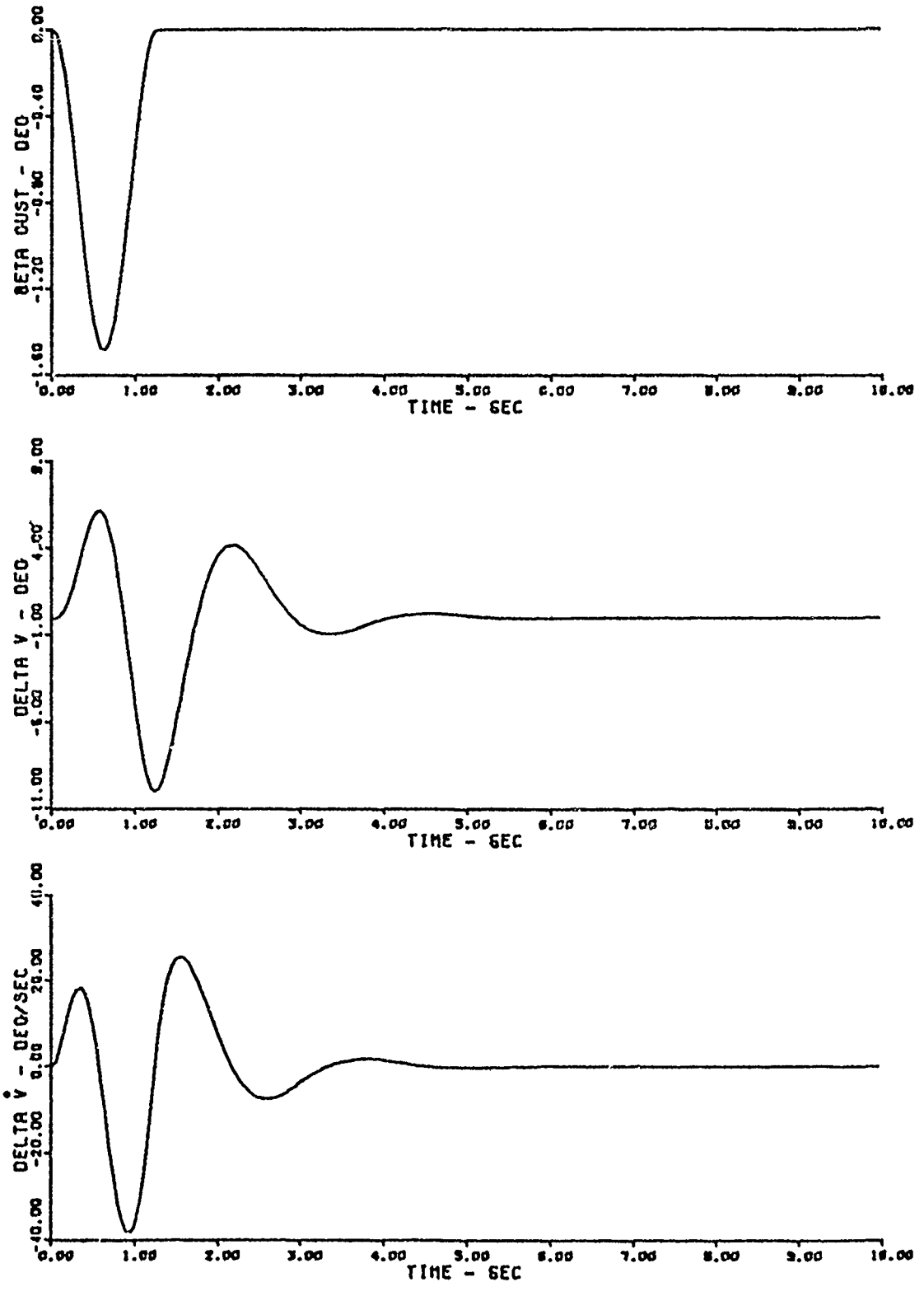

Figure 36. Flt. Cond. 2, Tail-off, Discrete Atmospheric Turbulence

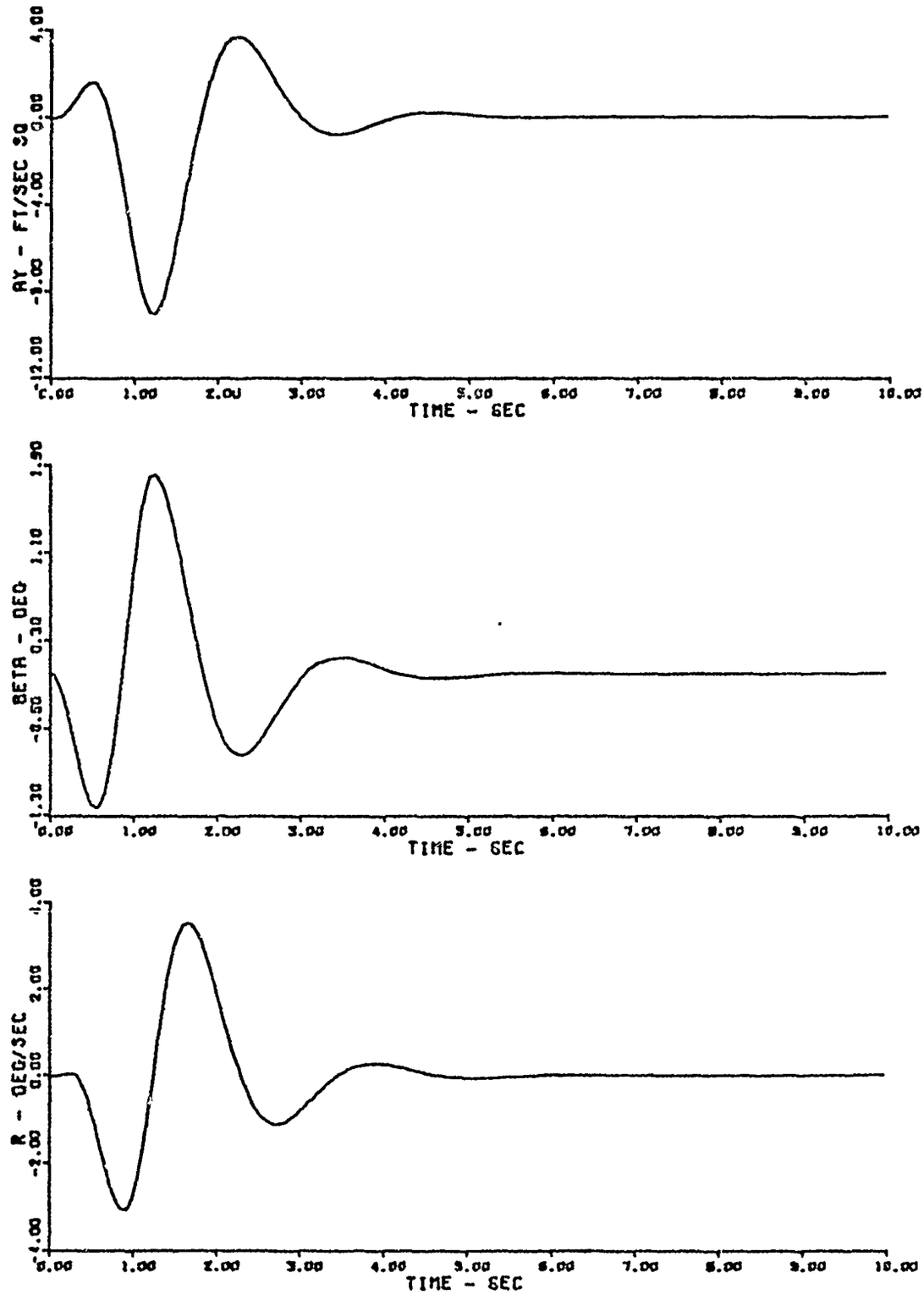

Figure 37. Flt. Cond. 2, Tail-off, Discrete Atmospheric Turbulence

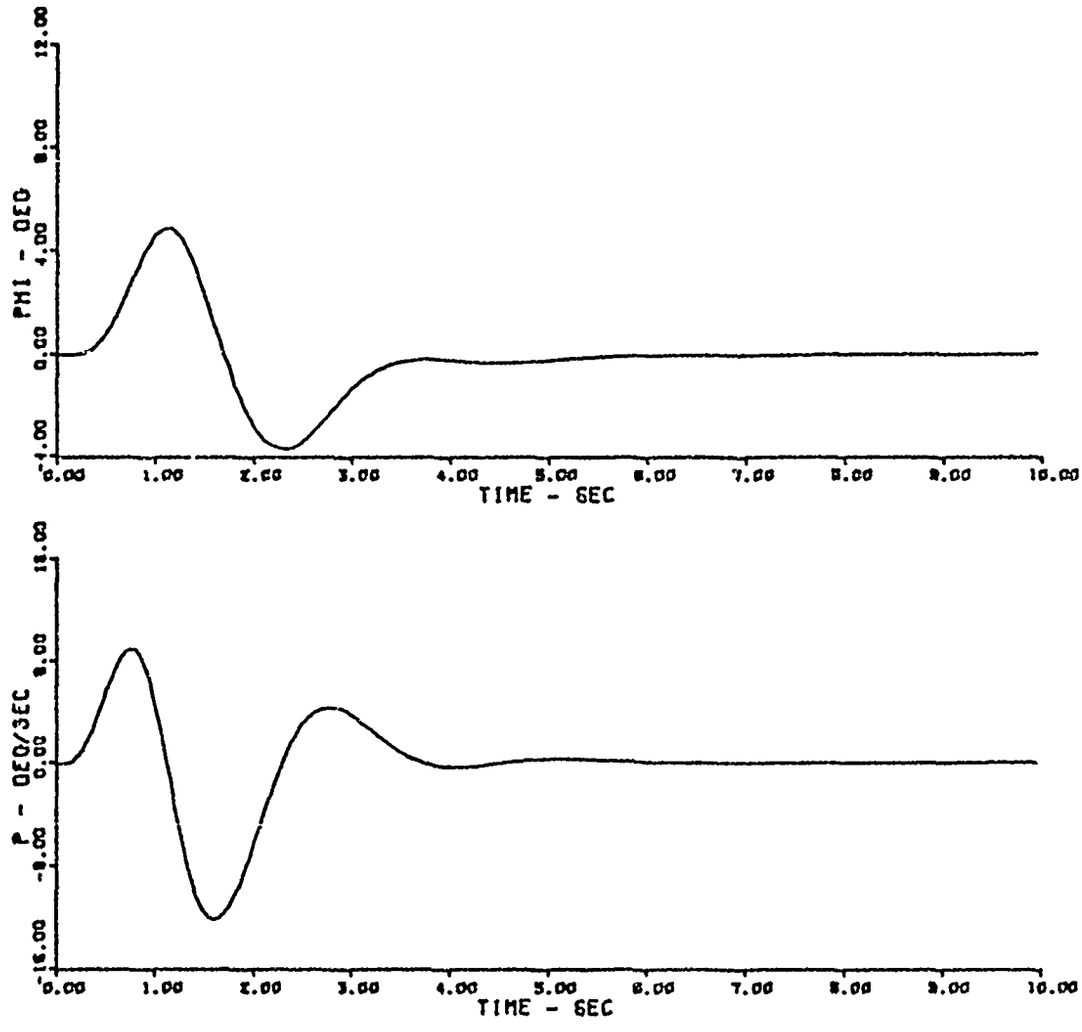

Figure 38. Flt. Cond. 2, Tail-off, Discrete Atmospheric Turbulence

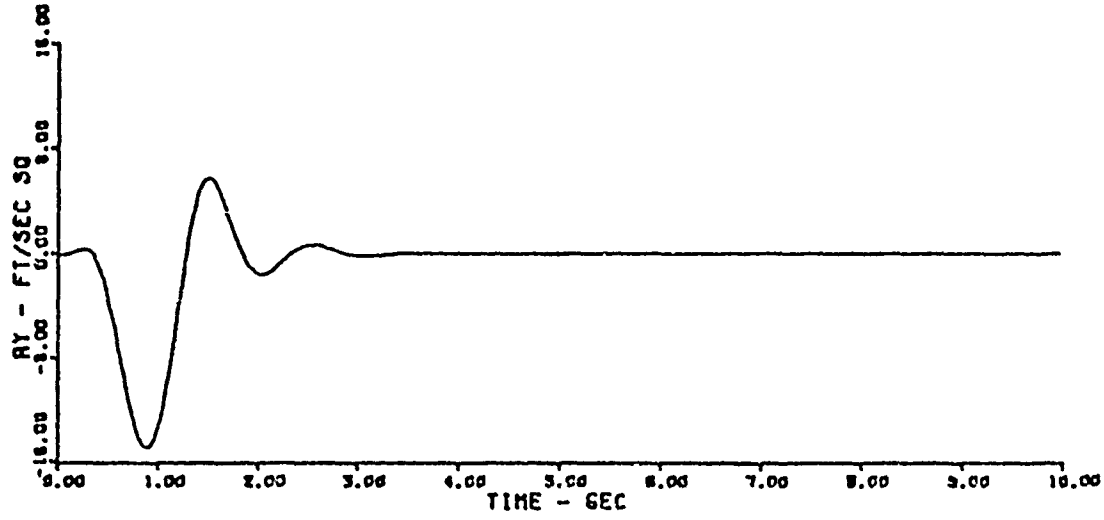

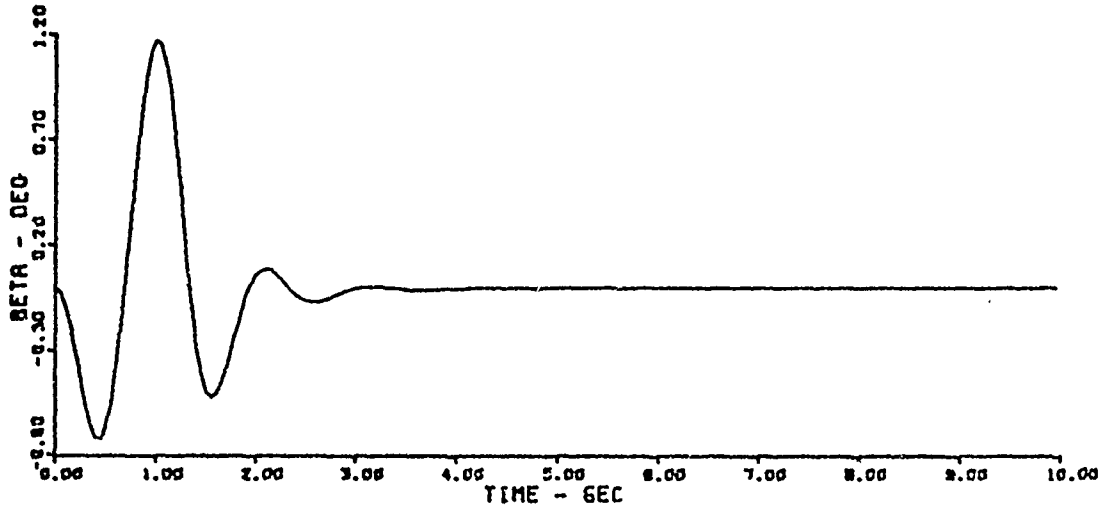

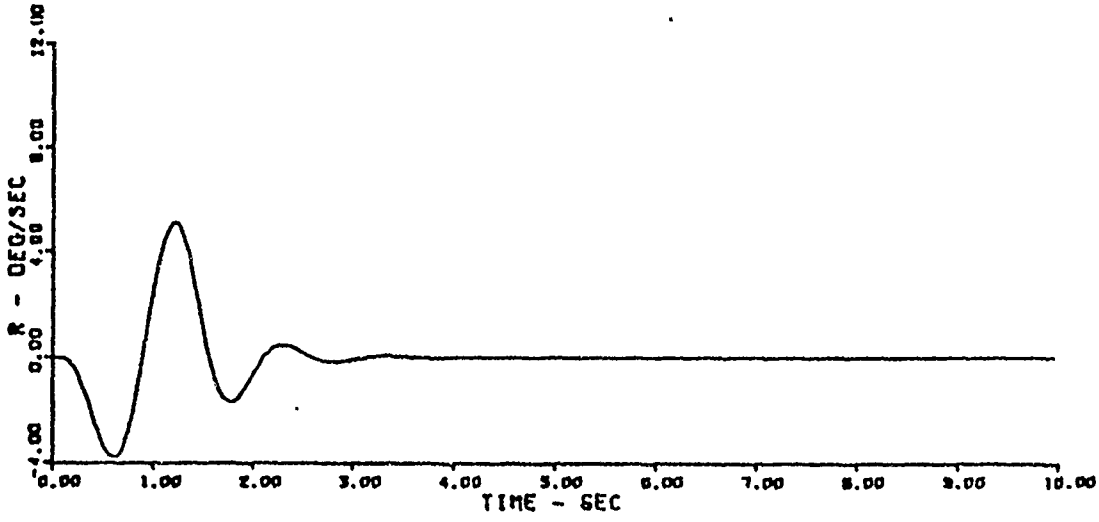

Figure 40. Flt. Cond. 2, Tail-on, Discrete Atmospheric Turbulence

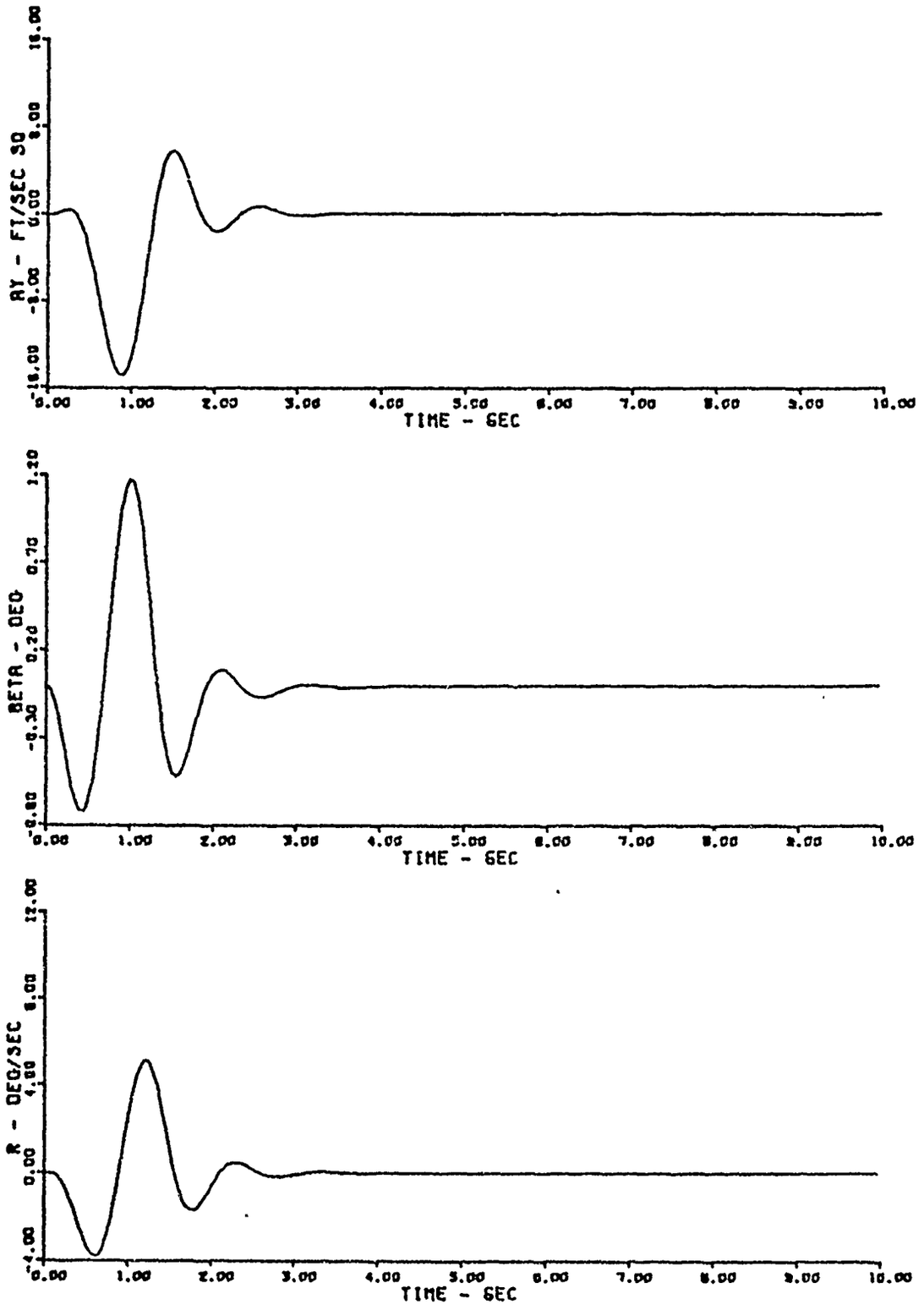

Figure 40. Flt. Cond. 2, Tail-on, Discrete Atmospheric Turbulence

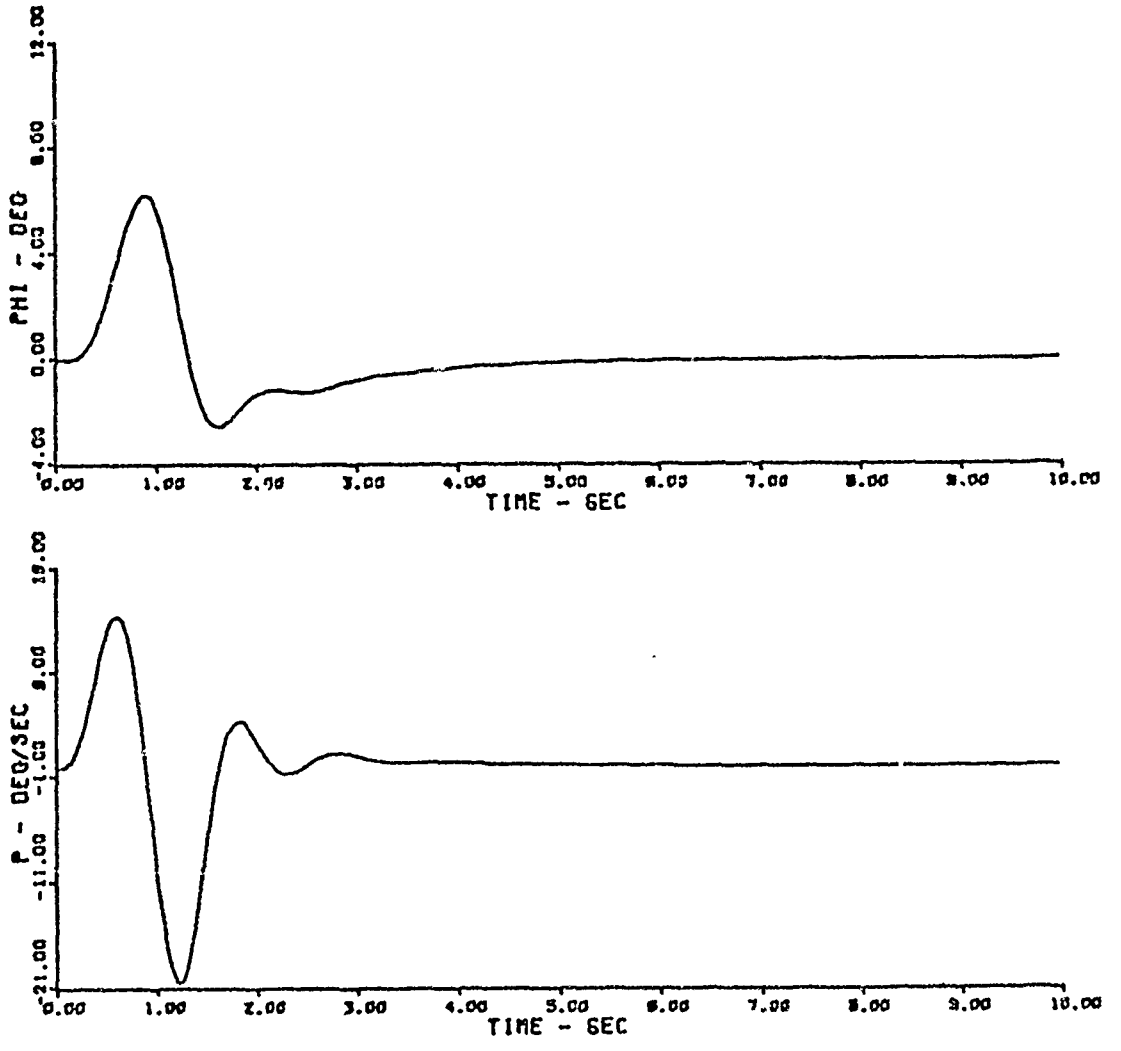

Figure 41. Flt. Cond. 2, Tail-on, Discrete Atmospheric Turbulence

Response To Continuous Random Atmospheric Turbulence

The response of the aircraft and control system to continuous random turbulence needs to be seen in order to complement the discrete turbulence evaluation. The random turbulence model and computer program explained previously were utilized for this part of the study. The input is in the form of white noise and the output is a matrix of variances or mean square error values for each state variable about a mean of zero. The results are presented in table 6 as the square root of the variances or standard deviation of the error.

From table 6 it is seen that for the Mach 0.8 flight condition the standard deviation of the aircraft output variables are reasonably close comparing the tail-off and tail-on values. Once again relatively large thrust vector excursions and rates are seen. In the Mach 2 flight condition the tail-off aircraft actually has a smaller standard deviation than the tail-on aircraft due to the large amount of yawing moment (figure 13) available. The tail-on aircraft exhibits a larger lateral acceleration at Mach 2 as it did for the discrete turbulence.

The results shown in this chapter have indicated that high thrust vector excursions and rates are commanded by the SAS in a low thrust flight condition (flight condition 1). While the linear assumptions made in the beginning become invalid, the trends should remain unchanged. The next step is to limit the thrust vector excursion and rate to more realistic values. The next chapter will show these effects. This feature also allows the linear assumptions to be acceptable so that the small perturbation equations can still be used.

Table 6

Response To Continuous Random Atmospheric Turbulence

Standard Deviation

		β (deg)	a_y (ft/sec^2)	δ_v(or δ_r) (deg)	$\dot{\delta}_v$(or $\dot{\delta}_r$) (deg/sec)	r (deg/sec)	ϕ (deg)	p (deg/sec)
Mach .8	Tail-off	1.32	1.06	14.4	72.7	2.14	2.50	3.31
	Tail-on	1.62	1.23	.78	3.90	1.05	5.00	5.50
Mach 2	Tail-off	.76	3.50	3.86	20.0	1.57	2.69	5.57
	Tail-on	.51	5.40	2.95	35.6	2.01	2.46	7.73

V. Thrust Vector Control Requirements

From the last chapter it was seen that large values of thrust vector excursion and rate were commanded by the control system due to atmospheric turbulence at the thunderstorm levels. Practically, there are limits imposed by the hardware. In addition longitudinal effects become increasingly important when the TV excursion is large. In this chapter, the results of a study of the effects of limiting the thrust vector excursion and rate is shown in order to establish the basic requirements to provide acceptable stability. By limiting the TV excursion the small perturbation equations of motion are again utilized with the longitudinal effects being ignored.

This chapter also examines the sensitivity of the closed loop system to variations in thrust, feedback gains, and actuator dynamics.

The effect on the lateral-directional modes of utilizing a fast and a slow TVC actuator is also addressed.

Thrust Vector Limit Study

The thrust vector excursion and excursion rate was limited to see the effect on the dutch roll frequency and damping. The discrete atmospheric turbulence model was again utilized. The integration program (Appendix 4) was modified to permit limiting of both the thrust vector deflection and rate of deflection. As the limits were decreased the point where the system did not meet the flying qualities requirements was determined. Further decrease in the limits caused the aircraft to become unstable.

As seen previously the maximum thrust vector excursion for a

discrete side gust of 4 rad/sec was 38 degrees with a maximum excursion rate of 119 deg/sec (Table 4). A limit on the TV excursion of 0.5 radians (28.7 degrees) with an excursion rate limit of 1.2 rad/sec (68.8 deg/sec) was tried first. Then subsequent reductions in the rate limit (holding the TV excursion limit constant) were made until divergence of the dutch roll mode was seen. This process of decreasing the rate while holding the excursion constant was continued for lower values of TV excursion down to 0.2 radians (11.5 degrees) of deflection.

In Table 7A a tabulation of the β peaks for various TV excursion and rate limits are shown. The response peaks at each half cycle of the dutch roll mode are shown and their time of occurance. In Table 7B is shown the dutch roll parameters of merit for each limit case. These parameters were obtained from the time and subsidence ratio for the second and fourth β peaks given in Table 7A. It can be seen from the table that decreasing the TV rate decreases the dutch roll frequency and damping. In general, if the TV excursion is decreased with the rate held constant the dutch roll frequency decreases but the damping increases. The effects of holding the thrust vector maximum excursion at 0.5 radians and decreasing the maximum rate from 1.2 rad/sec, to 1 rad/sec, and then to 0.9 rad/sec are shown in figures 42-50. For the last case the dutch roll mode is divergent. Seen from the plots is that as the TV rate is decreased the dutch roll mode takes longer to damp out. From the δ_v and $\dot{\delta}_v$ plots it is seen that as the allowable $\dot{\delta}_v$ is decreased (slower moving) the thrust vector stays at the deflection limit longer. Eventually

Table 7 A

δ_v, $\dot{\delta}_v$ Limit Study

(Flt. Cond. 1, 4 rad/sec Discrete Gust)

β Peaks

δ_v	$\dot{\delta}_v$	Time [1]	Amplitude	Time [2]	Amplitude	Time [3]	Amplitude	Time [4]	Amplitude	Time [5]	Amplitude
(rad)	(rad/sec)	(sec)	(deg)	(sec)	(deg)	(sec)	(deg)	(sec)	(deg)	(sec)	(deg)
Tail-on		0.70	-2.38	1.65	2.12	4.15	-.076	6.80	0.22	——	——
Tail-off											
0.66	2.08	0.65	-2.10	1.50	3.17	2.80	-1.27	4.35	0.31	5.8	-0.08
0.5	1.2	0.60	-2.07	1.60	3.98	3.10	-2.44	4.50	0.72	6.00	-0.20
0.5	1.0	0.65	-2.10	1.70	4.46	3.45	-4.38	5.10	3.62	6.55	-2.41
0.4	1.2	0.60	-2.07	1.70	4.01	3.20	-2.21	4.70	0.63	6.2	-0.18
0.4	1.0	0.60	-2.07	1.70	4.49	3.60	-3.59	5.00	1.83	6.5	-o.56
0.3	1.2	0.70	-2.10	1.70	3.96	3.50	-2.0	5.00	0.60	6.50	-0.18
0.3	1.0	0.70	-2.10	1.80	4.32	3.70	-2.85	5.30	1.05	6.80	-0.32
0.25	1.2	0.65	-2.15	1.80	3.78	3.70	-1.88	5.15	0.58	6.70	-0.18
0.25	1.0	0.70	-2.14	1.80	4.05	3.90	-2.43	5.40	0.88	7.00	-0.27
0.25	0.9	0.70	-2.15	1.90	4.25	4.00	-2.86	5.60	1.12	7.10	-0.34
0.2	1.2	0.70	-2.21	1.80	3.47	3.80	-1.75	5.40	0.59	6.90	-0.18
0.2	1.1	0.70	-2.21	1.85	3.56	3.95	-1.84	5.45	0.63	7.00	-0.20

Table 7 B

δ_v and $\dot{\delta}_v$ Limit Study

(Flt. Cond. 1, 4 rad/sec Discrete Gust)

δ_v (rad)	$\dot{\delta}_v$ (rad/sec)	Dutch Roll Parameters ω_n (rad/sec)	ζ	$\zeta\omega_n$ (rad/sec)
Tail-on		1.28	0.35	0.45
Tail-off				
0.66	2.08	2.20	0.35	0.77
0.5	1.2	2.17	0.26	0.56
0.5	1.0	1.85	0.085*	0.16*
0.4	1.2	2.09	0.28	0.59
0.4	1.0	1.90	0.13*	0.25*
0.3	1.2	1.90	0.28	0.53
0.3	1.0	1.80	0.22	0.40
0.25	1.2	1.88	0.29	0.55
0.25	1.0	1.74	0.23	0.40
0.25	0.9	1.70	0.20	0.34*
0.2	1.2	1.75	0.28	0.49
0.2	1.1	1.75	0.26	0.46

* Does Not Meet Flying Qualities Specification

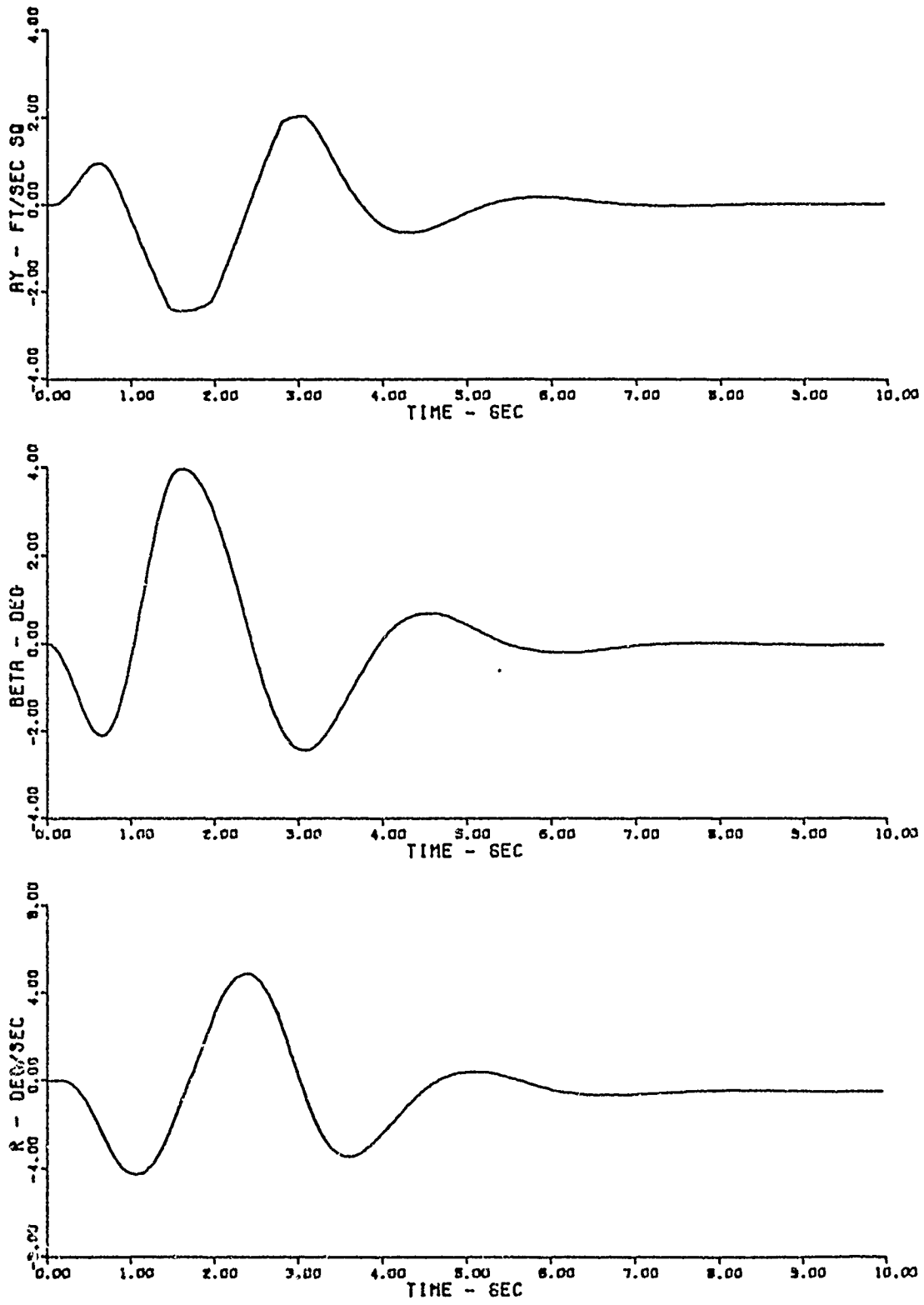

Figure 42. Flt. Cond. 1. Tail-off Discrete Atmospheric Turbulence
δ_V Max = .5 rad, $\dot{\delta}_V$ Max = 1.2 rad/sec

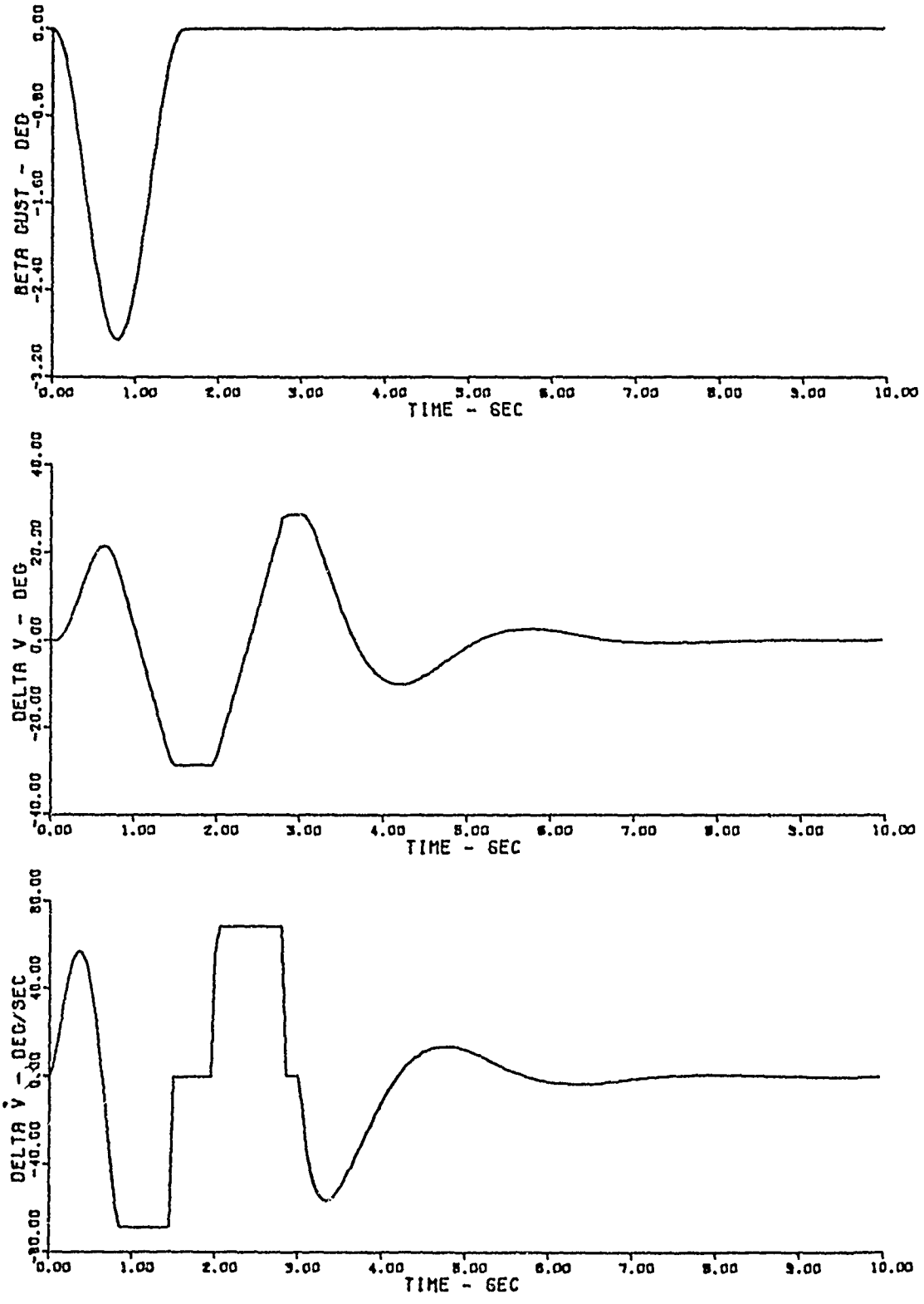

Figure 43. Flt. Cond. 1, Tail-Off, Discrete Atmospheric Turbulence

δ_v Max = .5 rad, $\dot{\delta}_v$ Max = 1.2 rad/sec

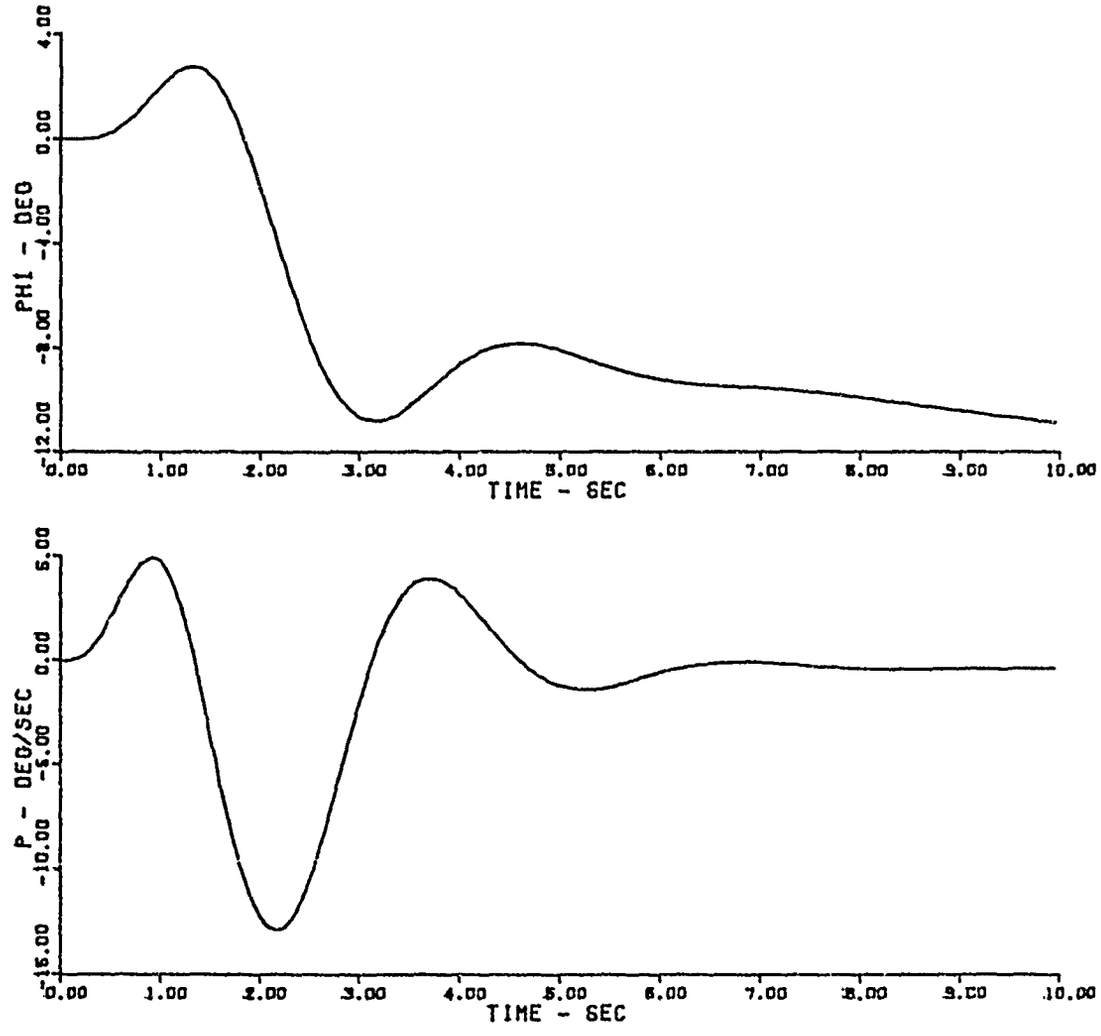

Figure 44. Flt. Cond. 1, Tail-off
Discrete Atmospheric Turbulence
δ_v Max = .5 rad, $\dot{\delta}_v$ Max = 1.2 rad/sec

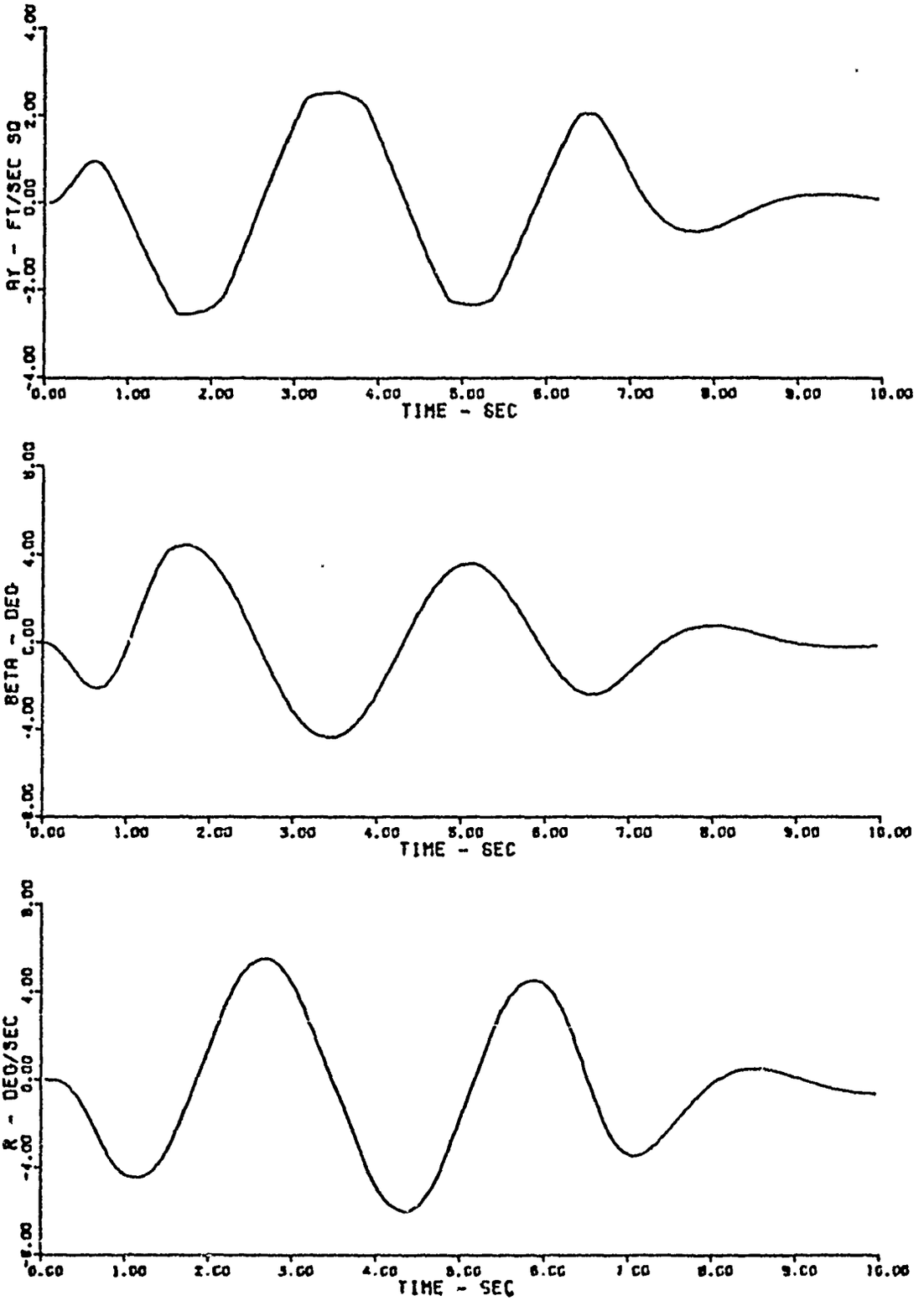

Figure 45. Flt. Cond. 1, Tail-off, Discrete Atmospheric Turbulence
δ_v Max = .5 rad, $\dot{\delta}_v$ Max = 1 rad/sec

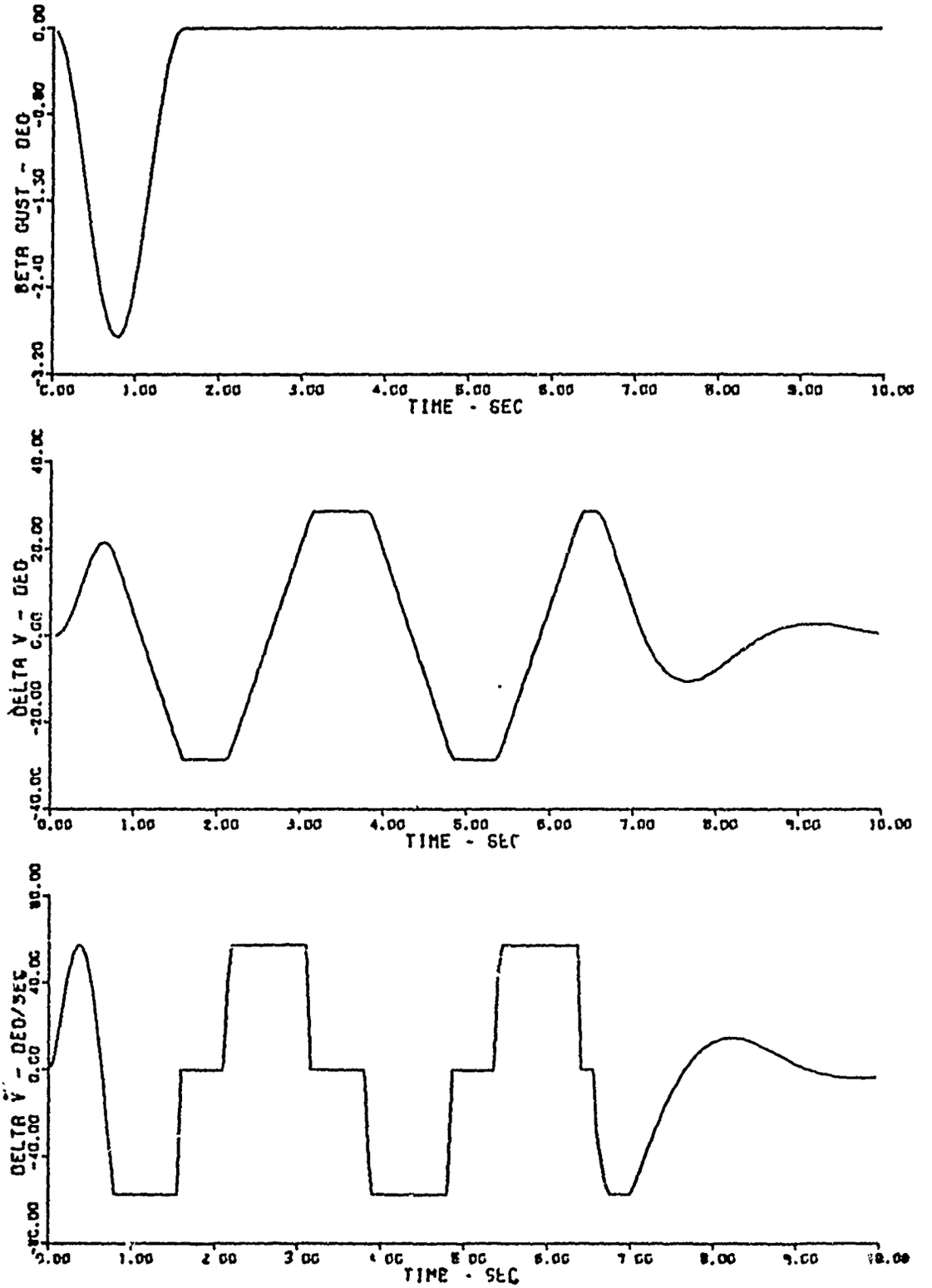

Figure 46. Flt. Cond. 1, Tail-off,
Discrete Atmospheric Turbulence
δ_v Max = .5 rad, $\dot{\delta}_v$ Max = 1 rad/sec

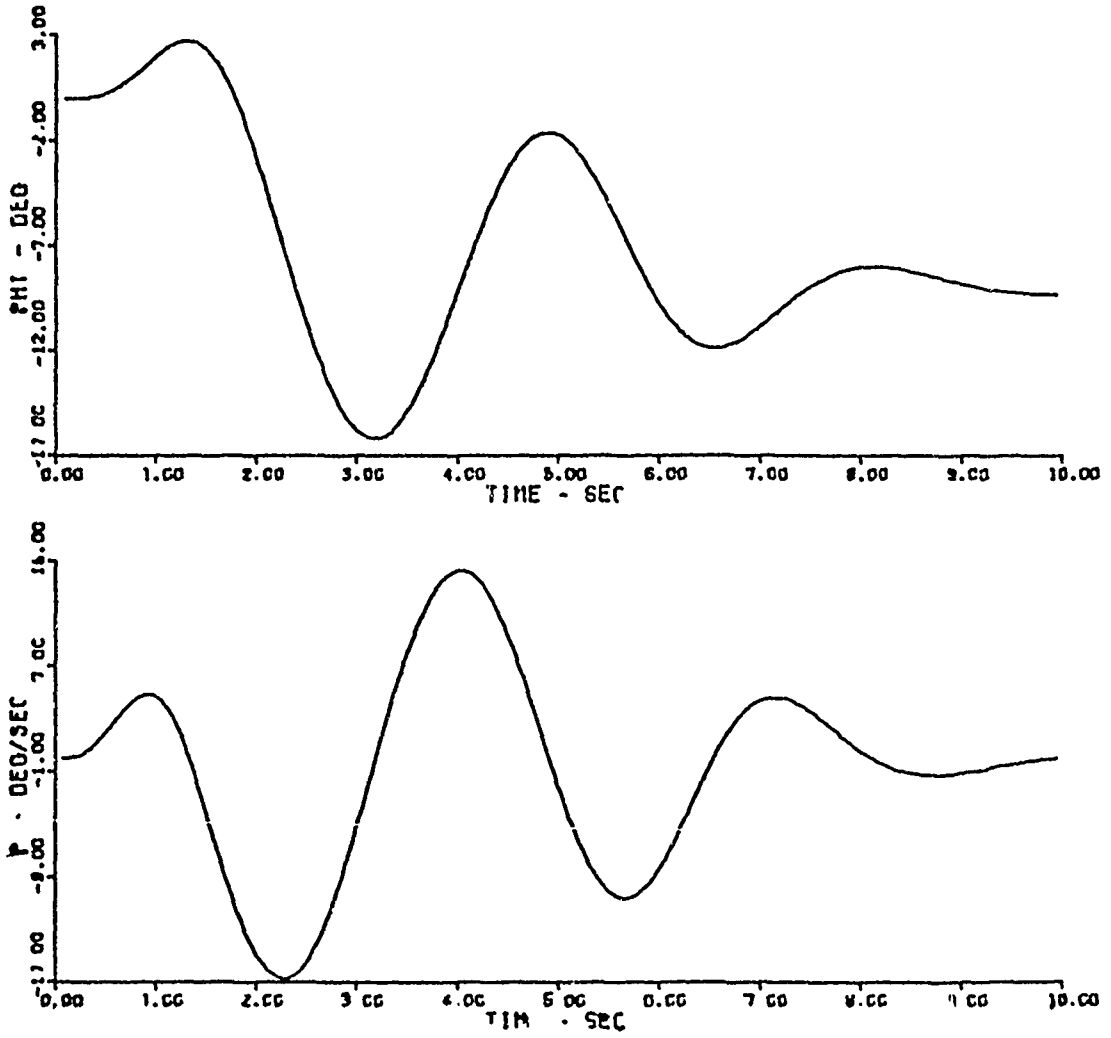

Figure 47. Flt. Cond. 1, Tail-off, Discrete Atmospheric Turbulence
δ_v Max = .5 rad, $\dot{\delta}_v$ Max = 1 rad/sec

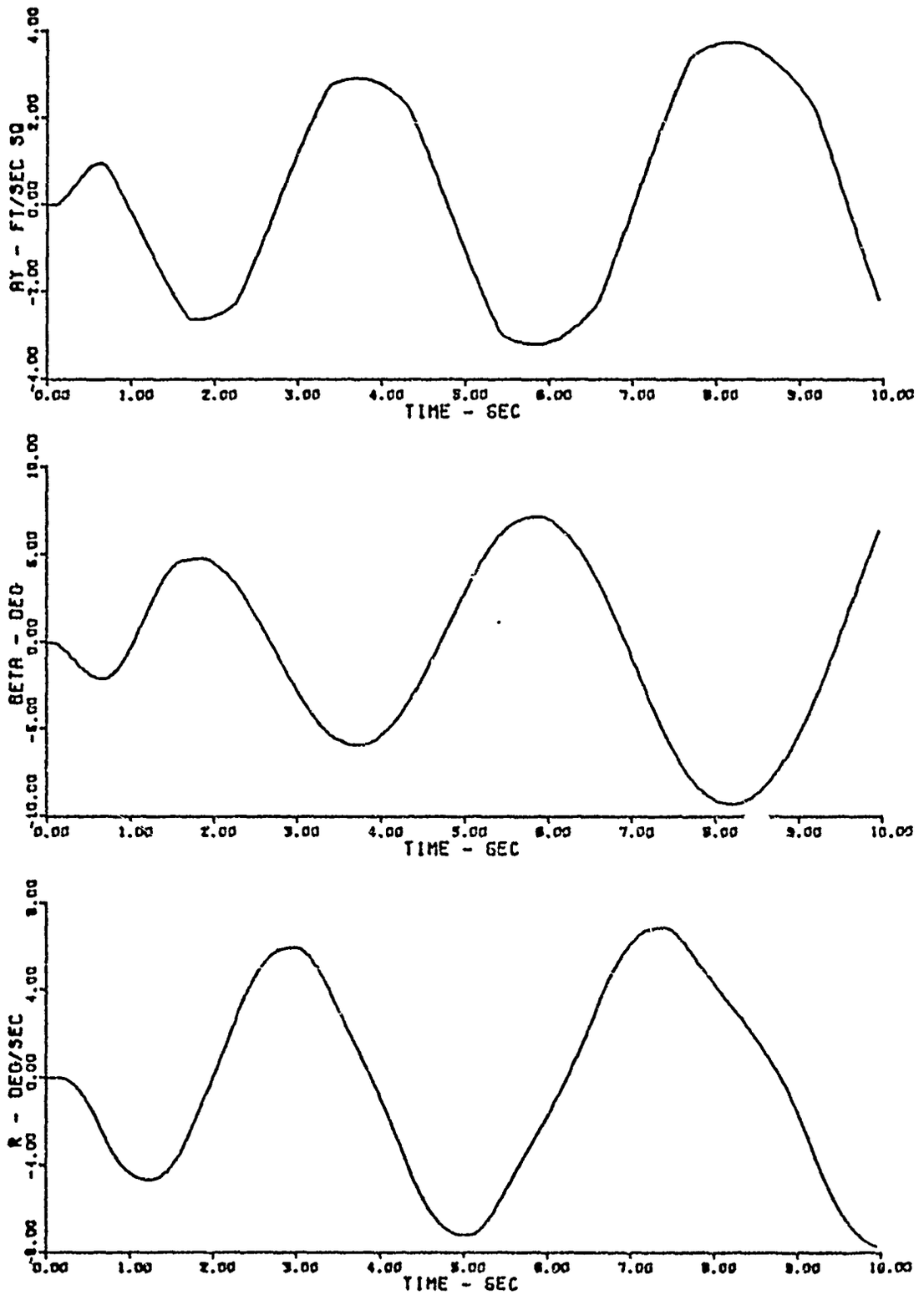

Figure 48. Flt. Cond. 1, Tail-off, Discrete Atmospheric Turbulence
δ_v Max = .5 rad, $\dot{\delta}_v$ Max = .9 rad/sec

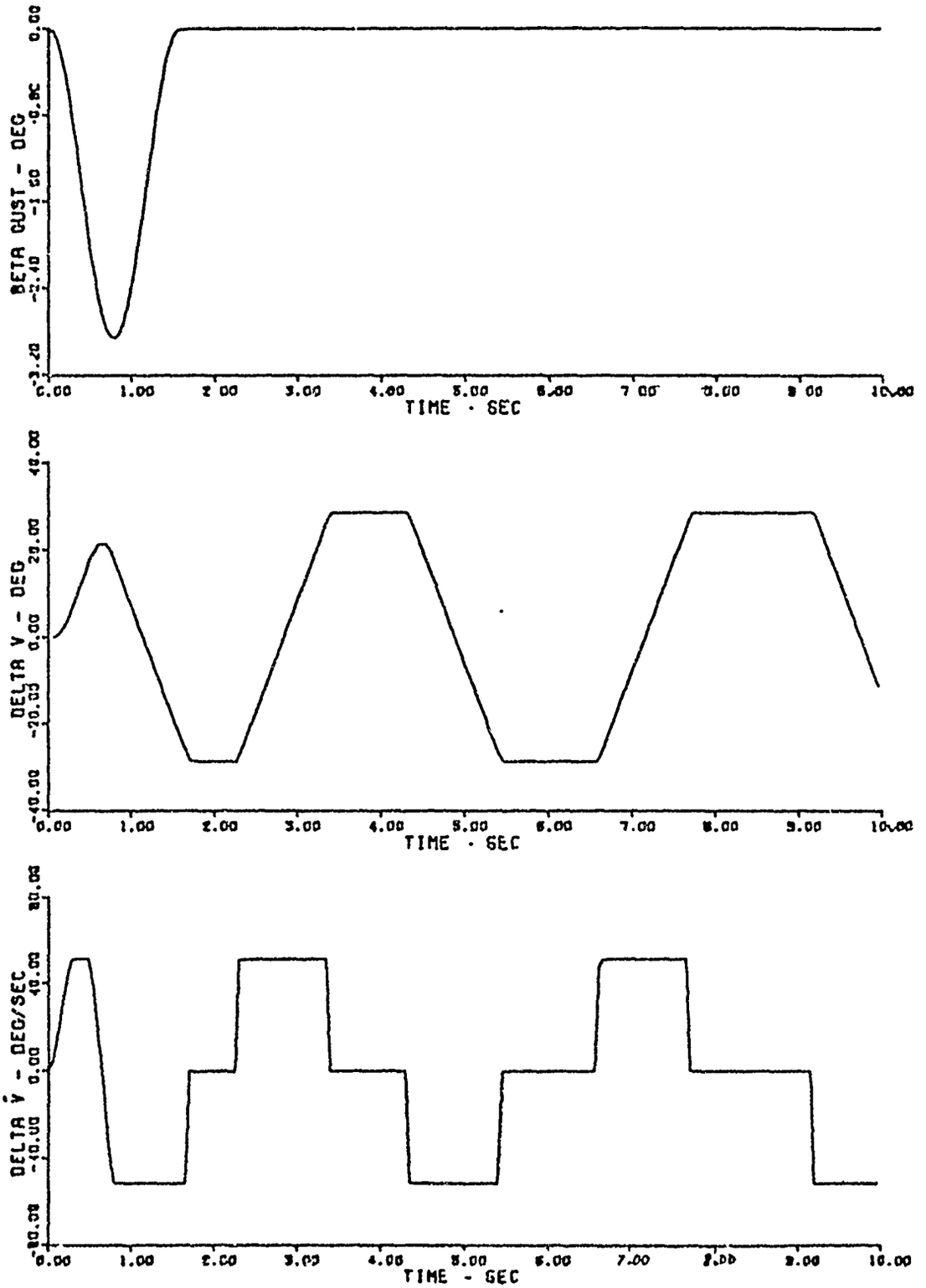

Figure 49. Flt. Cond. 1, Tail-off, Discrete Atrospheric Turbulence
δ_v Max = .5 rad, $\dot{\delta}_v$ Max = .9 rad/sec

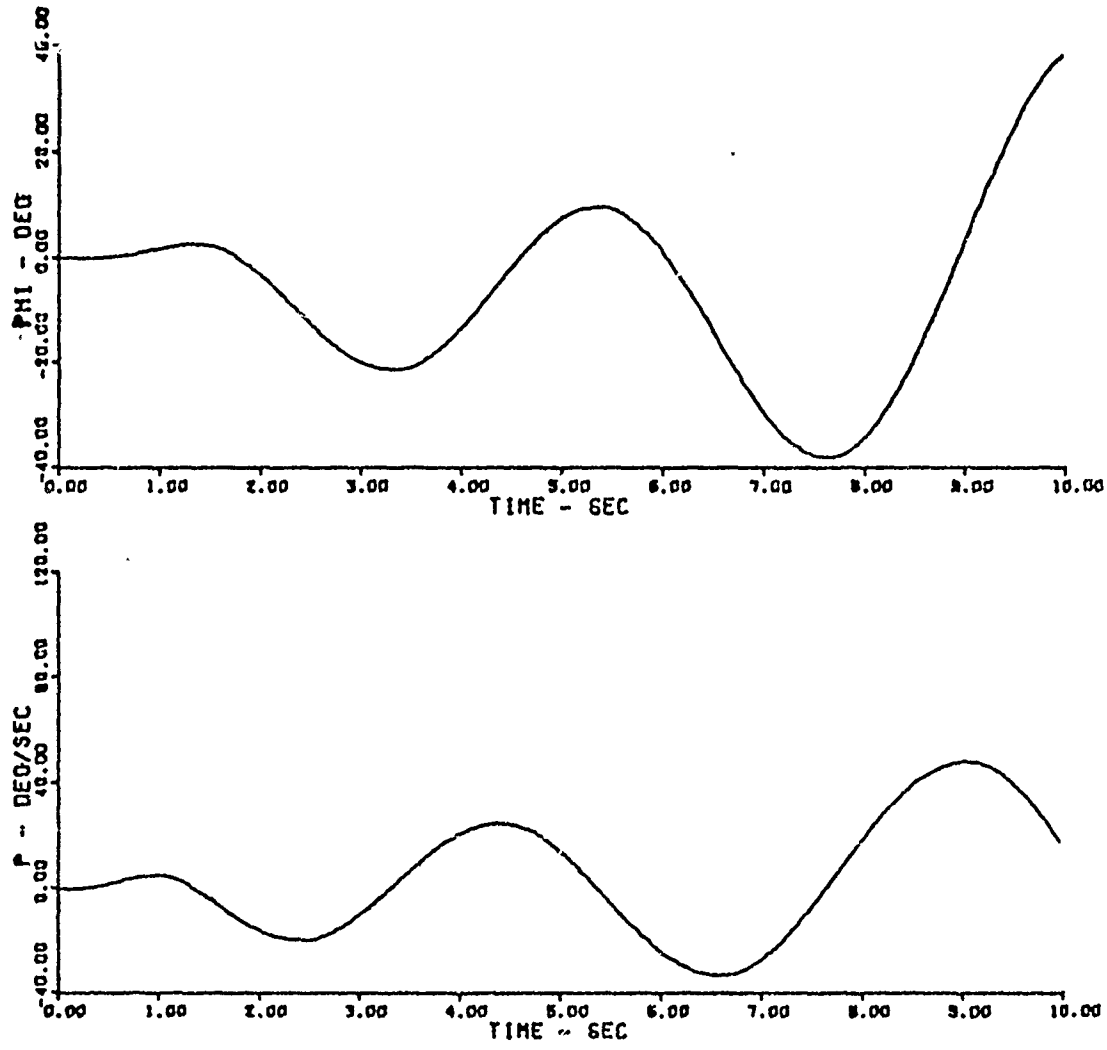

Figure 50. Flt. Cond. 1, Tail-off, Discrete Atmospheric Turbulence
δ_v Max = .5 rad, $\dot{\delta}_v$ Max = .9 rad/sec

it can no longer stabilize the aircraft. From tables 7A and 7B it can also be seen that if the TV excursion is reduced the rate can be reduced also (to a point) and still maintain acceptable stability. To further substantiate this, time response plots for a maximum TV deflection of 0.3 radians and a maximum rate of 1 rad/sec are shown in figures 51-53. From these plots it is seen that for a constant TV excursion rate, the dutch roll mode damps out faster than for the case with a larger excursion (figures 45-47).

The limit study can be summed up in figure 54 in which satisfactory combinations of TV deflection and TV rate of deflection for the discrete atmospheric turbulence environment (side gust) is shown. Areas of convergence, marginal stability and divergence of the dutch roll mode are indicated. This plot shows the deflection and rate requirements to meet the flying qualities specification requirements for the dutch roll mode.

No attempt was made to limit the thrust vector maximum deflection and rate for flight condition 2 as the maximum values were low (table 5). It is believed that flight condition 1 will drive the design choice (for cruise).

Parameter Study

A study of the effect on the dutch roll frequency and damping of varying the thrust, feedback gains and TVC actuator dynamics by $\pm$ 10% was done. The TV maximum deflection was limited to 0.5 radians and the rate was limited to 1.2 rad/sec. Both the discrete and the continuous random turbulence models were used for this study.

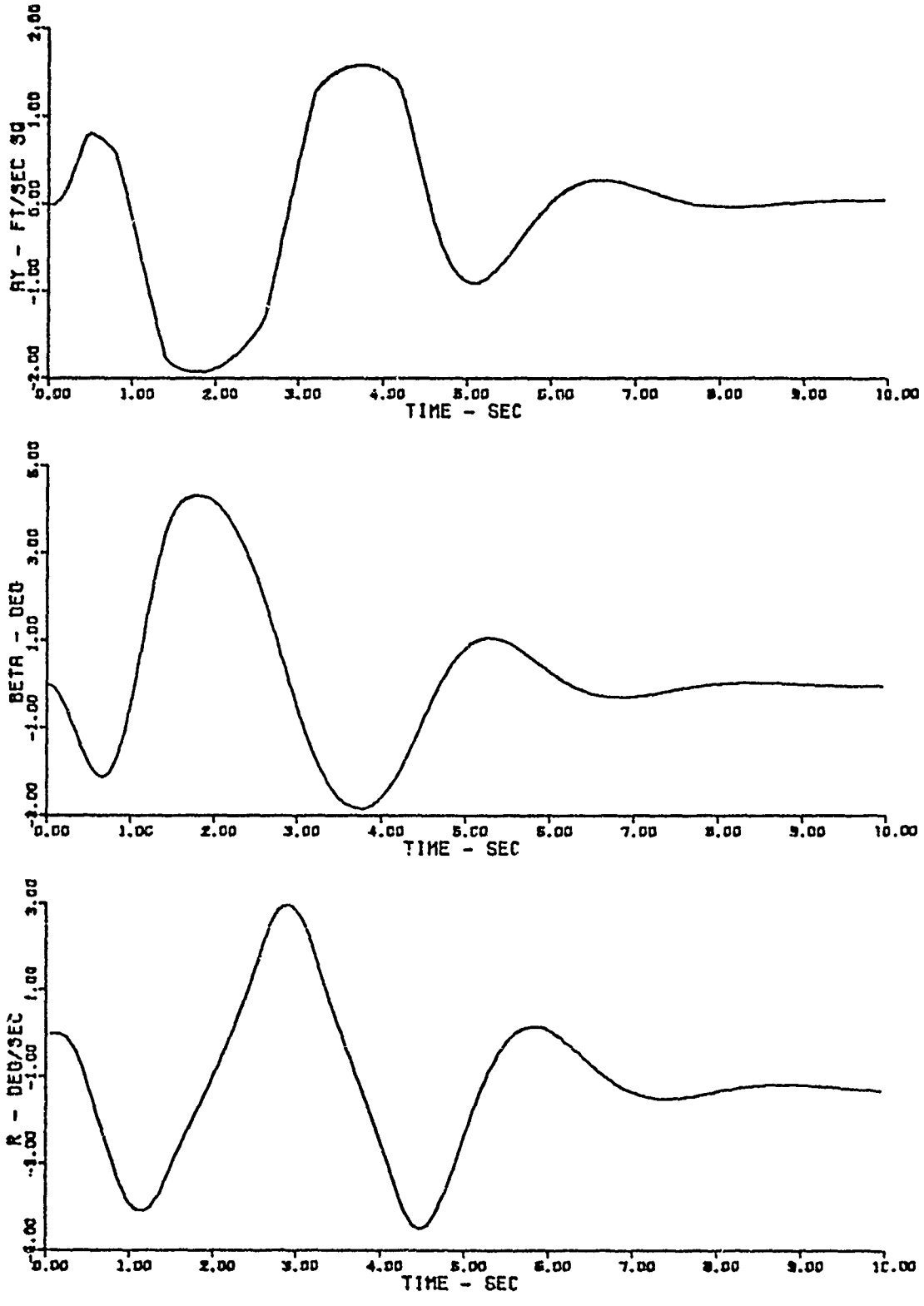

Figure 51. Flt. Cond. 1, Tail-off, Discrete Atmospheric Turbulence
δ_v Max = .3 rad, $\dot{\delta}_v$ Max = 1 rad/sec

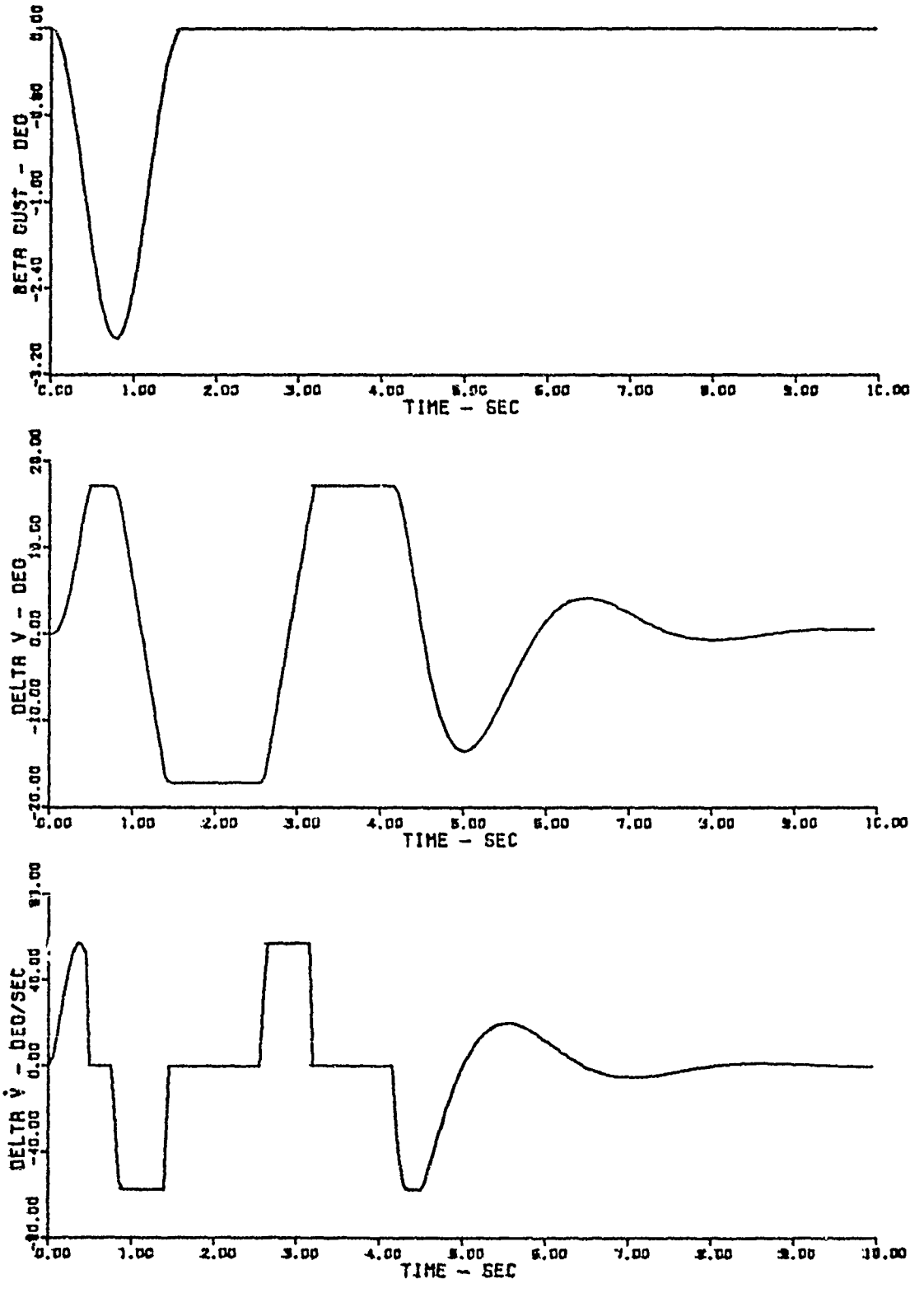

Figure 52. Flt. Cond. 1, Tail-off, Discrete Atmospheric Turbulence δ_V Max = .3 rad, $\dot{\delta}_V$ Max = 1 rad/sec

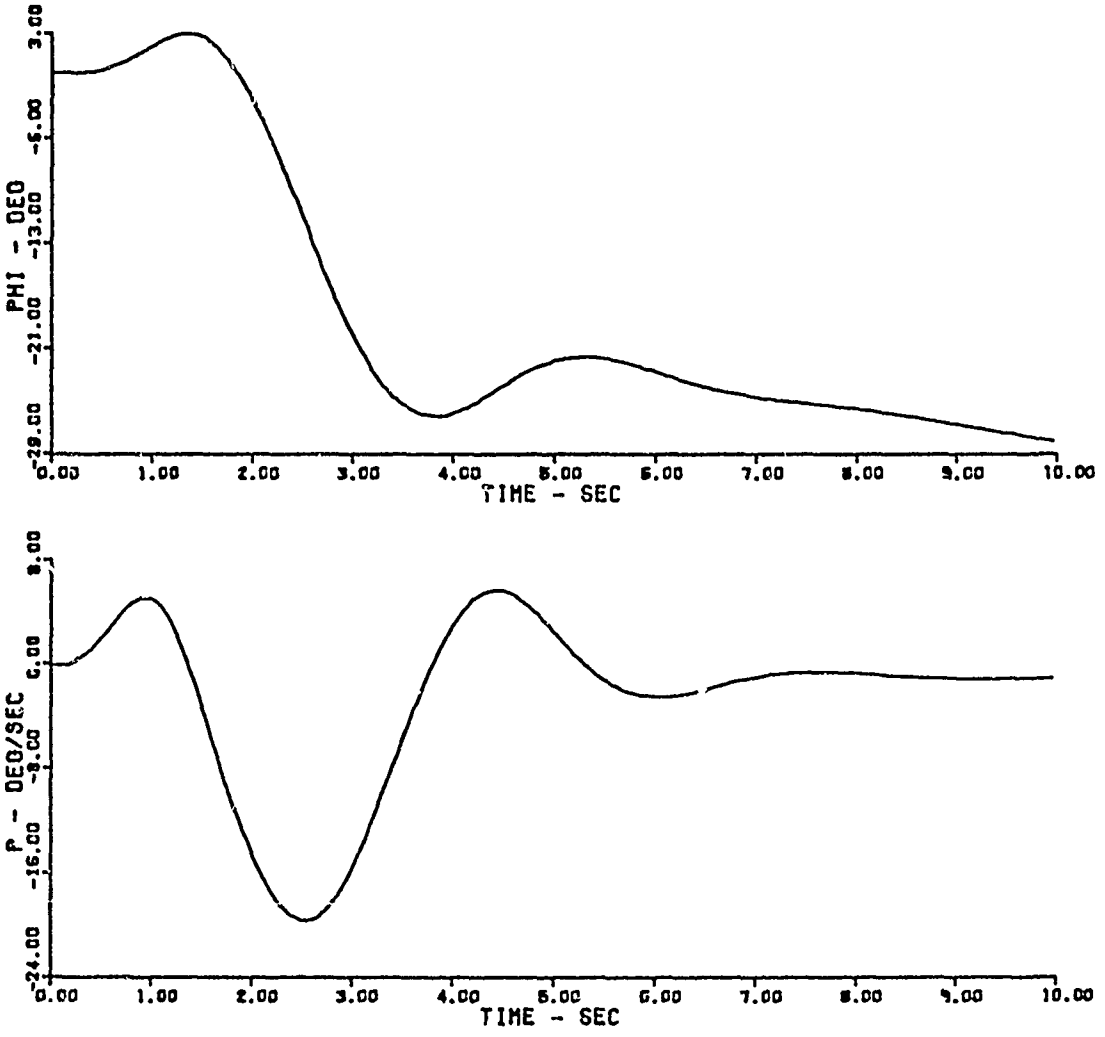

Figure 53. Flt. Cond. 1, Tail-off, Discrete Atmospheric Turbulence δ_v Max = .3 rad, $\dot{\delta}_v$ Max = 1 rad/sec

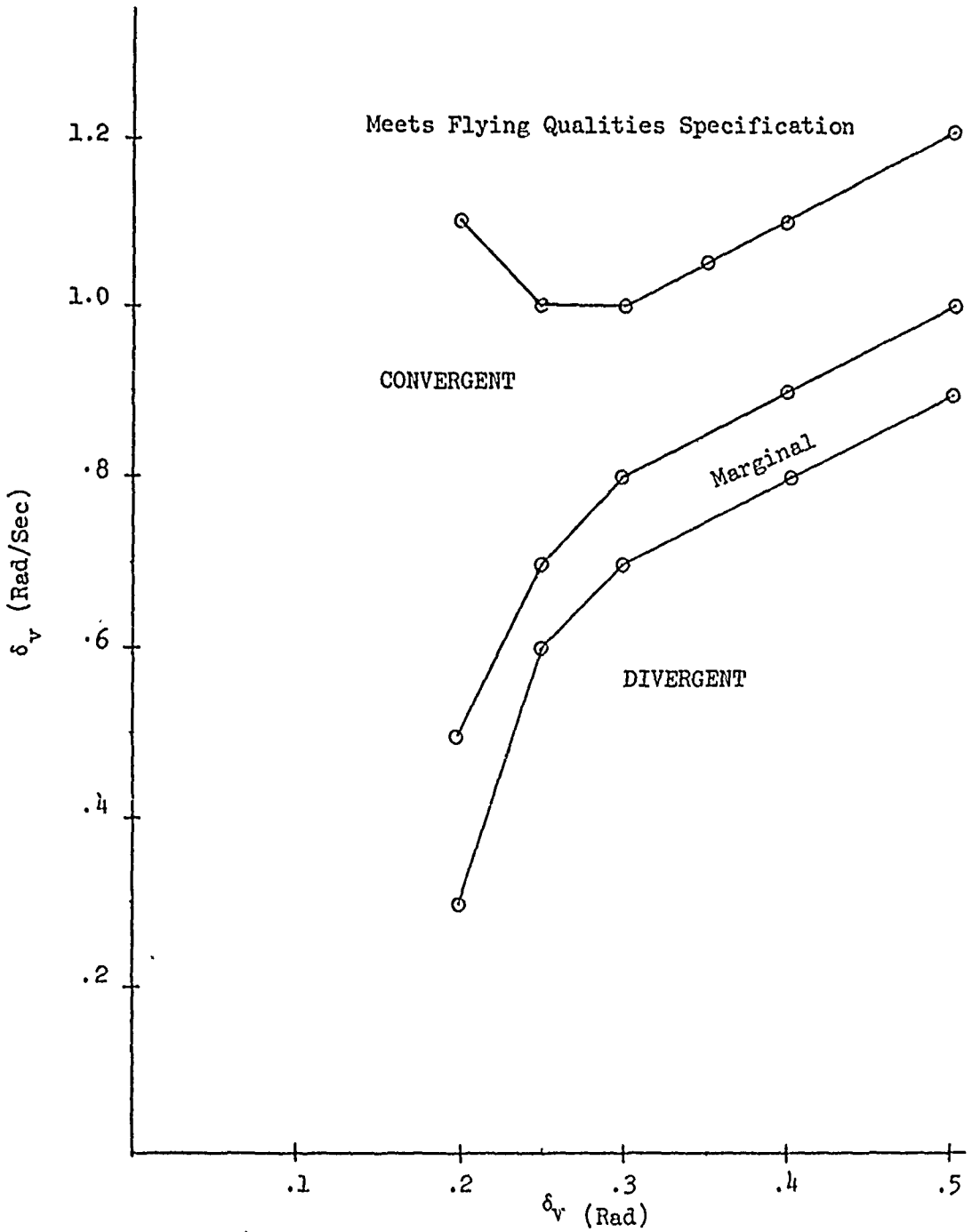

Figure 54. Thrust Vector Deflection / Deflection Rate Requirements for Discrete Turbulence at Flt. Cond. 1.

Table 8 indicates the results for discrete atmospheric turbulence at flight condition 1. The Maximum values of β and a_y are tabulated along with the dutch roll mode parameters. What is indicated is that the system is most sensitive to the actuator time constant variations. For the slower actuator the dutch roll mode became unacceptable from the requirements standpoint.

The results of the parameter study for flight condition 2 are shown in table 9. Values for δ_v and $\dot{\delta}_v$ were included since the magnitudes of these quantities were not limited. It can be seen from table 9 that the system is less sensitive to the actuator variations than to the thrust and gain changes. What is indicated is that the gains need to be closely correlated with the thrust and the actuator needs to be accurately modelled. Table 10 shows the effects of the parameter variations using the continuous random atmospheric turbulence input. It substantiates the previous results.

TVC Actuator Model

The basic TVC actuator model used as a baseline in this study utilized a 0.1 second time constant. It could be useful from a hardware standpoint to see how slow an actuator could be used and still maintain acceptable flying qualities. This would be of interest in the selection of the type of TVC device to be used. Values of the actuator time constant were tried at 0.2, 0.25 and 0.33 seconds. The design process described in Chapter III was repeated to develop new feedback gains to optimize the dutch roll dynamics. It was determined that with an actuator time constant larger than 0.25 seconds the coupled roll-spiral mode in flight condition 1 would

Table 8

Parameter Study, Flt. Cond. 1

Discrete Atmospheric Turbulence

	Peak Values		Dutch Roll		
	β (deg)	a_y (ft/sec^2)	ω_n (rad/sec)	ζ	$\zeta\omega_n$ (rad/sec)
Tail-On	2.25	1.5	1.28	0.35	0.45
Tail-off					
Baseline	3.98	2.4	2.17	0.26	0.56
-10% Thrust	3.76	2.2	1.96	0.32	0.63
+10% Thrust	4.17	2.6	2.24	0.18*	0.40
Actuator $\frac{9}{s+9}$	4.49	2.5	1.96	0.08*	0.16*
Actuator $\frac{11}{s+11}$	3.58	2.3	2.03	0.32	0.65
-10% Gains	3.80	2.4	2.09	0.28	0.59
+10% Gains	4.14	2.4	2.17	0.22	0.48

δ_v Max = $\pm$ .5 rad

δ_v Max = $\pm$ 1.2 rad/sec

* Does Not Meet Flying Qualities Specification

Table 9

Parameter Study, Flt. Cond. 2

Discrete Atmospheric Turbulence

	Peak Values				Dutch Roll		
	a_y (ft/sec^2)	β_a (deg)	δ_v (deg)	$\dot{\delta}_v$ (deg/sec)	ω_n (rad/sec)	ζ	$\zeta\omega_n$ (rad/sec)
Tail-on	14.9	1.17	7.06	32.36	6.53	0.32	2.09
Tail-off							
Baseline	9.0	1.80	9.86	38.15	3.00	0.41	1.24
-10% Thrust	7.2	1.50	8.50	34.90	2.71	0.63	1.70
+10% Thrust	10.5	2.05	11.02	40.74	3.38	0.28	0.95
Actuator $\frac{9}{s+9}$	10.2	2.00	11.74	43.84	3.56	0.30	1.07
$\frac{11}{s+11}$	8.0	1.65	8.48	33.60	2.48	0.46	1.14
-10% Gains	8.6	1.78	9.27	34.80	2.66	0.37	0.98
+10% Gains	9.3	1.82	10.58	40.90	3.44	0.45	1.55

Table 10

Parameter Study, Continuous Random Atmospheric Turbulence

	Standard Deviation a_y (ft/sec^2)		β_a (deg)		δ_v (deg)		$\dot{\delta}_v$ (deg/sec)	
Mach No.	.8	2	.8	2	.8	2	.8	2
Tail-on	1.23	5.40	1.62	0.51	0.78	3.95	3.9	35.6
Tail-off Baseline	1.06	3.50	1.32	0.76	14.4	3.86	72.7	20.0
-10% Thrust	1.05	2.99	1.34	0.7	14.2	3.47	71.3	18.7
+10% Thrust	1.07	3.92	1.31	0.83	14.55	4.28	73.0	21.7
Actuator $\frac{9}{s+9}$	1.15	3.85	1.32	0.79	16.24	4.49	79.0	22.7
$\frac{11}{s+11}$	0.99	3.27	1.33	0.76	12.98	3.48	67.8	18.3
-10% Gains	1.04	3.56	1.38	0.81	13.79	3.78	65.6	17.9
+10% Gains	1.07	3.42	1.28	0.72	14.93	3.93	79.6	72.1

not uncouple, which is an unacceptable condition. With an actuator time constant of 0.25 seconds an acceptable dutch roll frequency and damping ratio was obtained although it was not as good as the baseline actuator. Table 11 is a tabulation of the figures of merit for the lateral-directional modes for the baseline actuator, the slower actuator and a 0.05 second time constant (faster) actuator. The faster actuator was included to indicate its advantage in the capability for higher dutch roll frequency and damping. The feedback gains selected for each configuration are also shown.

Table 11

Effect Of Actuator Time Constant Changes

Mach .8	Dutch Roll ω_n (rad/sec)	ζ	$\zeta\omega_n$ (rad/sec)	Roll τ_r (sec)	Spiral τ_s (sec)	Feedback Gains K_β	K_r
Tail-on	1.28	0.35	0.45	0.35	62.9	K_{a_y} = .01745	1.5
Tail-off							
$\frac{10}{s+10}$ (baseline)	2.24	0.398	0.89	2.13	22.2	16.22	6.35
$\frac{4}{s+4}$	1.8	0.385	0.69	2.25	25.2	13.51	8.42
$\frac{20}{2+20}$	2.17	0.49	1.06	2.13	21.7	20.27	8.09
Mach 2							
Tail-on	6.53	0.32	2.04	0.36	(stable)	K_{a_y} = .01745	1.5
Tail-off							
$\frac{10}{s+10}$ (baseline)	3.0	0.41	1.24	0.25	92.6	6.43	1.34
$\frac{4}{s+4}$	1.38	0.37	0.51	-2.36±5.11j	163.9	4.95	3.05
$\frac{20}{s+20}$	2.67	0.59	1.58	0.23	90.9	6.93	1.52

VI. Conclusions and Recommendations

Conclusions

It has been seen in this study that removal of the vertical stabilizer on the F-111 results in an unstable aircraft. The analyses of this study have shown that lateral-directional thrust vector control (TVC) can not only stabilize the F-111 in the tail-off configuration, but also, can achieve a better dutch roll frequency and damping ratio than the baseline tail-on aircraft. For the two flight conditions examined, the response of the tail-off aircraft to atmospheric turbulence was as good as or better than the tail-on aircraft. The price that must be paid for this stability is a momentary reduction of the forward thrust due to the deflection of the thrust vector. If the thrust vector is allowed higher maximum excursions and rates, the dutch roll stability is better than that of the tail-on aircraft. The problem is that about 12% of the forward thrust (for a maximum deflection of 0.5 radians) is lost momentarily at the full deflection of the thrust vector. It was seen that the maximum TV excursion could be limited to as low as 0.2 radians (11.5 degrees) and still maintain acceptable flying qualities. This would only be a 2% loss in forward thrust for full deflection. This assumes a worst case cruise condition (low thrust) in an environment represented by the discrete atmospheric turbulence model at the thunderstorm levels. But, a TV excursion rate of 1.1 rad/sec (63 deg/sec) is required with the above excursion value.

Requirements for the thrust vector deflection and rate of deflection were specified for an actuator model with a 0.1 second

time constant. It was seen that the lowest TV rate of deflection for acceptable flying qualities was 1 rad/sec, so a device to deflect the thrust vector having at least this capability would be required. It was seen that a TVC actuator with faster dynamics (than the 0.1 sec. time constant) produced a better dutch roll frequency and damping ratio. The slowest actuator possible was one with a 0.25 second time constant. Slower actuator dynamics resulted in a closed loop coupled roll-spiral mode.

The control system feedback gains found in this study were dependent on the flight condition and thrust level, implying that gain scheduling is necessary. Since it was shown that the closed loop system was very sensitive to unmodelled changes in feedback gains, thrust level, and actuator dynamics, the gains must be closely matched with the actual thrust and actuator dynamics.

Recommendations

This study was done using the lateral-directional small perturbation equations of motion. It is recommended that the study be continued using the non-linear longitudinal and lateral-directional equations of motion. Flight conditions such as a landing configuration and maneuvering flight should be considered. A model of the amount of thrust deflection that can be practically realized needs to also be considered in further analyses.

A problem unique to utilizing TVC for lateral-directional stability is one of an engine out condition. Since the F-111 is a twin engine aircraft, this would help minimize the problem, but there still may be consideration to provide a small vertical surface to produce a more neutrally stable aircraft.

Bibliography

1. Baldwin, A. W. Kinsey, D. W., and Lash, S.F., Transonic Aircraft Technology (TACT) Program Summary, AFFDL-TM-78-7-FXS, Air Force Flight Dynamics Laboratory, Wright-Patterson AFB, Ohio, January 1978.

2. Roskam, J., Flight Dynamics of Rigid and Elastic Airplanes-Part One, Roskam Aviation and Engineering, Corporation, 1976.

3. Griffin, J.M., Digital Computer Solution of Aircraft Longitudinal and Lateral-Directional D; iamic characteristics, as revised by Yeager, R. B., Maj., Jordan, L. B., Maj., Ratino, D. A., Capt., SEG-TR-66-52, Aeronautical Systems Division, Wright-Patterson AFB, Ohio.

4. Larimer, S. J., An Interactive Computer-Aided Design Program For Digital And Continuous Control System Analysis And Synthesis, AFIT/GGC/EE/78-2, Air Force Institute of Technology, Wright-Patterson AFB, Ohio, March 1978.

5. Woodcock, R. J., Background Information And User Guide For Mil-F-8785 B (ASG), "Military Specification-Flying Qualities Of Piloted Airplanes", AFFDL-TR-69-72, Air Force Flight Dynamics Laboratory, Wright-Patterson AFB, Ohio, August 1969.

6. Blakelock, J. H., Automatic Control of Aircraft and Missiles, John Wiley and Sons, Inc., 1965.

7. Guttram, I. and Wilks, S.S., Introductory Engineering Statistics, John Wiley and Sons, Inc., 1965.

8. Baldwin, A.W., Drag Polars, Air Force Flight Dynamics Laboratory, Wright-Patterson AFB, Ohio, 1979.

Appendix 1

F-111 TACT Aircraft Physical Description

WING		
Area		603.9 Sq. Ft.
Aspect Ratio (Λ = 16°)		5.83
Taper Ratio (")		.542
Span-Extended (")		712 In.
Sweep, Leading Edge		10° to 58°
Root Chord		158.5 In.
Tip Chord		85.8 In.
Airfoil		Supercritical
Thickness Ratio	B.L. 93	9.89%
	Theo. Tip	5.35%
Incidence (Jig)	SS 124	-3.15°
Incidence (Shape)	SS 356	-6.70°
Dihedral		0°
LEADING EDGE FLAPS		
Type		Krueger
No. Sections/Wing		3
Total Area (Stowed)		55.01 Sq. Ft.
Deflection (Nominal)		45° (From Local Chord)
SPOILERS		
Type		Flap
No. Per Side		2
Total Area (Aft of Hinge)		26.6 Sq. Ft.
Hinge Line		61.4%C
Deflection (max)		45°
TRAILING EDGE FLAPS		
Type		Fowler, Single-Slotted
No. Per Side		4
Area (Total)		135 Sq. Ft.
Hinge Line		78%
Deflection (max)		30°
SPEED BRAKE		
Area (Projected-L'K'g Aft)		17.03 Sq.Ft.
Deflection		50°
Hinge Line	Fus. Sta.	472.5
VENTRALS (Total Area)		25.0 Sq.Ft.

VERTICAL TAIL		
Area		111.7 Sq. Ft.
Aspect Ratio		1.419
Taper Ratio		.411
Sweep, Leading Edge		55°
Span		106.8 in.
Airfoil	Root	3.2% Biconvex
	Tip	3.0% Biconvex
RUDDER		
Area		29.3 Sq. Ft.
Span		95.8 in.
Root Chord		60 in.
Tip Chord		28 in.
Deflection		± 30°
HORIZONTAL TAIL		
Total Area (Exposed)		172.9 Sq. Ft.
(Movable)		152.8 Sq. Ft.
Aspect Ratio (Movable)		2.12
Span (Total)		352 in.
Sweep, Leading Edge		57° 30'
Root Chord (@ B.L. 68.2)		180.1 in.
Pivot Location		F.S. 770.25
Airfoil	B.L. 68.2	4% Biconvex
	Tip	3% Biconvex
Incidence		1°
Dihedral		-1°
Deflection		30° T.E. Up, 15° T.E. Dwn.
POWER PLANT		
Engine		P & W TF 30-P-3 Turbofan

Figure 1-1. F-111 Transonic Aircraft Technology Program (TACT) Physical Description

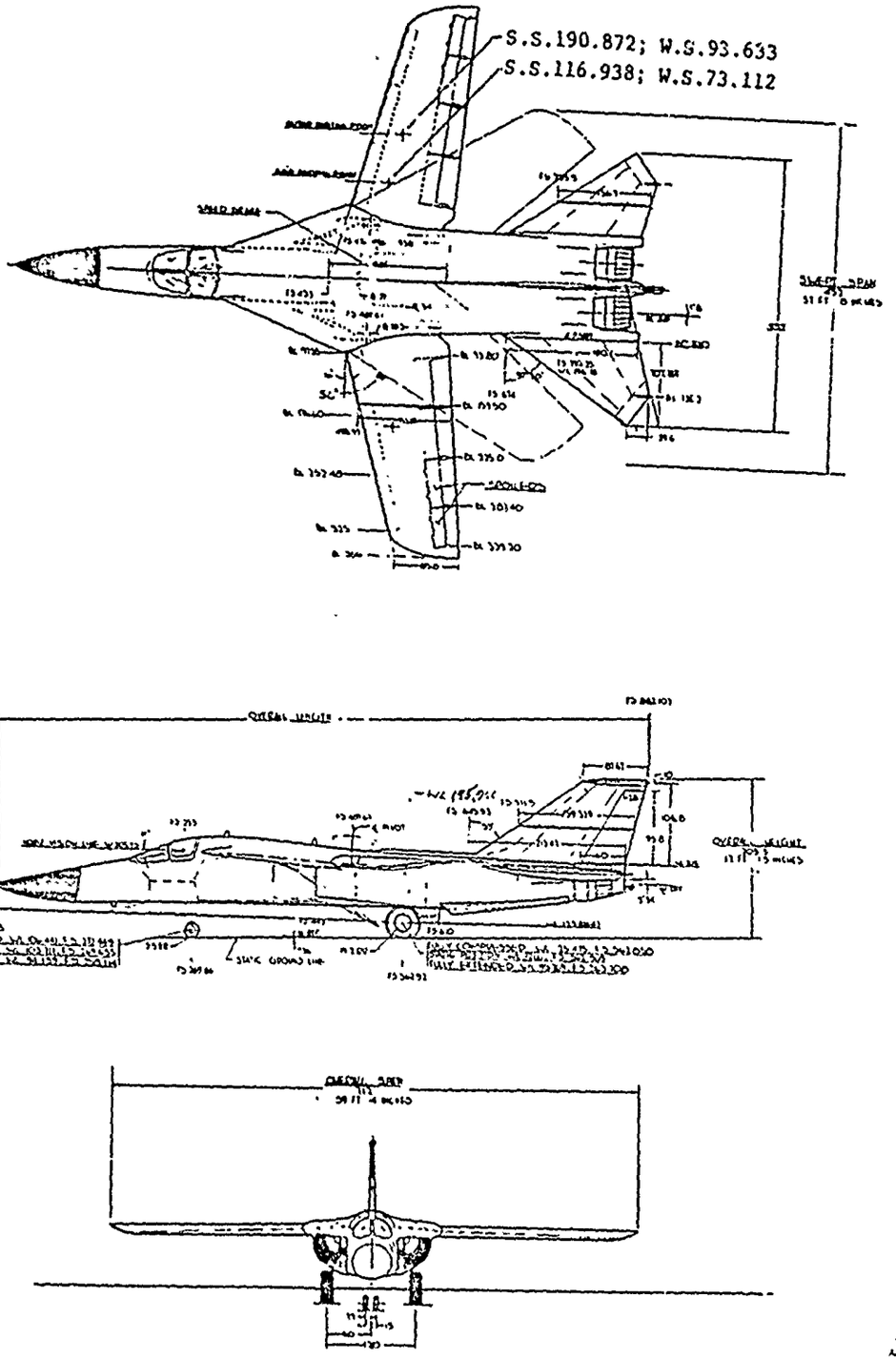

Figure 1-2. F-111 TACT Aircraft

Appendix 2

F-111 TACT Stability Deriviatives

Body Axes

		MACH 0.8 $\alpha = 9°$		MACH 2.0 $\alpha = 2°$	
		TAIL-ON	TAIL-OFF	TAIL-ON	TAIL-OFF
C_{ℓ_β}	(1/deg)	-.0014	-.0016	-.0012	-.00042
C_{y_β}	(1/deg)	-.0122	-.0050	-.0126	-.0060
C_{n_β}	(1/deg)	.0012	-.0012	.0012	-.0012
C_{ℓ_p}	(1/rad)	-.30	-.25	-.11	-.09
C_{y_p}	(1/rad)	.07	-.05	.05	-.04
C_{n_p}	(1/rad)	-.03	-.009	-.01	-.003
C_{ℓ_r}	(1/rad)	.31	.29	.017	.086
C_{y_r}	(1/rad)	0.0	0.0	0.0	0.0
C_{n_r}	(1/rad)	-.25	-.08	-.21	-.07
$C_{y_{\delta_a}}$	(1/deg)	.0001	.0001	.00013	.00013
$C_{\ell_{\delta_a}}$	(1/deg)	-.0008	-.0008	-.000067	-.000067
$C_{n_{\delta_a}}$	(1/deg)	-.000067	-.000067	-.000067	-.000067

		MACH 0.8 $\alpha = 9°$		MACH 2.0 $\alpha = 2°$	
		TAIL-ON	TAIL-OFF	TAIL-ON	TAIL-OFF
$*C_{y_{\delta_v}}$	(1/deg)	.0034	.001	.0008	.0007
$*C_{\ell_{\delta_v}}$	(1/deg)	.0003	0.000	.00005	0.000
$*C_{n_{\delta_v}}$	(1/deg)	-.0013	-.0006	-.00026	-.0004

$*\delta_r$ control derivatives in Tail-on Case

Appendix 3

Thrust Vector Control Derivatives

Thrust vector control derivatives are required in the same form as the rudder control derivatives in order to directly apply them to the lateral - directional small perturbation equations of motion.

The usual sign convention for rudder control is that left rudder is positive, which causes a negative yawing moment. The same sign convention will be used for the thrust vector deflection in that a thrust deflection that causes a negative yawing moment is considered a positive angle (δ_v). This is shown in figure 3-1.

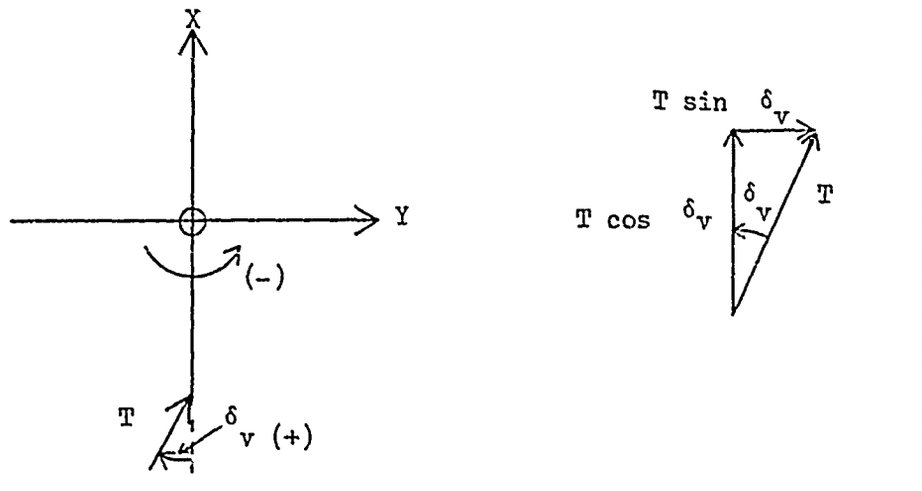

Figure 3-1. Thrust Vector Sign Convention

From figure 3-1 the force in the Y direction due to thrust vectoring is:

$$Y_t = T \sin \delta_v$$

Using a small angle approximation:

$$\text{Sin } \delta_v \tilde{=} \delta_r \text{ (rad)}$$

Then:

$$Y_t = T \delta_v$$

Since the engine thrust is assumed to be parallel to the roll axis in the X - Y plane the rolling moment due to thrust is zero. That is:

$$L_t = 0$$

The yawing moment due to thrust vectoring is (using the small angle approximation):

$$N_t = - T \delta_v l_t$$

where l_t is the distance between the aircraft's center of gravity and the nozzle. To non-dimensionalize the thrust vector dimensional stability derivatives, control surface derivatives used in the lateral-directional small perturbation equations are defined as follows:

$$Y_\delta = \frac{q s}{m} C_{y_\delta}$$

$$L_\delta = \frac{q s b}{Ixx} C_{\ell_\delta}$$

$$N_\delta = \frac{q s b}{Izz} C_{n_\delta}$$

Now let:

$$Y_t = T \delta_v = m Y_{\delta_v} \delta_v$$

$$L_t = 0$$

$$N_t = - T \delta_v l_t = - Izz N_{\delta_v} \delta_v$$

and defining the thrust vector control derivatives as:

$$Y_{\delta_v} = \frac{q\ s}{m}\ C_{y_{\delta_v}}$$

$$L_{\delta_v} = 0$$

$$N_{\delta_v} = \frac{q\ s\ b}{Izz}\ C_{n_{\delta_v}}$$

So finally the non-dimensional thrust vector control derivatives are:

$$C_{y_{\delta_v}} = \frac{m\ Y_{\delta_v}}{q\ s} = \frac{T}{q\ s}$$

$$C_{l_{\delta_v}} = 0$$

$$C_{n_{\delta_v}} = -\frac{Izz\ N_{\delta_v}}{q\ s\ b} = -\frac{T\ l_t}{q\ s\ b}$$

For steady level equilibrium flight conditions:

$$T = D = C_D\ qs$$

Then:

$$C_{y_{\delta_v}} = \frac{C_D qs}{qs} = C_D$$

$$C_{\ell_{\delta_v}} = 0$$

$$C_{n_{\delta_v}} = -\frac{C_D qs\ l_t}{qsb} = -\frac{C_D\ l_t}{b}$$

The drag coefficient was obtained from reference 8.

Appendix 4

Listing of Integration and Plot Program

```
      PROGRAM DISC(INPUT,OUTPUT,PLOT)
      DIMENSION Y(7),YP(7),X(7,8),IWORK(5),WORK(247),BETA(202),TIME(202)
     1,AYY(202),P1(202),PH(202),R(202),DV(202),DD(202),BGG(202),YD(7)
      COMMON X,N,P,W,A
      EXTERNAL F
C
C     MACH .8
C
      READ*,N,W,A,VT,YPP
      M=N+1
      DO 1 I=1,N
    1 READ 5,(X(I,J),J=1,M)
    5 FORMAT(8F10.5)
      WRITE 28
   28 FORMAT(40X,"A MATRIX")
      PRINT*," "
      DO 29 I=1,N
   29 WRITE 30,(X(I,J),J=1,M)
   30 FORMAT(2X,8F10.5)
      PRINT*," "
      PRINT*," "
      P=6.283185/W
      DO 2 I=1,N
    2 Y(I)=0.
      T=0.
      TOUT=.05
      IFLAG=1
      RELERR=ABSERR=.000005
      WRITE 9
    9 FORMAT(3X,*T*,7X,*BETA*,7X,*P*,9X,*R*,8X,*PHI*,6X,*DELTA V*,2X,
     1*DELTA VDOT*,4X,*BG*,6X,*AY*,5X,*IFLAG*)
      PRINT*," "
      PRINT*," "
      DO 10 I=1,200
```

```
      CALL ODE(F,N,Y,T,TOUT,RELERR,ABSERR,IFLAG,WORK,IWORK)
      AY=X(1,1)*Y(1)*VT+YPP*Y(2)+X(1,6)*Y(6)*VT
      T1=TOUT
      IF(T1.GT.P)T1=0.
      BG=A-A*COS(W*T1)
      CALL DEG(YD,Y,BG)
      BA=YD(1)+BG
      DVD=X(6,1)*YD(1)+X(6,6)*YD(6)+X(6,7)*YD(7)+X(6,8)*BG
      IF(DVD.GE.51.57)DVD=51.57
      IF(DVD.LE.-51.57)DVD=-51.57
      IF(YD(6).GE.28.5)DVD=0.
      IF(YD(6).LE.-28.5)DVD=0.
      WRITE 15,T,BA,YD(2),YD(3),YD(4),YD(6),DVD,BG,AY,IFLAG
   15 FORMAT(1X,F5.2,8F10.4,3X,I2)
      PRINT*," "
      J=I+1
      BETA(J)=BA
      TIME(J)=T
      AYY(J)=AY
      P1(J)=YD(2)
      R(J)=YD(3)
      DV(J)=YD(6)
      PH(J)=YD(4)
      DD(J)=DVD
      BGG(J)=BG
   10 TOUT=TOUT+.05
      BETA(1)=0.
      TIME(1)=0.
      AYY(1)=0.
      P1(1)=0.
      PH(1)=0.
      R(1)=0.
      DV(1)=0.
      DD(1)=0.
      BGG(1)=0.
```

```
      NJ=20
      L=NJ+1
      M=NJ+2
      CALL FACTOR(1.1)
      PRINT*,"PLOT"
      CALL PLOT(0.,.5,-3)
      PRINT*,"SCALE"
      CALL SCALE(TIME,10.,NJ,1)
      CALL SCALE(P,4.,NJ,1)
      CALL AXIS(0.,0.,10HTIME - SEC,-10,10.,0.,TIME(L),TIME(M))
      CALL AXIS(0.,0.,11HP - DEG/SEC,11,4.,90.,P(L),P(M))
      CALL LINE(TIME,P,NJ,1,0,50)
      CALL PLOT(0.,5.,-3)
      CALL SCALE(BETA,4.,NJ,1)
      CALL AXIS(0.,0.,10HTIME - SEC,-10,10.,0.,TIME(L),TIME(M))
      CALL AXIS(0.,0.,11HBETA - DEG,10,4.,90.,BETA(L),BETA(M))
      CALL LINE(TIME,BETA,NJ,1,0,50)
      CALL PLOT(0.,5.,-3)
      CALL SCALE(AYY,4.,NJ,1)
      CALL AXIS(0.,0.,10HTIME - SEC,-10,10.,0.,TIME(L),TIME(M))
      CALL AXIS(0.,0.,14HAY - FT/SEC SQ,14,4.,90.,AYY(L),AYY(M))
      CALL LINE(TIME,AYY,NJ,1,0,50)
      CALL PLOT(12.,-10.,-3)
      CALL SCALE(P1,4.,NJ,1)
      CALL AXIS(0.,0.,10HTIME - SEC,-10,10.,0.,TIME(L),TIME(M))
      CALL AXIS(0.,0.,11HP - DEG/SEC,11,4.,90.,P1(L),P1(M))
      CALL LINE(TIME,P1,NJ,1,0,50)
      CALL PLOT(0.,5.,-3)
      CALL SCALE(PH,4.,NJ,1)
      CALL AXIS(0.,0.,10HTIME - SEC,-10,10.,0.,TIME(L),TIME(M))
      CALL AXIS(0.,0.,9HPHI - DEG,9,4.,90.,PH(L),PH(M))
      PRINT*,"LINE"
      CALL LINE(TIME,PH,NJ,1,0,50)
      CALL PLOT(12.,-5.,-3)
      CALL SCALE(CD,4.,NJ,1)
```

```
      CALL AXIS(0.,0.,17HDELTA V - DEG/SEC,17,4.,90.,DD(L),DD(M))
      CALL AXIS(0.,0.,10HTIME - SEC,-10,10.,0.,TIME(L),TIME(M))
      CALL LINE(TIME,DD,NJ,1,0,50)
      CALL PLOT(0.,5.,-3)
          CALL SCALE(DV,4.,NJ,1)
      CALL AXIS(0.,0.,10HTIME - SEC,-10,10.,0.,TIME(L),TIME(M))
      CALL AXIS(0.,0.,13HDELTA V - DEG,13,4.,90.,DV(L),DV(M))
      CALL LINE(TIME,DV,NJ,1,0,50)
      CALL PLOT(0.,5.,-3)
      CALL SCALE(BGG,4.,NJ,1)
      CALL AXIS(0.,0.,10HTIME - SEC,-10,10.,0.,TIME(L),TIME(M))
      CALL AXIS(0.,0.,15HBETA GUST - DEG,15,4.,90.,BGG(L),BGG(M))
      CALL LINE(TIME,BGG,NJ,1,0,50)
      PRINT*,"PLOTE"
      CALL PLOTF(NI)
      STOP
      END

      SUBROUTINE F(T,Y,YP)
      DIMENSION Y(7),YP(7),X(7,8)
      COMMON X,N,P,W,A
      T1=T
      IF(T1.GT.P)T1=0.
      BG=A-A*COS(W*T1)
      IF(Y(6).GE..5)Y(6)=.5
      IF(Y(6).LE.-.5)Y(6)=-.5
C     STATE EQUATIONS
      DO 10 I=1,N
   10 YP(I)=X(I,1)*Y(1)+X(I,2)*Y(2)+X(I,3)*Y(3)+X(I,4)*Y(4)+X(I,5)*Y(5)+
     1X(I,6)*Y(6)+X(I,7)*Y(7)+X(I,8)*BG
      IF(YP(6).GE..9)YP(6)=.9
      IF(YP(6).LE.-.9)YP(6)=-.9
      IF(Y(6).EQ..5)YP(6)=0.
      IF(Y(6).EQ.-.5)YP(6)=0.
      RETURN
      END
```

```
1                SUBROUTINE DEG(YD,Y,RG)
                 DIMENSION Y(7),YD(7)
                 RG=RG*57.29578
                 DO 1: I=1,7
5          10    YD(1)=Y(I)*57.29578
                 RETURN
                 END
```

Appendix 5

Listing of Continuous Random Variance Program

```
      1                 PROGRAM GUST(INPUT,OUTPUT)
                        DIMENSION A(100),H(30),C(30),CQ(30),CQCT(9),Q(100)
                        DIMENSION DUM1(100),DUM2(100),DUM3(100),DUM4(100)
                  C
      5           C      MACH .8
                  C     TAIL-ON
                  C
                        PRINT 100
                        READ *,N,M,L
     10                 N2=N*N $L2=L*L $NM=N*M $NL=N*L
                   1    CONTINUE
                        DO 10 I=1,N
                        READ*,(A(J),J=I,N2,N)
                   10   IF(EOF(5LINPUT).NE.0.)GO TO 99
     15                 READ*,(H(I),I=1,N)
                        DO 20 I=1,L
                  20    READ *,(C(J),J=I,NL,L)
                        PRINT 250
                        DO 40 I=1,N
     20           40    PRINT 500,(A(J),J=I,N2,N)
                        PRINT 280
                        DO 45 I=1,N
                  45    PRINT 500,(H(J),J=I,NM,N)
                        PRINT 300
     25                 DO 50 I=1,L
                  50    PRINT 500,(C(J),J=I,NL,L)
                        CALL KLEIN(A,H,Q,N,M,DUM1,DUM2,DUM3,DUM4)
                        PRINT 320
                        DO 80 I=1,N
     30           80    PRINT 500,(Q(J),J=I,N2,N)
                        CALL MPRD(C,Q,CQ,L,N,N)
                        CALL MPRDT(CQ,C,CQCT,L,N,L)
                        PRINT 340
                        DO 85 I=1,L
```

```
      85    PRINT 500,(CQCT(J),J=I,L2,L)
            GO TO 1
      99    STOP
     100    FORMAT(*  FINDS THE STEADY STATE VARIANCE MATRIX FOR THE SYSTEM:*
           1 /5X,"XDOT = A * X + H * W"/
           2 *  WHERE W IS UNIT VARIANCE WHITE NOISE.*//*  SOLVES THE *
           3 "EQUATIONS:  A * Q + Q * AT + H * HT = 0"/ 5X,"WHERE Q IS THE"
           4 " VARIANCE OF X."// "  THE PROGRAM THEN COMPUTES THE VARIANCE "
           5 "MATRIX OF Y, WHERE Y = C * X"//8X"A(N,N), H(N,M), C(L,N)"/
           6 5X,"MAX DIMENSIONS: N=10, M=3, L=3"//5X"ENTER N,M,L"/)
     260    FORMAT(/"    'A' MATRIX IS:")
     280    FORMAT(/"    'H' MATRIX IS:")
     300    FORMAT(/"    'C' MATRIX IS:")
     320    FORMAT(/" STATE VARIANCE MATRIX 'Q' IS:")
     340    FORMAT(//" OUTPUT VARIANCE MATRIX IS:")
     500    FORMAT(1X,8E13.3)
            END


      1     SUBROUTINE KLEIN(A,H,Q,N,L,G,U,V,W)
            DIMENSION A(N,N),H(N,L),Q(N,N),G(N,N),U(N,N),V(N,N),W(N,N)
            DATA D,D2/1.,2./
      C     TRANSPOSE A
      5     DO 2 I=1,N
            DO 2 J=1,N
      2     G(I,J)=A(J,I)
      C     FORM (D*I-G) AND (D*I+G)
            DO 5 I=1,N
     10     DO 4 J=1,N
      4     U(I,J)=-G(I,J)
            U(I,I)=U(I,I)+D
      5     G(I,I)=G(I,I)+D
      C     FORM U=(D*I-G)INV, V=(D*I+G)*U, D=D2*UT*H*HT*U
     15     CALL MINV(U,U,N)
            CALL MPRO(G,U,V,N,N,N)
            CALL MTPRO(H,U,G,L,N,N)
```

```
      CALL MTPRD(G,G,W,N,L,N)
      CALL MADD(W,W,Q,N,N,D2,0.)
C     PERFORM THE FOLLOWING LOOP UNTIL CONVERGENCE
C     QNEW=QOLD+VOLDT*DOLD*VOLD
C     VNEW=VOLD**2
C     QOLD=QNEW
C     VNEW=VOLD
      K=0
10    K=K+1
      CALL MPRD(Q,V,U,N,N,N)
      CALL MTPRD(V,U,G,N,N,N)
      CALL MADD(Q,G,Q,N,N,1.,1.)
      CALL MPRD(V,V,U,N,N,N)
      CALL MADD(U,U,V,N,N,1.,0.)
      TRACE=0. $ CHANG=0.
      DO 20 I=1,N
      TRACE=TRACE+Q(I,I)**2
20    CHANG=CHANG+G(I,I)**2
      IF (CHANG/TRACE .LT. 1.E-8) GO TO 30
      IF (K.LT.12) GO TO 10
      PRINT 100,CHANG,TRACE
      RETURN
30    PRINT 200,CHANG,TRACE,K
      RETURN
100   FORMAT(* DID NOT CONVERGE, CHANG =*E12.4,*  TRACE =*,E12.4/)
200   FORMAT(/* VARIANCE ANALYSIS COMPLETE*/* CHANG,TRACE,ITERATIONS =*
     1  2E12.4,I5/)
      END
```

```
      1                 SUBROUTINE  MPRD(A,B,C,L,M,N)
                        DIMENSION A(L,M),B(M,N),C(L,N)
                  C     C=A*B
                        DO 10  I=1,L
      5                 DO 10  J=1,N
                        SUM=0.
                        DO 5  K=1,M
                  5     SUM=SUM+A(I,K)*B(K,J)
                  10    C(I,J)=SUM
     10                 RETURN
                        END
```



```
      1                 SUBROUTINE MTPRD(A,B,C,L,M,N)
                        DIMENSION A(M,L),B(M,N),C(L,N)
                  C     C=AT*B
                        DO 10  I=1,L
      5                 DO 10  J=1,N
                        SUM=0.
                        DO 5  K=1,M
                  5     SUM=SUM+A(K,I)*B(K,J)
                  10    C(I,J)=SUM
     10                 RETURN
                        END
```

```
      SUBROUTINE MPRDT(A,B,C,L,M,N)
      DIMENSION A(L,M),B(N,M),C(L,N)
C     C=A*BT
      DO 10 I=1,L
      DO 10 J=1,N
      SUM=0.
      DO 5 K=1,M
5     SUM=SUM+A(I,K)*B(J,K)
10    C(I,J)=SUM
      RETURN
      END
```



```
      SUBROUTINE MADD(A,B,C,L,M,ASCALE,BSCALE)
      DIMENSION A(L,M),B(L,M),C(L,M)
C     C=ASCALE*A+BSCALE*B
      DO 10 I=1,L
      DO 10 J=1,M
10    C(I,J)=ASCALE*A(I,J)+BSCALE*B(I,J)
      RETURN
      END
```

Vita

Roy Edward La Froth

He received a Bachelor of Science degree in Aerospace Engineering in December 1973 from the University of Arizona and was commissioned as a 2nd Lieutenant at the School of Military Sciences, Officer in April 1974. He worked as a project officer for the Deputy for Intercontinental Ballistic Missiles, Space and Missile Systems Organization (SAMSO) at Norton AFB, California from April 1974 to June 1978 at which time he entered the School of Engineering, Air Force Institute of Technology in the Graduate Aeronautical Engineering Program.

Unclassified

SECURITY CLASSIFICATION OF THIS PAGE (When Data Entered)

REPORT DOCUMENTATION PAGE		READ INSTRUCTIONS BEFORE COMPLETING FORM
1. REPORT NUMBER AFIT/GAE/AA/79D-9	2. GOVT ACCESSION NO.	3. RECIPIENT'S CATALOG NUMBER
4. TITLE (and Subtitle) THRUST VECTORING TO ELIMINATE THE VERTICAL STABILIZER		5. TYPE OF REPORT & PERIOD COVERED MS Thesis 6. PERFORMING ORG. REPORT NUMBER
7. AUTHOR(s) Roy E. La Froth Captain, USAF		8. CONTRACT OR GRANT NUMBER(s)
9. PERFORMING ORGANIZATION NAME AND ADDRESS Air Force Institute of Technology (AFIT-EN)		10. PROGRAM ELEMENT, PROJECT, TASK AREA & WORK UNIT NUMBERS
11. CONTROLLING OFFICE NAME AND ADDRESS Air Force Flight Dynamics Laboratory (AFFDL-FGC) Wright-Patterson AFB, Ohio 45433		12. REPORT DATE December 1979 13. NUMBER OF PAGES
14. MONITORING AGENCY NAME & ADDRESS (if different from Controlling Office)		15. SECURITY CLASS. (of this report) Unclassified 15a. DECLASSIFICATION/DOWNGRADING SCHEDULE

16. DISTRIBUTION STATEMENT (of this Report)

Approved for public release, distribution unlimited

17. DISTRIBUTION STATEMENT (of the abstract entered in Block 20, if different from Report)

18. SUPPLEMENTARY NOTES

Approved for public release; IAW AFR 190-17

Joseph P. Hipps, Major, USAF
Director of Public Relations

19. KEY WORDS (Continue on reverse side if necessary and identify by block number)

Control Systems
Flight Control System
Thrust Vector Control System

20. ABSTRACT (Continue on reverse side if necessary and identify by block number)

Root locus analysis techniques are used to design an active thrust vector control system to provide the directional stability for an F-111 without the vertical stabilizer. A linear analysis of the lateral-directional modes is performed for the aircraft both with and without the vertical stabilizer. The aircraft with the vertical stabilizer is used as a baseline. Computer histories for discrete atmospheric turbulence and a covariance analysis for random turbulence are used for

DD FORM 1 JAN 73 1473 EDITION OF 1 NOV 65 IS OBSOLETE

Unclassified

SECURITY CLASSIFICATION OF THIS PAGE (When Data Entered)

the evaluation. It is found that the thrust vector control produces a response as good as or better than the baseline aircraft.

Requirements for the thrust vector deflection and rate of deflection are generated. The lowest possible rate of deflection for acceptable flying qualities is shown to be 1 rad/sec.